University of Strathclyde

Department of Civil Engineering

Case Study for Sustainable Management of Tributyltin Contamination in the Environment

by

Sornnarin Bangkedphol

A thesis presented in fulfilment of the requirements for the degree of Doctor of Philosophy

2010

Declaration of Author's Rights

This thesis is the result of the author's original research. It has been composed by the author and has not been previously submitted for examination which has led to the award of a degree.

The copyright of this thesis belongs to the author under the terms of the United Kingdom Copyright Acts as qualified by University of Strathclyde Regulation 3.50. Due acknowledgement must always be made of the use of any material contained in, or derived from, this thesis.

Signed: *Date:*

Acknowledgements

I wish to express my gratitude towards my supervisor, Dr. Helen Keenan for her kind assistance and suggestions. I also wish to express my appreciation to Dr. Christine Davidson for her valuable support and constructive criticism. I express my gratitude to Dr. Apisit Songsasen for his great attention on my experimentation. I am grateful to Dr. Alec Gaines for his valuable comment. Special thanks to Mr. Weekit Sirisaksoontorn for his valuable and generous time on the photocatalytic laboratory equipments.

I would like to acknowledge the Department of Civil Engineering, University of Strathclyde, Glasgow, UK and the Department of Chemistry, Faculty of Science, Kasetsart University, Thailand for research facilities.

I would like to dedicate my indebtedness to Mr. Arthit Sakultantimetha for his immense assist, patience, encouragement and attention throughout the duration of my study.

I wish to express my high appreciation and deepest gratitude to my mother, Arthit's parents and Dr. Helen Keenan for inspiration, encouragement, and the financial assistance which made my graduate studies possible. I thank you for all you have done to get me this far.

Sornnarin Bangkedphol

April, 2010

Abstract

Tributyltin (TBT) has been widely used as an antifoulant for ship hulls since the 1980s. This has led to widespread contamination in the environment by this persistent organic pollutant (POP). Meanwhile, sustainable management has become an essential solution to solve the problem. This study includes the development of an analysis method, modeling with partition coefficients and remediation techniques.

A low cost determination using normal phase high performance liquid chromatography was optimised for environmental samples which encourages further research. The separation was performed on a cyanopropyl column with hexane containing 5% tetrahydrofuran and 0.03% acetic acid. Under the experimental conditions, limit of detection (LOD) of TBT and dibutyltin (DBT) were 0.70 and 0.50 μg mL^{-1}, respectively. The optimised extraction of butyltins in water and sediment samples was achieved using hexane containing 0.05-0.5% tropolone and 0.2% sodium chloride at pH 1.7. The quantitative extraction in a certified reference material (BCR-646) and naturally contaminated samples were achieved with recoveries ranging from 95 to 108% with RSD 0.02-1.00%. This method was then used to determine the contamination level and partition coefficients of TBT in samples collected from the Forth and Clyde canal, Glasgow, UK. The environmental quality standards (EQS) values allowed comparison between the values obtained and the guidelines in order to assess the levels of pollution. Furthermore, the modeling program EPISuite (V4.0) was used to determine the partitioning and toxicity of TBT within the different environmental compartments. The experimental model involving K_d, K_{oc} and K_{ow} was compared with the default model. This modeling provides a preliminary evaluation of the fate of TBT, and potential for treatment within the specific environment which leads to effective remediation studies. Photo-degradation of TBT has been focused and enhanced by TiO_2 nanoparticle doped with nitrogen (N-doped TiO_2). Under natural light, this effective catalyst demonstrated the highest photocatalytic degradation of TBT at 28% in 3 h.

Publications

• From this thesis

S. Bangkedphol, H. E. Keenan, C. Davidson, A. Sakultantimetha, A. Songsasen. Enhancement of Tributyltin Degradation under Natural Light by N-doped TiO_2 Photocatalyst, *Journal of Hazardous Materials* **2010,** submitted in April 2010

S. Bangkedphol, H. E. Keenan, C. Davidson, A. Sakultantimetha, A. Songsasen. The Partition Behavior of Tributyltin and Prediction of Environmental Fate, Persistence and Toxicity in Aquatic Environments, *Chemosphere* **2009**, 77(10), 1326-1332.

S. Bangkedphol, H. E. Keenan, C. Davidson, A. Sakultantimetha, M. Dyer, A. Songsasen. Development and Application of an Analytical Method for the Determination of Partition Coefficients of Tributyltin in the Forth and Clyde Canal, Glasgow, Scotland. *Journal of ASTM International* **2009**, 6(7), 3-19.

S. Bangkedphol, H. E. Keenan, C. Davidson, A. Sakultantimetha, A. Songsasen. Development of a Low Cost Method of Analysis for the Qualitative and Quantitative Analysis of Butyltins in Environmental Samples. *Journal of Environmental Science and Health, Part A* **2008**, 43(14), 1744-1751.

Publications

• Related to this thesis

A. Sakultantimetha, H. E. Keenan, T. K. Beattie, T. J. Aspray, **S. Bangkedphol**, A. Songsasen. Acceleration of Tributyltin Biodegradation by Sediment Microorganisms under Optimized Environmental Conditions. *International Biodeterioration & Biodegradation* **2010**, in press.

A. Sakultantimetha, H. E. Keenan, M. Dyer, T. K. Beattie, **S. Bangkedphol**, A. Songsasen. Isolation of TBT-Degrading Bacteria *Citrobacter braakii* and *Enterobacter cloacae* from Butyltin-Polluted Sediment. *Journal of ASTM International* **2009**, 6(6), 369-377.

H.E. Keenan, A. Sakultantimetha, **S. Bangkedphol**. Environmental Fate and Partition Co-efficient of Oestrogenic Compounds in Sewage Treatment Process. *Environmental Research* **2008**, 106(3), 313-318.

H.E. Keenan, P. Sentenac, **S. Bangkedphol**, A. Songsasen, A. Sakultantimetha. Monitoring and Modeling of Metals and PAHs Contaminants in Thai: Laos Mekong River. *Recent Progress in Computational Sciences and Engineering* **2006**, 7A-B, 682-689.

Table of Contents

List of Tables

List of Tables (Continued)

List of Tables (Continued)

List of Figures

List of Figures (Continued)

List of Figures (Continued)

List of Figures (Continued)

List of Figures (Continued)

Abbreviations

AAS	Atomic Absorption Spectrophotometer
APVMA	Australian Pesticides and Veterinary Medicines Authority
BCF	Bioconcentration Factor
BET	Brunauer Emmett Teller
CAS	Chemical Abstracts Number
CI	Confident Interval
CRM	Certified Reference Materials
DBT	Dibutyltin
DPT	Diphenyltin
EA	Elemental Analysis
EDC	Endocrine Disrupting Chemical
EPISuite	Estimation Program Interface Suite program
EPIWIN	Estimation Program Interface for Windows
ETAAS	Electrothermal Atomic Absorption Spectrophotometer
EQS	Environmental Quality Standard
FAP	Free Association Paint
FPD	Flame Photometric Detector
GC	Gas Chromatography
HPLC	High Pressure Liquid Chromatography, High Performance Liquid Chromatography
ICP	Inductive Coupled Plasma
IMO	International Maritime Organisation
JCPDS	Joint Committee on Powder Diffraction Standard
LC_{50}	Lethal Concentration 50
LD_{50}	Lethal Dose 50
LOD	Limit of detection
LOQ	Limit of Quantification
MAE	Microwave Assisted Extraction
MAF	Marine Antifouling
MBT	Monobutyltin

Abbreviations (Continued)

MEPC	Marine Environment Protection Committee
MS	Mass Spectrophotometer
N-doped	Nitrogen doping
OTC	Organotin Compound
PAH	Polycyclic Aromatic Hydrocarbon
PBT	Persistent, Bioaccumulative and Toxic
POP	Persistent Organic Pollutant
PVC	Polyvinyl Chloride
QFAAS	Quartz Furnace Atomic Absorption Spectrophotometer
SDME	Single Drop Micro Extraction
SEM	Scanning Electron Microscopy
SEPA	Scottish Environment Protection Agency
SMILES	Simplified Molecular Input Entry Specification
SPC	Self-Polishing Copolymers
SPE	Solid Phase Extraction
SPM	Suspended Particulate Matter
SPME	Solid Phase Micro Extraction
SRC	Syracuse Research Corporation
TBT	Tributyltin
TBTB	Tributyltin Benzoate
TBTC	Tributyltin Chloride
TBTF	Tributyltin Fluoride
TBTH	Tributyltin Hydride
TBTO	Tributyltin Oxide
TBTOAc	Tributyltin Acetate
TEM	Transmission Electron Microscopy
TEtT	Triethyltin
TMPD	*N,N,N′,N′*-Tetramethyl-*p*-phenylenediamine
TPT	Triphenyltin
TPrT	Tripropyltin

Abbreviations (Continued)

UNEP	United Nations Environment Programme
USEPA	US Environmental Protection Agency
UV/Vis	Ultra Violet/Visible

CHAPTER 1

Introduction on Tributyltin

1.1 Scope of thesis

This thesis is focused on the tributyltin compound (TBT) which is regarded as a persistent organic pollutant (POP), and an endocrine disruptor compound (EDC). There are three research areas relating to TBT studied in this work including environmental monitoring, modelling and remediation by photo-degradation. To monitor the amount of TBT, a cost-saving analytical method has been developed. This developed method is used to determine the amount of TBT in the samples which is also vital for the research in the modelling section. To determine TBT in environmental samples, an effective extraction method has to be developed by varying various extraction parameters. Then, the extractant containing TBT is analyzed by the developed HPLC method which is verified by GC-MS, which is a standard recognized method. The sampling sites in Glasgow that this research focuses on are Bowling Basin and Port Dundas, where organotin compounds in the collected samples were analyzed for two years. To predict the environmental fate and toxicity level of TBT using modelling program, the EPISuite (Estimation Programs Interface) version 4.0 is used to predict % partitioning and toxicity of TBT in the environments. The partitioning of TBT for solid-water and octanol-water provide the experimental partition coefficient values which lead to accurate modelling for prediction of environmental fate. The parameters that affect the adsorption and partition of TBT are also indicated in this work. Moreover, desorption of TBT from solid to water is identified. This present, the contamination of TBT in water could then become considerable. It is therefore necessary to study the remediation process of TBT in water. Therefore, catalytic photo-degradation of TBT in water under natural light is studied and the degradation efficiency is enhanced.

1.2 Properties of TBT

Organotin compounds have a central tin (Sn) atom, with sp^3 hybridisation. They are organic derivatives of tetravalent tin, which is characterised by the presence of covalent bonds between a tin atom and carbon atoms. TBT (Bu_3Sn^+) is a member of the trialkyl organotin family, containing three butyl groups. The planar structure of the TBT ion is shown in Figure 1.1

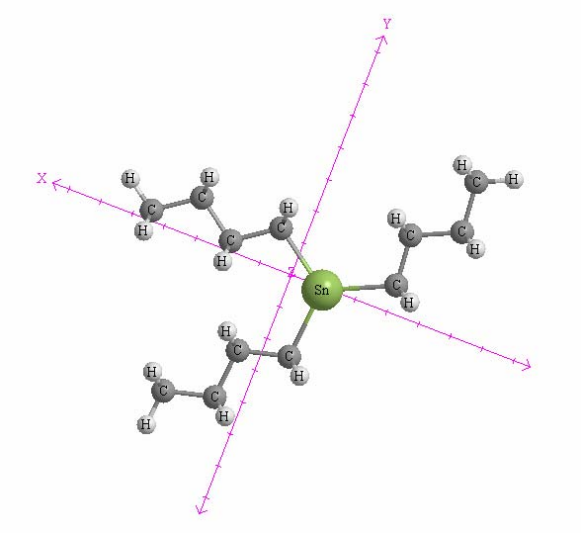

Figure 1.1 Molecular structure of TBT ion, Bu_3Sn^+ from the Cambridge Chemdraw Ultra 11 software (CambridgeSolf, 2009)

Organotin compounds are represented by the formula R_nSnX_{4-n}, in which R is an alkyl or aryl group and X is an anionic mono-valence species. The tetrahedral structure of butyltin compound, Bu_3SnX is shown in Figure 1.2.

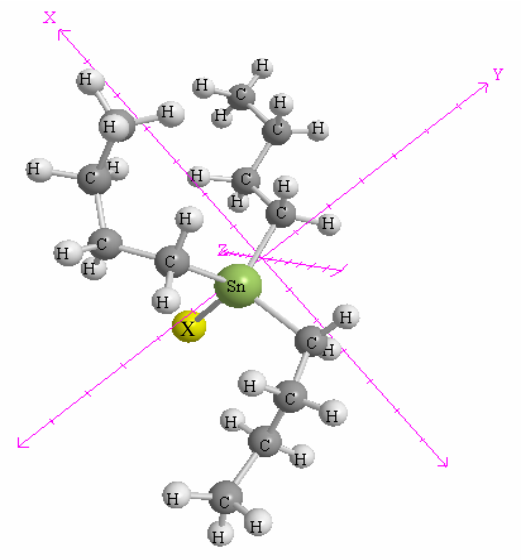

Figure 1.2 Molecular structure of butyltin compounds from the Cambridge Chemdraw Ultra 11 software, where X is Cl atom (CambridgeSolf, 2009)

TBT^+ by itself is unstable and will break down in the environment unless it is combined with anionic substituents, such as hydride (TBTH), halide (TBTF, TBTCl), acetate (TBTOAc), and oxide (TBTO). TBT can be liquid or solid at ambient temperature dependent on the anion group and has a characteristic odour. It is considered lipophilic and thus has poor water solubility (Laughlin et al., 1986, Chen et al., 2006), but it is soluble in hexane and most organic solvents. The solubility of TBT in water is influenced by such factors as the oxidation-reduction potential, pH, temperature, ionic strength, and concentration and composition of the dissolved organic matter (Hall et al., 2000). TBT compounds will become positively charged after the tin-anionic bond is broken down in a solvent. In sea water, TBT exists mainly as a mixture of the chloride, the hydroxide, the aqua complex, and the carbonate complex (Laughlin et al., 1986). The physical properties of TBT are varied and dependent upon their anionic group. The behaviour of TBT biocides may be described by equation Equation 1.1 for un-dissociated compounds (neutral) and for the dissociated cation (positively charged) upon reaction with water. The behaviour and toxicity of TBT with the biocide in the natural environment are attributed to the cation, but not to the associated anion (Antizar-Ladislao, 2008).

$$Bu_3SnX + H_2O \rightarrow Bu_3Sn(H_2O)^+ + X^- \quad \text{(Equation 1.1)}$$

1.3 Production and application of TBT compounds

Organotin compounds (OTCs) were discovered about 150 years ago in the first study by Sir Edward Frankland who successfully synthesised diethyltin-diiodide (Kerk, 1975). Further investigations on the OTCs have led to the discovery of more than 800 organotin compounds to date. All compounds in the organotin family are anthropogenic, except methyltins which are the only compounds that can be produced by biomethylation. Organotins were not widely used due to the fact that no applications existed until it was found to have potential advantages in industrial production, i.e. production of plastics and polyvinyl chloride (PVC). During the development of OTCs, the biocidal property of mainly trisubstituted organotin species was discovered 50 years ago in the Netherlands (Kamruddin et al., 1996). Tributyltin compounds were then seen as important toxic ingredients in fungicides, molluscicides, repellants, wood preservatives and antifouling paint.

1.3.1 Synthesis pathways

Organotin is a man-made organometal, the preparation process has been successfully used since 1848 (Hoch, 2001). It can be synthesized by several methods, Grinard route, Wurtz route, and alkyl aluminium route. These routes to produce organotin halides involve two step reactions (Figure 1.3). The first step is a reaction of tin tetrachloride ($SnCl_4$) with suitable reagents to form various tetraalkyltin compounds (R_4Sn). In the second step, R_4Sn reacts with $SnCl_4$ to form less alkylated organotin chlorides, like R_3SnCl, R_2SnCl_2 or $RSnCl_3$.

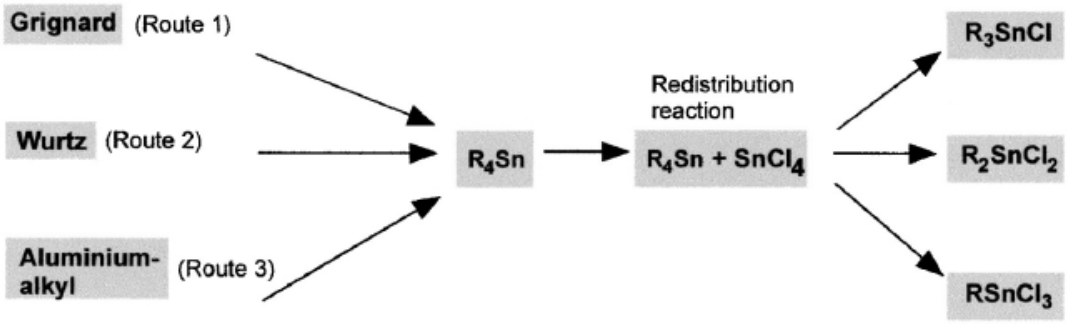

Figure 1.3 Two step preparation of organotins (Hoch, 2001)

The commercial production of organotin compounds by using the Grignard reagent (nRMgX; X represents halides) began in the late 1940s. This process gives a high yield but the use of large amounts of solvents is required. This is also a problem with the Wurtz synthesis. Because of the large solvent volumes and use of sodium metal together with side reactions and uncompetitive economics this process was disregard for industrial production. The alkyl aluminium route started in 1962. This process can be operated continuously and no solvents are needed. Organotin halides can also be prepared by direct synthesis where tin reacts with alkyl iodide resulting in dialkyltin iodide as presented in Equation 1.2 (Hoch, 2001).

$$Sn + 2RI \longrightarrow R_2SnI_2 \qquad \text{(Equation 1.2)}$$

1.3.2 Global production

Greenpeace (1999) reported that there are three major companies producing TBT. The world's largest producer is the German chemical company Witco that has 75% of the world market (Greenpeace, 1999). On the European market almost all TBT (99%) comes from Witco. The remaining percentage comes from A. Song Woun, a Korean producer that has 5% of the global market share. Atochem produces TBT in the USA and has 20% of the world market, but no market share in the EU. The EU production of TBT is around 3,000 tonnes annually. The global production is therefore around 4,000 tonnes. The EU consumption is around 1,300 tonnes. Several paint producers manufacture TBT ship paints by incorporating the chemical into the paint. The largest producer on the world market is the British company International Paint that is owned by Akzo Nobel. Other global players are Sigma Coatings in the Netherlands, Hempel in Denmark, Jotun in Norway, Chugoku in Japan and Ameron in the US. These have made extensive use of TBT in the past.

1.3.3 Application of TBT compounds

In the 1950s, scientists first recognised tin compounds to have strong toxic properties against molluscs (Huang et al., 2004). Organotins with three organic groups were also found to be the most powerful fungicides and bactericides in their family. Extensive use of TBT worldwide began in the 1970s. The major applications are as antifouling agents and as pesticides in agriculture and wood preservation.

1.3.3.1 Antifouling coatings

Antifoulants prevent the settlement and growth of organisms on submerged structures like fishing nets, ship hulls and buoys (Figure 1.4). TBT-containing products have been extremely effective as antifouling paints on ship hulls and underwater structures. These products protect surfaces and structures from the growth of marine organisms.

Figure 1.4 The fouling on ship hull (Yebra et al., 2004)

The most common organotin used in these paints is TBT oxide. Protection from fouling lasts more than two years and is superior to copper- and mercury-based paints by not promoting bimetallic corrosion. Further development of organotin antifouling paints has been in the production of paints containing copolymers that control the release of the organotins and result in longer useful life of the paint as an antifoulant (Bennett, 1996, Champ and Seligman, 1996, Kirk-Othmer, 1981).

Antifouling paints are grouped into 2 types by their mechanism, free association paints (FAP) and self polishing copolymer (SPC) paints**.** Further information on the paints utilising TBT is provided by Anderson and Dalley (Anderson and Dalley, 1986, Hoch, 2001). The primary use is the free association paints, where the active ingredients are dispersed in a resinous matrix. TBT leaches out of this matrix and the painted surface is covered with a TBT containing film so that no organisms will settle on it. In this type of antifouling paint the release rate is uncontrolled, beginning with a very high rate that exponentially decreases in time. The effective period of such paints is up to 2 years. In many countries the use of free association TBT paints are forbidden. Figure 1.5 shows the mechanism of free association paint.

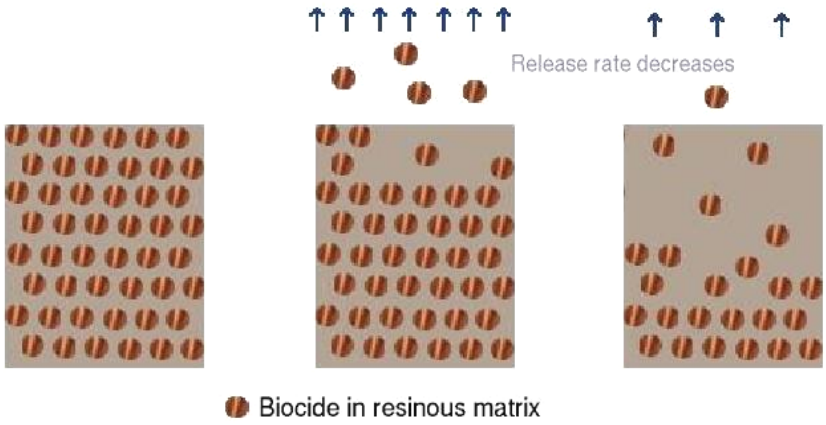

Figure 1.5 Free association paint mechanism (Anderson and Dalley, 1986)

In self polishing copolymer paints, the antifouling component is chemically bonded with a polymer. The antifoulant is then released from the paint surface due to hydrolysis of the polymer with seawater. The surrounding water is in fact slowly eroding the coat of paint and the antifoulant is always released at the same rate dependent on the condition of polymer. These paints are much more environmentally friendly than the free association paints. Antifouling lifetimes are proportional to the thickness of the coating and therefore very predictable up to 7

years. The paint film surface is in constant renewal, which can reduce hull roughness. This is advantageous in that old coatings do not have to be removed before a ship can be repainted (Omae, 2003). Figure 1.6 shows the mechanism of self polishing copolymer paint.

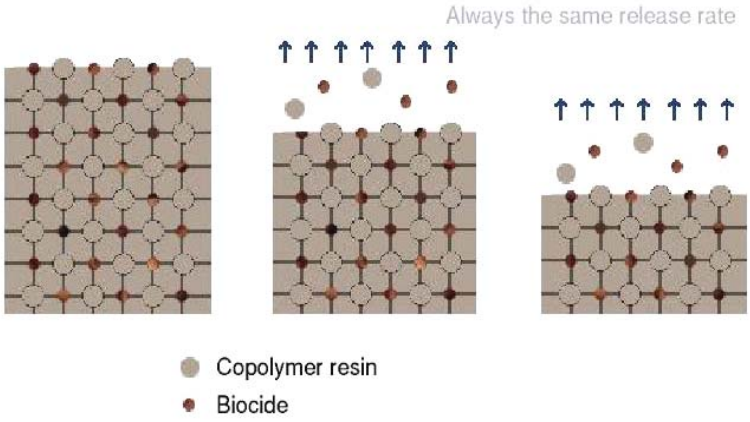

Figure 1.6 Self polishing copolymer paint mechanism (Anderson and Dalley, 1986)

Pollution from ships painted with self polishing copolymer paints is still considerably high, given the amount of TBT released each day (Hoch, 2001). Effective antifouling however does have environmental benefits.

- Growth of aquatic organisms on vessel hulls creates roughness, this leads to more friction thus higher fuel consumption for the same vessel speed. The increase in fuel used leads to greater concentrations of sulfur being released to the atmosphere and also contributing to climate change.
- Ordinary paint needs to be repainted more often, this causes increases release of volatile chemicals to the atmosphere.
- Effective antifouling also prevents the spread of alien species across the world by travel along with ships. Fouled ships are often responsible for the introduction of these species or diseases which could endanger the populations of native species.

By now it is clear that antifouling paints are the major source of TBT compound in the environment. Major shipping routes, harbours and docks show very elevated TBT concentrations (Table 1.1).

Table 1.1 Butyltins in seawater (ng Sn L^{-1}) reported for several regions in the world (Antizar-Ladislao, 2008)

Sampling		Levels of organotin compounds		
Location	Year	MBT	DBT	TBT
American harbours and marinas				
-West and east coast, Canada	1995	<d.l.-460	<d.l.-270	<d.l.-500
Asian harbour and marinas				
-Coast, Korea	1997-1998	<d.l.-13.4	<d.l.-22.3	<d.l.-4.5
-North coast of Kyoto, Japan	2003	2.5-23	2.1-13	3.9-27
Euroean harbours and marinas				
-South west coast, Spain	1993	<d.l.-51	6.8-20	9.1-79
-South east coast, France	1998	-	-	<0.015-0.12
-Coastal waters, Greece	1998-1999	<d.l.-19	<d.l.-159	<d.l.-70
-North west coast, Spain	Not provided	0.8-11.6	0.3-33.7	0.4-196.6

<d.l.: below detection limit

1.3.3.2 Wood treatment

TBT was investigated as a wood preservative to prevent the attack of timber from insects, fungi and bacteria in the breakdown of cellulose. Tributyltin oxide, tributyltin naphthenate and tributyltin phosphate are used as fungicidal components in wood preservative. The applications include dipping, spraying, brushing and double vacuum impregnation in a chamber. TBT is then overspread or remains absorbed within the wood. TBT can be released into the environment by leakage,

accidental spills, effluents, air emission in the spraying process and leaching from treated wood (Hoch, 2001).

1.3.3.3 Pesticides

Since the 1960s, the agricultural applications of pesticides containing TBT have been excessively used as both a fungicide and also to prevent certain tropical diseases in plants. Because of the severe toxic effects against various organisms, its use is restricted in most countries; therefore the chance of significant human intake by food consumption is considered low (Anderson and Dalley, 1986). Another extensive use of TBT is as a biocide and as a preservative to prevent the growth of mould and mildew. Other minor applications of TBT are an antifungal agent in textiles, industrial and water systems, such as cooling tower and refrigeration water systems, wood pulp and paper mill systems, breweries and electrical equipment (Extoxnet, 1996).

1.4 Effects on organisms in the environment

TBT is toxic to non-target organisms even at minute concentration, ng L^{-1}, due to its effectiveness as a biocide. The legislation and ban of the TBT compound was brought into world concern after its toxicity was realized. Unfortunately, high amounts of this compound have already been introduced to the terrestrial and aquatic environment. It is also classed as persistent organic pollutants (POPs) by the United Nations Environment Programme (UNEP), where POPs are chemical substances that persist in the environment, bioaccumulate through the food web, and pose a risk of causing adverse effects to human health and the environment. With the evidence of long-range transport of these substances to regions where they have never been used or produced and the consequent threats they pose to the environment of the whole

globe, the international community has on several occasions called for urgent global actions to reduce and eliminate releases of these chemicals (UNEP, 2005).

Therefore, TBT is regarded as an organic compound that is resistant to environmental degradation and will persist in the environment for a long time. The accumulation of TBT in environmental media and organisms' tissue has become an important issue, as it can biomagnify in the food chain which impacts greatly on the top predator, humans (UNEP, 2005). Moreover, TBT is an endocrine disruptor chemical (EDCs) which interferes with the endocrine system in organisms and humans. It causes physical damage, reproductive effects, teratogenic effects, immunological effects, and imposex of gastropods (Smith, 1981). It is still uncertain if it is a carcinogen (Extoxnet, 1996). Understanding of its fate and transport in the environment is of primary importance to prevent its migration.

1.4.1 Endocrine disrupting chemicals (EDCs)

Endocrine disrupting chemicals are naturally occurring compounds or man-made chemicals that may interfere with the production or activity of hormones of the endocrine system leading to adverse health effects (UNEP, 2005). Environmental pollution has been the source of much public discussion and media attention. EDCs have caused particular concern because they may interfere with the normal function of the hormonal systems of humans and animals. Endocrine disrupting properties are found in several classes of chemicals released into the environment such as some insecticides and fungicides, dioxins and anti-fouling paints. TBT is an endocrine disrupting chemical (Matthiessen and Gibbs, 1998). Despite the lack of information on the effect on humans of EDCs in the environment, strong evidence links EDCs exposure to effects on some organisms in the environment, most notably the effect of TBT on molluscs. The action of EDCs has resulted in the localised destruction of certain species and is a cause for serious concern. The possible effect of EDCs on humans are: reproductive (sperm quality, fertility, sex ratio and abnormalities of

male sex organs), endometriosis, precocious puberty, nervous system function, immune function and cancer (WHO, 2002). Even when there is no firm evidence on the interactions, the biological plausibility of possible damage to certain human functions from exposure to EDCs seems strong when viewed against the background of known influences of endogenous and exogenous hormones on many of these processes. Therefore, despite the difficulties and uncertainties, concern remains about the possible role of exposure to EDCs in adverse health effects in humans. It is pertinent to describe the endocrine system briefly and discuss the mechanisms of endocrine disruption.

1.4.1.1 Endocrine system

The endocrine system is a main body system working together with the nervous system, reproductive system, kidneys, gut, liver and fat to communicate and control the growth and development, body responses, energy levels, reproduction and homeostasis. A gland is a group of cells that produces and secretes chemicals. A gland selects and removes materials from the blood, processes them, and secretes the finished chemical product for use in the body. Endocrine glands release more than 20 major hormones directly into the bloodstream where they can be transported to the target cells in other parts of the body upon which they act. The major glands that make up the human endocrine system are the hypothalamus, pituitary, thyroid, parathyroid, adrenals, pineal body, and the reproductive glands, which include the ovaries and testes. The pancreas is also part of this hormone-secreting system, even though it is also associated with the digestive system because it also produces and secretes digestive enzymes (Boyer, 1989, Kaloyanova, 1991). The positions of glands in the body are shown in Figure 1.7.

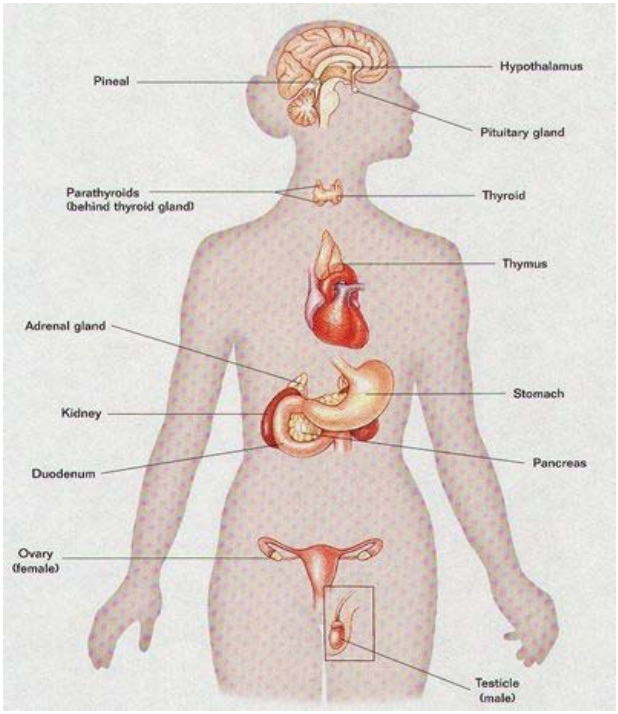

Figure 1.7 The endocrine system and glands in human body (EPA, 1996)

As the body's specific chemical messengers, hormones are synthesised and secreted by glands and travel throughout the body. Each hormone's shape is specific and can be recognised by the corresponding target cells that contain matching receptors in or on their surfaces. The hormone binds with the receptor, much like a key would fit into a lock. The hormones need to find compatible receptors to work properly. Although hormones reach all parts of the body, only target cells with compatible receptors are equipped to respond. Once a receptor and a hormone bind, the receptor carries out the hormone's instructions by either altering the cell's existing proteins or turning on genes that will build a new protein. Both of these actions create reactions throughout the body (UNEP, 2005).

1.4.1.2 Endocrine disruptors

Endocrine disruptors have been linked with production, release, transport, metabolism, binding, biological action or elimination of natural ligands in the body that are responsible for the maintenance of homeostasis and the regulation of developmental process (Zacharewski, 1998). These chemicals also may be adversely affecting human health in similar ways resulting in declined fertility and increased incidences or progression of some diseases including endometriosis and cancers (NIEHS, 2006). These chemicals have also been referred to as endocrine modulators, environmental hormones, and endocrine active compounds. Endocrine disruptors may act is several different ways to disrupt normal body function (Rajesh, 1999) including:

• Mimic or partly mimic naturally occurring hormones in the body by duplicating normal hormone responses, but produce slightly different variations, leading to potentially producing over-stimulation of the chemicals or false communication which can negatively affect reproductive organs, behaviour and other biological functions.

• Interact or bind with receptors within a cell to block the endogenous hormone, to produce an abnormal response, or to exaggerate the hormones effect. The normal signal then fails to occur and the body fails to respond properly, either having a decreased or increased effect on the gene.

• Interrupt or block normal signalling mechanisms of natural hormones or their receptors that control the body's ability to make proteins, enzymes, and other hormones.

• Stimulate receptor formation of hormone receptors on or within target cells which leads to hormone signals being multiplied. Therefore, the effects of both natural and foreign hormones are amplified.

• Interfering with the synthesis of natural hormones. Endocrine disruptors can alter their structures, or alter and influence the pattern of the hormone synthesis.

• Interfering with the removal of hormones from circulation. Chemicals can accelerate the rate at which the hormones are broken down, effectively reducing the concentration of a given hormone, or interfere with the natural enzymes within the body that break down hormones resulting in higher than required concentrations of hormones within the body.

• Disrupt by alternation of genes that control critical pathways and interfere with neurotransmitters, causing a disruption in menstrual and reproductive cycles. This also occurs by direct toxic activity on the nerve cells in the pituitary, the ovaries and the testes.

• Bind to hormone receptors on sperm and oocytes to cause abnormal function and impair fertility.

1.4.2 Toxicity of TBT compounds

Toxicity of organotin compounds is strongly influenced by the length of the alkyl chains attached to the tin (Clarkson, 1991). Generally, the toxicity of organotin compounds is influenced more by the alkyl substituent than the ionic substituent, which form the rest of the molecule (Kaloyanova, 1991). TBT compounds are moderately toxic via both ingestion and dermal absorption. TBT leads to acute and chronic effect in non-target organisms even at low concentration in the level of parts per billion (ppb or $\mu g\ L^{-1}$) (UNEP, 2005). When exposed to TBT, effects on reproduction, organ toxicity, carcinogenicity and imposex may occur.

1.4.2.1 Effect on humans

Although the effects of TBT on humans are not clear, several incidents of human exposure to the biocide have been reported (Goh, 1985). TBT is a skin, eye and mucous membrane irritant, and severe dermatitis has been reported after direct contact with the skin. The potential problem is made worse by the lack of an immediate skin response. Skin burns or severe lesions were most commonly caused by contact with liquid TBT chlorides. The irritancy is not immediately apparent, thus contact with TBT was frequently ignored. This compound causes an acute burn which heals relatively quickly, or a more diffuse dermatitis which persists. Treatment of undiluted TBT compounds on human skin established that the TBT chloride, acetate, and oxide all produces acute burns. Reddening, inflammation of the hair follicles, minute pustules and a faint erythema are the main symptoms that happen after exposure to the compound. The burns were not reported to be painful, but itching and adherence of clothes to skin was problematic (Goh, 1985).

Exposure to TBT results in severe dermatitis where the compound had been retained on the skin for long periods. Inhalation of TBT causes nausea and vomiting. TBT-exposed suffers also report irritant effects by the development of rashes, severe itching, redness, swelling, and blistering. Moreover, hospital examination has shown extensive vesiculobullous lesions, erythema, and oedema (Goh, 1985).

Miscellaneous effects reported from poisoning with TBT compounds were, along with symptoms of lassitude, slight occipital headaches, and stiffness in the shoulders; there was also marked disturbance of the sense of smell (IPCS, 1990). Symptoms reported following: inhalation of TBTO dust and vapours included irritation of the upper respiratory tract and eyes. Sufferers also developed lower chest symptoms, reduced sense of smell, breathing problems, irritated skin, chronic headaches, colds, flu-like symptom, fatigue, dizziness, stomach ache and feelings of musculoskeletal stiffness (Kaloyanova, 1991).

1.4.2.2 Effect on microorganisms

TBT is toxic to various microorganisms and has been used commercially as a bactericide and algaecide (Fent, 1996). The concentrations that produce toxic effects vary considerably according to the species. For example, the 48 h and 72 h LC_{50} for the estuarine zooplankter *Eurytemora affinis* were 2,200 and 600 ng L^{-1} TBT, respectively (Aguilar-Martinez et al., 2008). TBT is more toxic to Gram-positive bacteria than to Gram-negative bacteria (Lascourreges et al., 2000). The concentration of TBT that cause toxicity in bacteria depends on the species of bacteria exposures to TBT and the surrounding conditions (Suehiro et al., 2006, Harino et al., 1997b). TBT present in the solid phase tends to have higher toxicity than presence in the liquid phase (Wuertz et al., 1991). The TBT acetate and TBTO were found to inhibit growth of fungi and of green alga *Chlorella pyrenoidosa* (IPCS, 1990).

1.4.2.3 Effect on aquatic organisms

TBT is lipophilic and tends to accumulate in aquatic organisms, for example, oysters, mussels, crustaceans, molluscs, fish, and algae. Freshwater species presented higher bioaccumulation of TBT than marine organisms, due to the bioavailability and aqueous solubility of TBT in different type of water (Extoxnet, 1996).

Marine and estuarine organisms; TBT is highly toxic to marine molluscs. It has been shown experimentally to affect shell deposition of growing oysters, gonadal development and gender of adult oysters, and to cause increased mortality of larval oysters and other bivalves (IPCS, 1990, Lawler and Aldrich, 1987). TBT causes imposex, the development of male characteristics in female gastropods (Smith, 1981). The toxicity of TBT to marine fish is highly variable. Larval stages are more sensitive than adults. In an effective concentration, a temporary opacity of the surface of the eyes developed. Other symptoms included sluggishness and difficulties with balance. Melanophores in the skin were found to be constricted but TBT did not seem to affect feeding behaviour (Hall et al., 1988). The injuries on

hard and soft corals in the Great Barrier Reef were consistent with the symptoms from contact with antifoulants, Figure 1.8 (Marshall et al., 2002).

Figure 1.8 The coral showing damage consistent with antifoulants (Marshall et al., 2002)

Freshwater organisms; Freshwater angiosperms were inhibited by a TBTO and killed in high concentration (μg L^{-1}). Freshwater snails were sensitive to TBT acetate (IPCS, 1990). Imposex, the development of male characteristics in females, has been initiated by TBT exposure in several snail species (Fent, 1996). Therefore, reproduction was inhibited when female snails exposed to TBT developed male characteristics (USEPA, 1985). Also the inhibition in growth rate and mortality of crustaceans was reported (Laughlin et al., 1986). In the exposure of TBT to freshwater fish, there was a dose-related retardation of growth, resulting in a decrease in body weight (Seinen et al., 1981).

1.4.2.4 Effect on terrestrial organisms

Exposure of terrestrial organisms to TBT derives primarily from its use as a wood preservative. However, little information is available. TBT compounds are

toxic to insects exposed either topically or via feeding on treated wood (IPCS, 1990). TBTO is moderately toxic to birds. It does not affect the bird mortality but reduces egg production, eggshell thickness, fertility, and hatchability (IPCS, 1990). The toxicity to mammals can be divided into the following:

Acute toxicity; TBT is moderately to highly toxic to laboratory mammals, acute oral LD_{50} values range from 94 to 234 mg kg^{-1} body weight for rats and from 44 to 230 mg kg^{-1} body weight for mice. The acute toxicity via the dermal route is low, the LD_{50} being >9000 mg kg^{-1} body weight for the rabbit (IPCS, 1990, Pelikan and Cerny, 1968). The variation comes from the anion component of the TBT salt. Other effects of acute exposure may include alterations in blood lipid levels, the endocrine system, liver, and spleen, and transient deficits in brain development (Ocallaghan and Miller, 1988, Matsui et al., 1982).

Short-term toxicity; TBT compounds have been studied most extensively in the rat. At dietary doses of 25 mg kg^{-1} body weight, high mortality rates were observed when the exposure time exceeded 4 weeks. The main symptoms at lethal doses were reduction in food consumption, weakness, and emaciation (Krajnc et al., 1984). Decreases in haemoglobin concentration and erythrocyte volume in rats, resulting from dosing with 8 mg kg^{-1} body weight, indicate an effect on haemoglobin synthesis, leading to microcytic hypochromic anaemia (IPCS, 1990).

Long-term toxicity; A long-term study in rats indicates effect of TBT on general toxicological parameters at a level of 0.25 mg kg^{-1} body weight (Wester et al., 1990, IPCS, 1990).

Reproductive toxicity; The potential embryo toxicity of TBTO has been evaluated after oral dosing of the mother. The main malformation noted in rat and mouse foetuses was cleft palate, but this occurred at dosages overtly toxic to the mothers. These results are not considered to be indicative of teratogenic effects of TBTO at doses below those producing maternal toxicity. The lowest TBT concentration, with

regard to embryotoxicity and fetotoxicity for all species, was 1.0 mg kg^{-1} body weight (IPCS, 1990, Crofton et al., 1989).

Carcinogenicity; Carcinogenicity studies have been carried out on rats, in which neoplastic changes were observed in endocrine organs at 50 mg kg^{-1} diet. The pituitary tumours reported at 0.5 mg kg^{-1} diet were considered as having no biological significance since there was no dose-response relationship. These tumour types usually appear in high and variable background incidences (Wester et al., 1990).

1.5 Management and current standards for TBT

1.5.1 Legislation and the banning of TBT

Organotins, which have been used as effective antifouling agents for over 30 years, have come under extensive environmental scrutiny. Over the past 10 to 15 years it has become apparent that TBT degraded very slowly in the environment resulting in appreciable concentrations in the aquatic environment. In addition, chronic toxicities have been observed at low concentration levels (Yebra et al., 2004). As a result of environmental scrutiny of TBT, several new antifouling agents have been developed. A number of these compounds possess characteristics that clearly make them environmentally preferable alternatives to TBT (Martinez et al., 2000), which was a key factor in the International Maritime Organisation (IMO) decision to ban the applications as antifouling agents from January 1, 2003 (IMO, 2002).

In the early 1970s, TBT was introduced as an ingredient in marine antifouling coatings for general use on sea-going vessels. TBT soon became the most cost-effective technology for antifoulant protection of deep-sea vessels. It was so

effective that TBT-based antifoulant paint spread to nonessential uses such as pleasure craft, coastal vessels, and fresh watercraft. After reports of TBT causing imposex in dogwhelks and chambering in oysters, the first legislative restrictions on the use of organotin antifoulants came in 1982. France prohibited the use of organotin antifoulants on boats smaller than 25 m. The UK, in 1987, banned the use of TBT based paints on vessels less than 25 m in length and on fish-farming equipment, and set an environmental quality standard for TBT and TPhT to protect marine life. Also from that date all antifoulants had to be registered as pesticides so that a special committee on pesticides must approve sale and used (Yebra et al., 2004).

By the Organotin Antifouling Paints Control Act (OAPCA), in 1988, the use of TBT compounds as marine antifoulants has been limited by the type of vessel and also to TBT paints that have laboratory tested release rates of ≤ 4 μg cm^{-2} per day (Cardwell et al., 1999). The US prohibited TBT paints on smaller than 25 m vessels and they also set a maximum leaching rate of 4 μg cm^{-2} per day for all vessels longer than 25 m. From 1990 only certified applicators can apply these paints and all antifoulants need special registration. The US Environmental Protection Agency (USEPA) has requested all registration holders of TBT antifouling products to voluntarily agree to cancel registration under the Federal Insecticide, Fungicide and Rodenticide Act (FIFRA) by 1/1/2003 (IMO, 2002).

The International Maritime Organisation (IMO) and Marine Environment Protection Committee (MEPC) agreed a recommendation that governments should promote legislation along the following lines (IMO, 2002, Jacobson and Willingham, 2000).

• Elimination of usage on non-aluminum vessels less than 25m in length

• Elimination of usage of paints having average release rate greater than 4 μg cm^{-2} day

• Development of alternative systems

Most western countries, including the European Community, largely adopted these recommendations into their legislation (Yebra et al., 2004). A ban on the application of TBT based antifouling paints from 1 January 2003 was proposed and **1 January 2008** as the last date for having TBT based antifouling paints on a vessel. On 5 October 2001, in London, the International Convention on the Control of Harmful Anti-Fouling Systems for Ships was approved during the International Conference on the Control of Harmful Anti-Fouling Systems for Ships organized by the IMO (IMO, 2002). This convention encompasses the proposed ban of TBT antifoulants. However many countries, including the EU, are well on the way to ban organotin antifoulants. Currently the use of organotin compounds, in the EU, are subject to restrictions under regulation (EC) No 782/2003 of 14 April 2003 (EUROPA, 2003), and directive on priority substance 2008/105/EC of 16 December 2008 (EUROPA, 2008).

1.5.2 Environmental quality standard (EQS)

Maximum concentration limits for pollutants, called Environmental Quality Standards (EQS), have been established to protect aquatic environments and organisms in the ecosystem. Each EQS is specific to an individual substance. The toxicity of an individual substance, not necessarily the amount, determines its potential for environmental damage.

The UK EQS for TBT is amended to 2 ng L^{-1}, as a maximum concentration, through the surface waters regulations for Scotland, with similar legislation for England and Wales (SEPA, 2003). The maximum allowable concentration (MAC-EQS) of TBT in surface water has a limit of 0.0015 µg L^{-1} for the directive 2008/105/EC of the European Parliament and the Council of the European Union (EUROPA, 2008). US standard values of TBT compound are separated into acute concentration and chronic concentration. In freshwater, EQS are 0.46 and 0.063 µg L^{-1} for acute and chronic exposure respectively. In marine water, EQS are 0.37 and 0.01 µg L^{-1} for acute and chronic exposure respectively (CEFAS, 2006). Unfortunately, neither European countries nor the USA provide EQS values of TBT in soil and sediment. However, the Communication Information Resource Centre Administration (CIRCA) in Canada has set such quality standard values by calculation. These are based on the available information on toxicity to the mollusc species *Nucella lapillus* (Dog Whelk) which is most sensitive to TBT compounds. EQS values calculated from these equations are shown in Table 1.2.

Table 1.2 Specific quality standards (CIRCA, 2005)

Protection Objective	Quality Standard
Pelagic community	0.0002 μg L^{-1}
All types of surface water covered by the Water Framework Directive (WFD)	corresponding conc. in suspended matter: 0.022 μg kg^{-1} (dry wt)
Benthic community	0.0046 μg kg^{-1} wet wt
Freshwater & marine sediment	0.02 μg kg^{-1} dry wt
Predators (second. poisoning)	230 μg kg^{-1} wet wt (corresponding conc. in water: 0.038 μg L^{-1})
Food uptake by man	15.2 μg kg^{-1} seafood (wet wt) (corresponding conc. in water: 0.0025 μg L^{-1})
Abstraction of water intended for human consumption (AWIHC)	< 1 μg L^{-1}
Water intended for human consumption (WIHC)	0.1 μg L^{-1}

The IMO has called for a global convention that bans the application of TBT-based paints starting 1 January 2003, and total prohibition by 1 of January 2008 (IMO, 2002). An article in 2008 reviews the state of the science regarding TBT, with special attention paid to the environmental level, toxicity and human exposure. TBT compounds (including DBT and MBT) have been detected in a number of environmental samples (Antizar-Ladislao, 2008). The contamination levels of butyltins in selected environmental samples are presented in Table 1.3 and 1.4.

Table 1.3 Butyltins in sediments (ng-Sn g^{-1}) reported for several regions in the world (Antizar-Ladislao, 2008)

Sampling		Levels of organotin compounds		
Location	Year	MBT	DBT	TBT
American harbours and marinas				
West and east coast, Canada	1995	<d.l.-330	<d.l.-1100	<d.l.-5100
Crystal Lake, US	2001-2003	21.3-320[a]	59-350[a]	1.5-14,000[a]
Asian an Oceanian harbour and marinas				
Port of Osaka, Japan	1995-1996	<d.l.	<d.l.	10-2100
Coast, Malaysia	1997-1998	5.0-360[a,b]	3.8-310[a,b]	2.8-1100[a,b]
Great Barrier Reef World Heritage Area, Australia	1999	<d.l.-161	<d.l.-71	<d.l.-1275
Alexandria harbour, Egypt	1999	<0.1-186[c]	<0.1-379[c]	1-2076[c]
Kochi harbour, India	2000-2001	<d.l.-470[b]	n.a.	16.4-16,816[b]
Mumbai habour, India	2000-2001	<d.l.-131[b]	n.a.	4.5-1193[b]
Fishing harbours, Taiwan	2001-2004	n.a.	n.a.	2.4-8548[b]
West coast, India	2002-2003	n.a.	<d.l.-469	5-2384[b]
North coast of Kyoto, Japan	2003	4.3-22	2.3-23	1.2-19
Coast, Vietnam	2003	3.9-30	8.1-42.7	8.3-51
Sanricu coast, Japan	2005	<d.l.-3300	<d.l.-3400	2-14,000

Table 1.3 (Continued) Butyltins in sediments (ng-Sn g^{-1})

Sampling Location	Year	Levels of organotin compounds MBT	DBT	TBT
European harbours and marinas				
West coast, France	1993	25-74	9-29	7-30
River Thames, UK	1994	12-172	12-219	1-60
South west coast, Spain	1998	2.5-95	2.1-284	1.2-130
Tagus Estaury, Portugal	1998-1999	n.a.	n.a.	5.4-35[b]
Danish harbours and marinas, Denmark	1998-1999	n.a.	n.a.	100-5000[b]
North west Sicilian coast, Italy	1999-2000	<d.l.	<d.l.	3-27
North east coast, Spain	1995-2000	5-1131	47-3519	51-7673
Coast, Portugal	1999-2000	<5.2-78	<5.3-65	<3.8-12.4
North coast, Spain	2000	860-2870[a]	150-710[a]	50-5480[a]
South west, France	2000	1.0-125	<d.l.-87	<d.l.-89
Barcelona harbour, Spain	2002	35-440	67-2607	98-4702
North west coast, Spain	2005	0.7-3.8	0.5-357	0.6-303

[a] Wet weight, <d.l.: below detection limit

[b] ng organotin instead of Sn

[c] not specified whether concentration is given on basis of dry or wet weight

Table 1.4 Butyltins in biological tissue (ng-Sn g^{-1}) (Antizar-Ladislao, 2008)

Sampling Location	Year	Biological sample	Levels of organotin compounds MBT	DBT	TBT
American harbours and marinas					
Coast, Canada	1995	Mussel	<d.l.-708	<d.l.-1062	20-1198
Saint Lawrence river, Canada	1996	Mussel			<1440[a,b]
Asian an Oceanian harbour and marinas					
Japan sea, Japan	1991	Walleye pollock	<3[a]	<2.5[a]	2.2-6.4[a]
Bangladesh	1994	Fish	<5.6-170[a,b]	<0.36-15[a,b]	0.47-3[a,b]
Aomori, Japan	1996	Fish	<d.l.-20[a,b]	<d.l.-50[a,b]	<d.l.-240[a,b]
Coast, Korea	1997-1998	Vivalves	<d.l.-461	23-699	16-1610
Coast, Korea	1997-1998	Starfish	51-2860	8-139	2-323
Coast, Malaysia	1998	Fish	2.3-7.4[a,b]	<1.3-13[a,b]	2.4-190[a,b]
Aquaculture area, Taiwan	2002	Oyster	<3.3-407[a,b]	<3.9-281[a,b]	<3.8-417[a,b]
North coast of Kyoto, Japan	2003	Mussel	0.8-2.9[a]	0.8-3.1[a]	0.8-11[a]
Coast, Vietnam	2003	Clam	2.8-18	4.4-27	3.8-15
Coastline of Hong Kong, China	2004	*T. clavigera*	<d.l.-336	<d.l.-197	<d.l.-18
Coastline of Hong Kong, China	2004	*T. luteostoma*	<d.l.-51	<d.l.-85	3.8-170
Sanricu coast, Japan	2005	Mussel	4-32	3-92	3-287

Table 1.4 (Continued) Butyltins in biological tissue (ng-Sn g^{-1})

Sampling Location	Year	Biological sample	Levels of organotin compounds MBT	DBT	TBT
European harbours and marinas					
Northwestern Mediterranean, Spain	1996	Deep sea fish	<d.l.-54[a]	4.0-67[a]	1.0-52[a]
River Elbe and North Sea	1993	Fish	<d.l.-89[a,b]	<d.l.-55[a,b]	66-490[a,b]
The Netherlands	1993	Fish	23-41[a,b]	13-183[a,b]	9.2-67[a,b]
South west coast, Spain	1993-1994	Oyster	28.1±12.6	59.3±21.3	269±96
Strait between Denmark and Sweden	1997	Vivalves	2.5-15[b]	-	200-300[b]
Baltic Sea, Poland	1998	Mussel	<1.4-4.7[a]	<1.4-24[a]	2.2-39[a]
South west coast, Spain	1999	*H. trunculus*	63	85	48
Coast, Portugal	1999-2000	Mussel	<7.9-41	<2.5-18	<5.7-489
North-Western Sicilian coasts, Italy	1999-2000	*H. trunculus*	<d.l.167	<d.l.-316	<d.l.-91
West coast, Portugal	2000	Mussel	<10-605	<10-345	11-789
Aegean Sea, Greece	2001-2003	Bivalves	<d.l.-151	<d.l.-366	<d.l.-109
North west coast, Spain	2005	Oyster	0.4-12.9	7.6-441	74-193
North west coast, Spain	2005	Mussel	52.8-96.1	20.2-25.7	52.8-96

[a] Wet weight, <d.l.: below detection limit

[b] ng organotin instead of Sn

Moreover, contamination levels of butyltins were surveyed in sediment and green mussels (*Perna viridis*) from the coastal area of Thailand. The concentration levels of TBT, DBT and MBT in sediments were in the range of 2-1,246 μg kg^{-1}, 1-368 μg kg^{-1}, and 1-293 μg kg^{-1} dry wt., respectively. A higher concentration of TBT was observed in industrial areas, where many tankers and cargo ships sail and moor. The concentration levels of TBT, DBT and MBT in green mussels were in the range of 4-45 μg kg^{-1}, 4-9 μg kg^{-1}, and 8-20 μg kg^{-1} dry wt., respectively (Harino et al., 2006). From the reviewed results, the contamination levels of TBT around the world are clearly significantly. This means that TBT can adversely affect the ecosystem and living organisms present in the environment. The accumulation detected also raises a possibility of biomagnification to the top of food chain as presented in Figure 1.9. For example, TBT were determined in various body tissues of common cormorants. Among other organs and tissues, TBT levels were highly found in kidney and liver (270-290 ng g^{-1}). Moreover, the average level of TBT in cormorants were also higher than the average level in fish from the same area (Guruge et al., 1996).

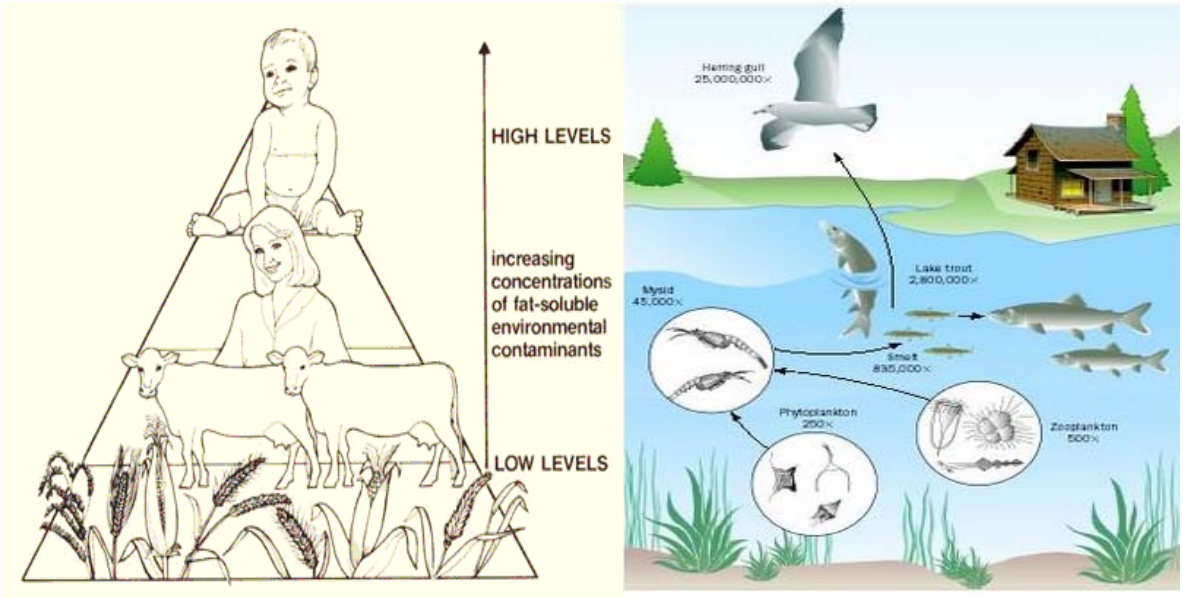

Figure 1.9 The biomagnifications of contaminants through the food chain (PRI, 2008, Stefan, 2009)

It is therefore necessary to develop improved a methods to evaluate the worldwide use of TBT and to study the environmental impact of this important pollutant. Key compounds of this work include further research on the partition behaviour of TBT, and study of its remediation/degradation process etc.

1.6 Project aims and objectives

The aims of this research are to present the sustainable management of TBT contamination in the environment. These include (i) the identification method for monitoring, (ii) using a model to predict environmental fate, and toxicity, and (iii) investigate the photo-degradation process with a view to remediation. Therefore, the objectives of this research are:

1. To develop an analysis method for organotins using HPLC
2. To optimize an extraction method of organotins from water and sediment samples suitablable with the developed analysis method
3. To monitor the organotin levels in environmental samples and compare to the EQS values
4. To study parameters that affects the partition behaviour of TBT and prediction of its environmental fate and toxicity in the aquatic environments
5. To investigate the experimental partition coefficient values and compare to the calculation values which are generated from EPISuite program
6. To study and enhance the photo-degradation of TBT contamination in aqueous samples under natural light

CHAPTER 2

Method Development and Environmental Analysis

2.1 Background

As stated in the **Chapter 1**, TBT is a persistent organic pollutant (POP), toxic and relatively resistant to environmental degradations though eventually generating the less toxic DBT and MBT. Since the significant increase in the production of TBT in the 1950s, TBT has contaminated many natural waters and sediments at concentrations that have adverse physiological effects on organisms and mammals (Antizar-Ladislao, 2008). TBT and its degradation products found in waters and sediments are a matter of growing environmental concern with many areas requiring costly determination and remediation (Maguire and Tkacz, 1985).

To determine the organotins in environmental samples, chromatography systems coupled with high sensitivity detection systems are widely used. Methods for the extraction and analysis of butyltins include, for example, sonication extraction with HCl in methanol followed by derivatized and determined with GC-quartz furnace atomic absorption spectrometry (QF-AAS) (Bowles, 2004) and extraction with tropolone and *n*-hexane followed by Grignard derivatization and determination with GC–flame photometric detection (FPD) (Caricchia et al., 1994, Gomezariza et al., 1992, Harino et al., 1992, Fent and Hunn, 1991, Muller, 1987, Hoang et al., 1982). However, this method was increasingly replaced by the less time consuming *in situ* ethylation with sodium tetraethylborate ($NaBEt_4$) and using sonication technique followed by GC–FPD, GC–atomic emission detection (AED) or GC–inductively coupled plasma mass spectrometry (ICPMS) (Moens et al., 1997, Ceulemans et al., 1994, Szpunarlobinska et al., 1993). Recently, solid-phase micro

extraction (SPME) developed by Arthur and Pawliszyn (Arthur and Pawliszyn, 1990) in combination with GC–ICPMS was applied for the analysis of $NaBEt_4$ derivatized volatile (Centineo et al., 2004, Moens et al., 1997) and semi-volatile (Vercauteren et al., 2000) butyltins in environmental samples. Moreover, with SPME the derivatized analyses were usually concentrated to the levels necessary for detection by headspace solid-phase micro extraction (HS-SPME) (Le Gac et al., 2003, Botana et al., 2002, Jiang et al., 2000, Moens et al., 1997), purge-and-trap (PT) (Reuther et al., 1999), headspace single-drop micro extraction (HDME) or liquid-phase micro-extraction (LPME) (Colombini et al., 2004, Shioji et al., 2004). These were based on the same principle as SPME but with a much higher volume of extracting phase and were applied for the determination of butyltins in environmental samples after *in situ* derivatization with $NaBEt_4$. In addition, the general extraction method for water samples was solid phase extraction (SPE): ODS(C-18) cartridges were used to extract butyltin compound from water samples (Serra and Nogueira, 2005, Gomes et al., 2003). Tripropyltin (TPT) and tricyclohexyltin (TCyT) were the most frequently used internal standards for the analysis of butyltin compounds in environmental samples (Vercauteren et al., 2001, Moens et al., 1997). It remains, however, questionable whether those compounds behave exactly the same as the target analytes and correct for all matrix interferences. More recently, isotope-labeled standards such as isotopically enriched TBT were introduced resulting in more reliable and accurate results (Colombini et al., 2004) for ICPMS detection. Bond et al., 1995, used an electrochemical technique for TBT measurement in aqueous media (Bond et al., 1995). However this was not successful for quantification when DBT and MBT were present due to polymerization reactions. For analysis using an HPLC method, there were a few reports using reverse phase systems to separate TBT, DBT and MBT with post column reaction by fluorescent detector (Ebdon and Alonso, 1987). Moreover, several normal phase HPLC was used to determine the amount of butyltins in sample using GF-AAS as the detection system (Astruc et al., 1992).

The methods above all consist of complicated sample preparation steps which are time consuming and increase the cost of analysis. They also require high

resolution detection which might not be available in some laboratories and require experienced operators.

Accordingly, this work presents an improvement of HPLC system with normal phase using simple UV/Vis detection to provide qualitative and quantitative analysis. This method omits pre-column, post-column and derivatisation steps. Previous studies using the same NPHPLC and UV methodology are available in the literature but not for environmental matrices. The disadvantages of the reported methods are that they only measure TBT and not the degradation products which limit the use of the methodology (Wang et al., 2006). Even though separation of TBT and DBT were studied by Praet, MBT was not (Praet et al., 1990). Also the conditions required iodine-chloride (ICl) on-column pretreatment which is stable for only a short period; however the main disadvantage is that this method gives only qualitative data.

Therefore the methodology described in this study is a useful and worthwhile addition to current methods of analysis for TBT and DBT, particularly due to the low cost of instrumentation. Analysis time and cost are also lower than the reported methods as derivatisation is unnecessary. This can enable more research in this field. The method described is suitable for qualitative and quantitative monitoring of contaminated sites and also for partition studies to determine environmental fate.

2.2 Experimental

2.2.1 Materials and equipments

All chemicals were used without additional purification. The analytical standards used were TBT chloride (96% purity), DBT chloride (98% purity) and MBT chloride (95% purity). Tetrabutyltin (TeBT) and triethyltin (TET) were used as internal standards for GC-MS and HPLC respectively. Tropolone (98% purity), tetrahydrofuran (THF), acetic acid and hexylmagnesium bromide solution (2*M* in diethyl ether) were obtained from Aldrich (Steinheim, Germany). The solvents hexane, methanol and ethanol were HPLC grade and obtained from Merck (Darmstadt, Germany). All reagents were of analytical grade. The PerkinElmer 785A UV/VIS HPLC system (Waltham, Massachusetts, USA) was equipped with an injection loop of 20 μL volume. All tubing in the HPLC system that came into contact with the sample was replaced by polyether ether ketone (PEEK) components. The chromatographic column was an ultra cyano column (5 μm, 250 mm x 4.6 mm i.d., Restek, UK). The GC-MS system comprised a Hewlett-Packard 5980 gas chromatograph/quadrupole mass spectrometer (Ramsey, Minnesota, USA) with a HP5 column (30 m x 0.25 mm i.d. x 0.25 μm). The UV/Vis spectrometer was carried out using a Perkin Elmer Lambda 45 UV/Vis system (Waltham, Massachusetts, USA).

2.2.2 Chromatographic separations

For the HPLC separation, firstly the absorption wavelength of butyltins was studied by UV/Vis scanning. The λ_{max} of TBT, DBT and MBT were investigated and used as the detection wavelength of HPLC UV/Vis system. From the spectra, TBT, DBT and MBT gave a maximum absorption at the same wavelength of 215 nm.

Normal phase HPLC was selected as many solvents used by RPHPLC are also absorb at this wavelength.

The separation of butyltins was optimised by varying the individual parameters e.g. the amount of tropolone and THF, pH, polarity of systematically mobile phase and the flow rate. Thus, various amounts of tropolone and THF were added into the mobile phase, hexane. The optimum quantity of added compound was then fixed and pH of the mobile phase was adjusted with concentrated acetic acid and varied from pH 2 to 7. The optimum pH was then fixed for the next variation. Ethanol, methanol and water were added to the hexane in order to increase its polarity. Finally, the flow rate was optimized. The optimised HPLC procedure was compared with a standard GC-MS method using the paired t-test at 95% confidence interval. This HPLC procedure was then used for further determinations (Miller and Miller, 2000).

Before GC-MS separation, the butyltins were derivatised with 0.5 mL 2M *n*-hexylmagnesium bromide (Grignard reagent) for 30 min under an inert atmosphere, 2M HCl was then added to stop the reaction. Anhydrous ammonium sulfate was added to remove moisture before the internal standard was added. The chemical reactions between butyltin compounds and the Grignard reagent are presented in Equations 2.1 to 2.3 (Harino et al., 1992).

$$\text{TBT, (n-butyl)}_3\text{Sn}^+ + \text{(n-hexylMgBr)} \rightarrow \text{(n-hexyl)(n-butyl)}_3\text{Sn (MW= 376)} \quad \text{(Equation 2.1)}$$

$$\text{DBT, (n-butyl)}_2\text{Sn}^{2+} + 2\text{(n-hexylMgBr)} \rightarrow \text{(n-hexyl)}_2\text{(n-butyl)}_2\text{Sn (MW= 404)} \quad \text{(Equation 2.2)}$$

$$\text{MBT, (n-butyl)Sn}^{3+} + 3\text{(n-hexylMgBr)} \rightarrow \text{(n-hexyl)}_3\text{(n-butyl)Sn (MW= 432)} \quad \text{(Equation 2.3)}$$

The GC-MS analysis employed an HP5, 30m x 0.25mm i.d., capillary column with a 0.25μm film thickness. The helium carrier gas had a flow rate of 1 ml min^{-1}. Injector and detector temperatures were held at 280 °C and 300 °C, respectively. The solvent delay was 8 min. The column oven temperature was programmed from an initial temperature of 100 °C, held for 2 min, to a final temperature of 300 °C at a rate of 15 °C min^{-1}, and held for 10 min. Sample injection was splitless for 1 min and followed by a split mode. The EI mass spectrometer was used in full scan mode. The detector acquisition method was employed for monitoring of TBT, DBT and MBT between m/z 105 and 390. The injection of each derivatised solution was in triplicate (n=3). Peak areas and mass spectra (Total Ion Chromatogram, TIC) were recorded. The average peak areas were plotted against solution concentration for standard solution to provide the calibration graph.

2.2.3 Extraction of butyltins

For spiked water sample preparation, 1,000 μg mL^{-1} stock solutions of TBT, DBT and MBT were prepared separately in methanol. From the stock solutions, a 100 μg mL^{-1} working solution was prepared in Nanopure water. Mixed standards 5-50 μg mL^{-1} were prepared in Nanopure water for method validation. A 30 mL aliquot of the sample solution was extracted into hexane by shaking 3 times with 10 mL of hexane in total at 350 rpm for 30 minutes. The organic phases collected from each step were mixed into one portion then evaporated close to dryness on a heating block (20 ^{o}C) under N_2. The internal standard was added to the evaporated sample and the volume adjusted with hexane. The extracted solutions were analysed by HPLC.

The extraction efficiency was improved by systematically varying individual parameters e.g. the amount of tropolone, pH and the amount of salt. Thus, selected amounts of tropolone were added into the extracting solvent, hexane. The optimised quantity of tropolone was employed for the next variation. The pH of water samples were adjusted with concentrated HCl from a pH of 1 to 6. The optimal extraction pH

was obtained. For the affect of ionic strength, selected amount of sodium chloride was added into a water sample containing optimal amount of acid. Optimisation of the extraction efficiency was confirmed by GC-MS.

The conditions optimised for water samples were adjusted by increasing the amount of tropolone for sediment samples. A 0.5% solution of tropolone in hexane was used. A 5 g (dry weight) sample of sediment was used to extract and quantify the contamination level of TBT. For the certified reference material (CRM): BCR-646, 5 g (dry weight) was used to determine the extraction efficiency of butyltin in the sediment. All experiments were performed in triplicate (n=3).

2.2.4 Sample collection

Sediment and water samples were collected from two potentially polluted areas. The samples were collected in March 2007 and 2008 at Bowling Basin and Port Dundas, Glasgow, UK. A map of the sampling sites is shown in Figure 2.1.

Figure 2.1 Map showing sampling sites in the Forth and Clyde canal; (a) Bowling Basin, and (b) Port Dundas (GoogleMap, 2009)

In the past, the sites were part of a main canal waterway between the west and east coast of Scotland. While boat activity is still present at Bowling Basin, Port Dundas has been inactive for many years and is no longer part of the canal network (Figure 2.2).

Figure 2.2 Photo showing the boat activity in the Forth and Clyde canal; (a) Bowling Basin, and (b) Port Dundas

Samples collected from the two sites were used to assess the persistence of butyltins in the environment. Sampling followed the ASTM: D6232-00 method (ASTM, 2001). All sediment samples were collected from the top 15 cm of the surface layer using a dredge sampler and sieved through 2 mm before storage in

polyethylene bags (Figure 2.3). Surface water samples were collected and stored in polypropylene bottles. The samples were kept refrigerated and analyzed within 3 days.

Figure 2.3 Surface sediment sampling using a dredge sampler

2.3 Results and discussion

2.3.1 Determination of butyltins by HPLC

Figure 2.4 shows the UV/Vis spectra of butyltins. From the spectra, TBT, DBT and MBT each gave a maximum absorption at the same wavelength of 215 nm which was subsequently used for butyltins analysis.

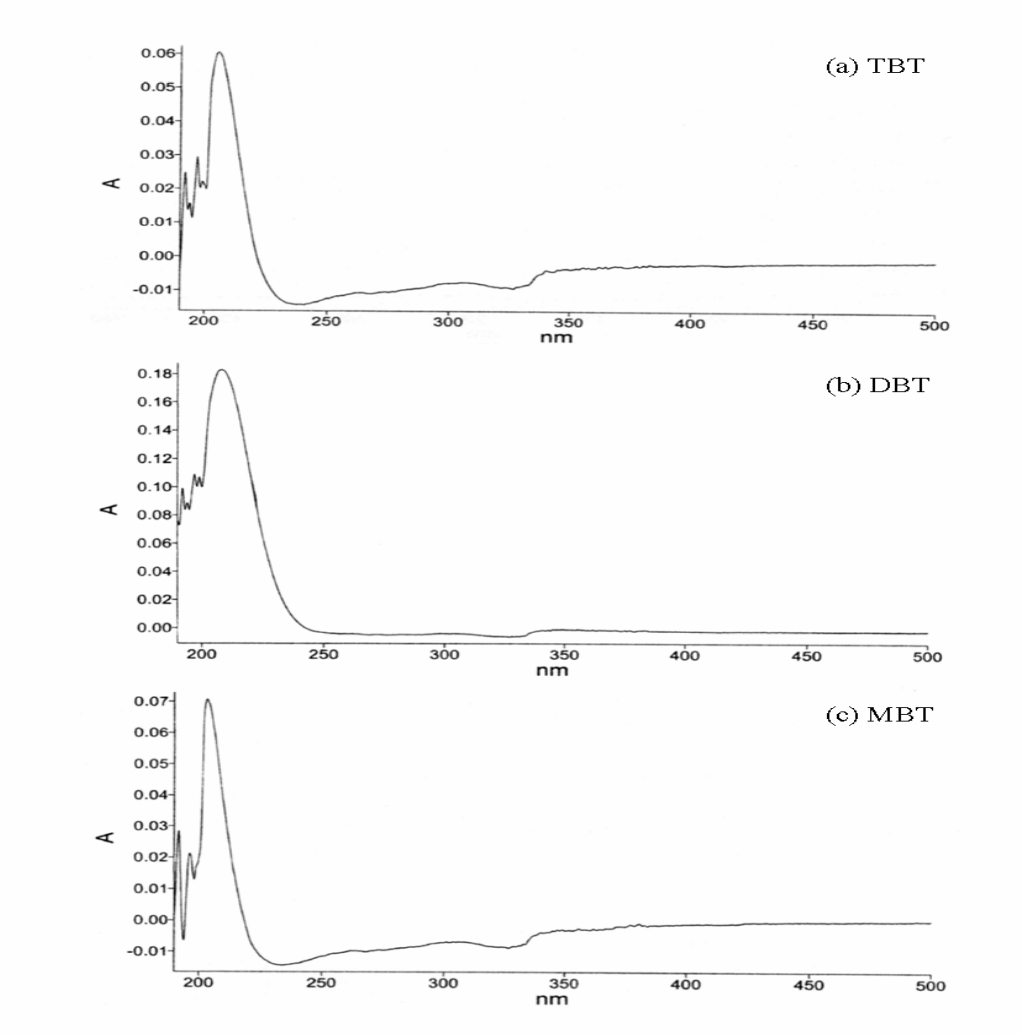

Figure 2.4 The UV/Vis spectra of TBT, DBT and MBT using hexane as reference

The amount of tropolone was varied from 5 to 50 mg L^{-1} of hexane at a flow rate 1 mL min^{-1} to optimise the HPLC separation of butyltins. The structure of tropolone is shown in Figure 2.5(a).

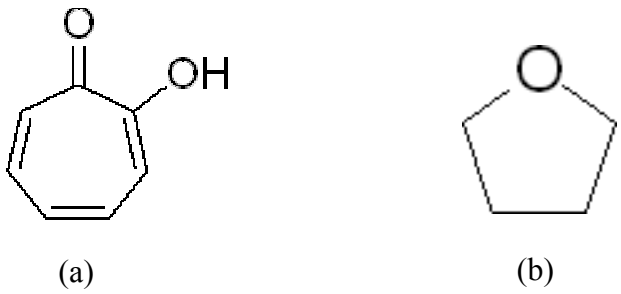

(a) (b)

Figure 2.5 The chemical structure of (a) tropolone, and (b) tetrahydrofuran

It was found that tropolone rapidly forms a stable complex with MBT and DBT cations but not TBT. Therefore, it has no effect on the elution of TBT (Astruc et al., 1992). The stoichiometry of the tropolone complex was ML_2 for MBT and ML for DBT, where M is MBT or DBT and L is tropolone. The complex formation reduces the effective positive charge of butyltin compounds which can enhance elution from the column. Thus, the presence of tropolone in the mobile phase helped elute DBT from the column. Since triply charged MBT binds strongly with the cyano group of the HPLC column, tropolone does not improve the elution of MBT.

Unfortunately, the mobile phase containing tropolone cannot be left overnight in contact with the column and detector as it degrades and produces a brown residue which contaminates the system. From this reason, tetrahydrofuran (THF) (Figure 2.5(b)) was selected to replace tropolone in improving the HPLC separation as it has an oxygen donor in the molecule and similar polarity to tropolone. The amount of THF in the mobile phase was varied systematically from 1 to 20% (v/v) at a flow rate 1 mL min^{-1}. The effect of THF on the chromatographic separation is shown in Figure 2.6(a).

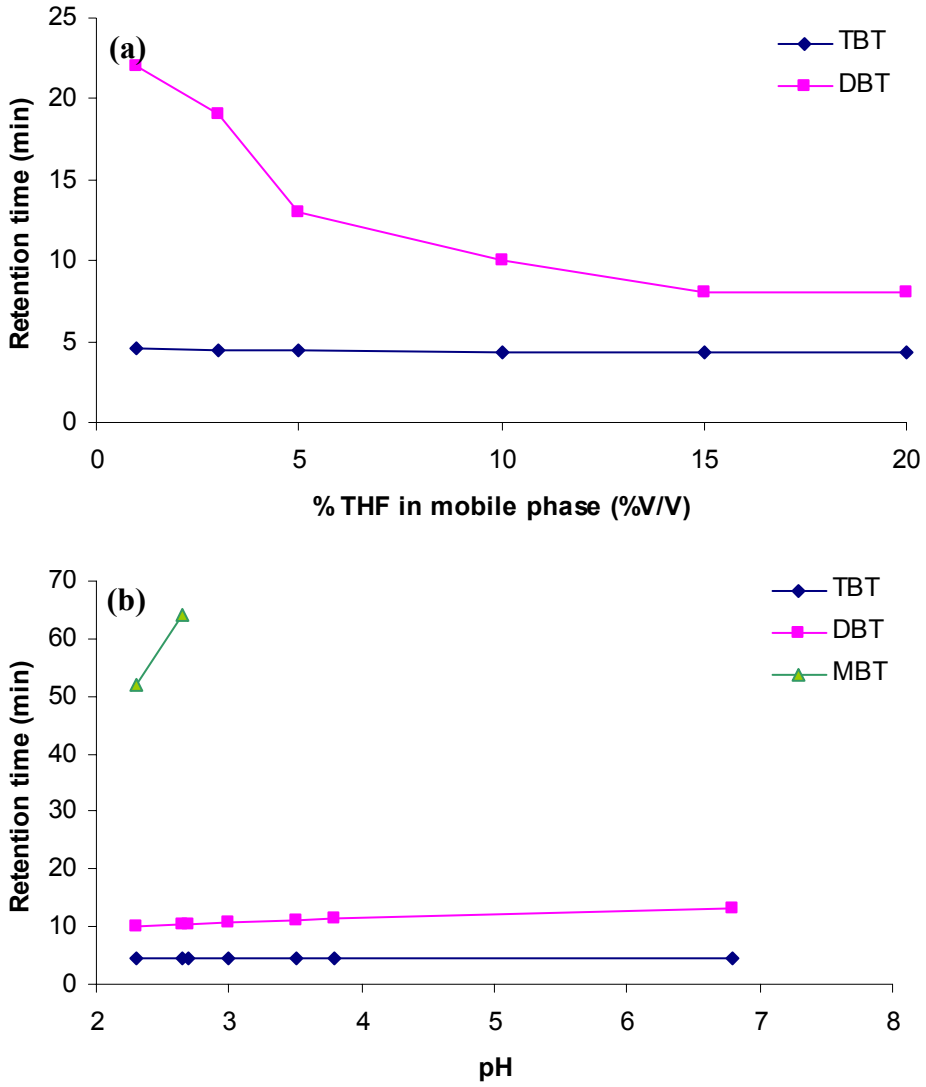

Figure 2.6 The separation of butyltins (a) effect of THF, and (b) effect of pH

The results show that THF contained in the mobile phase gave the same efficiency as tropolone and can therefore be used to improve the separation. The amount of THF which is suitable for the separation is 5% in mobile phase, due to higher amounts of THF increasing the baseline at 215 nm. However, a mobile phase containing THF still cannot aid the elution of MBT from the column. Therefore, other parameters which increase separation were considered.

The results of the addition of acid to the mobile phase at a flow rate of 1 mL min^{-1} are presented in Figure 2.6(b). The Figure shows that the mobile phase containing acid assists the elution of butyltins; protons (H^+) bind with the cyano-groups (CN) in the column and release butyltins. pH 3 was chosen for optimum separation. However, MBT cannot be eluted at pH 3 due to the strong interaction between MBT and the cyano-group. At pH lower than 3, MBT was eluted but gave an unsatisfactory peak shape and also the pH is below the column recommended limit (pH 2.5) which may damage the column.

Previous studies using a cyanopropyl-bonded silica column increased the elution strength of the mobile phase (toluene) for di-substituted tin compounds (Langseth, 1984) by adding of methanol varying from 1-5%. Therefore, the polarity of the mobile phase was studied by adding polar solvent e.g. 1% ethanol, 1% methanol and 4% water respectively. It was found that high polarity of the mobile phase increased the retention time of butyltins (Appendix Table A1) and also the added solvent gave a very high background at the absorption wavelength of 215 nm. Consequently, the adjustment of polarity could not be used to improve the separations.

The flow rate of mobile phase was varied from 0.05 to 1 mL min^{-1}. Increasing the flow rate improved the elution of organotins from the column but reduced the absorption signal thereby affecting the sensitivity of the system. The optimum flow rate was found to be 0.8 mL min^{-1}. Figure 2.7 shows a typical chromatogram obtained from the optimised procedure (isocratic mode) at 0.8 mL min^{-1} using a cyanopropyl column with a mobile phase of hexane containing 5% THF and 0.03% acetic acid.

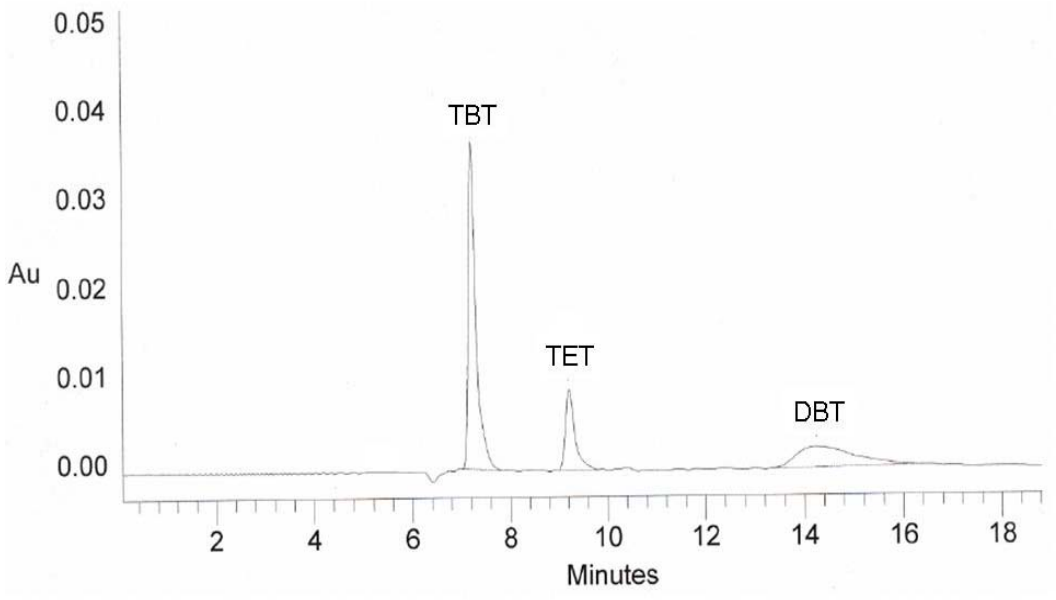

Figure 2.7 The chromatogram of butyltins by NPHPLC (triethyltin (TET): internal standard)

This developed HPLC technique was compared with the standard GC-MS method using the paired t-test method at the 95% confidence limit. 10 samples of various concentrations of TBT (5, 10, 15, 20, 25, 30, 35, 40, 45 and 50 μg mL^{-1}) were analysed by both techniques (Figure 2.8).

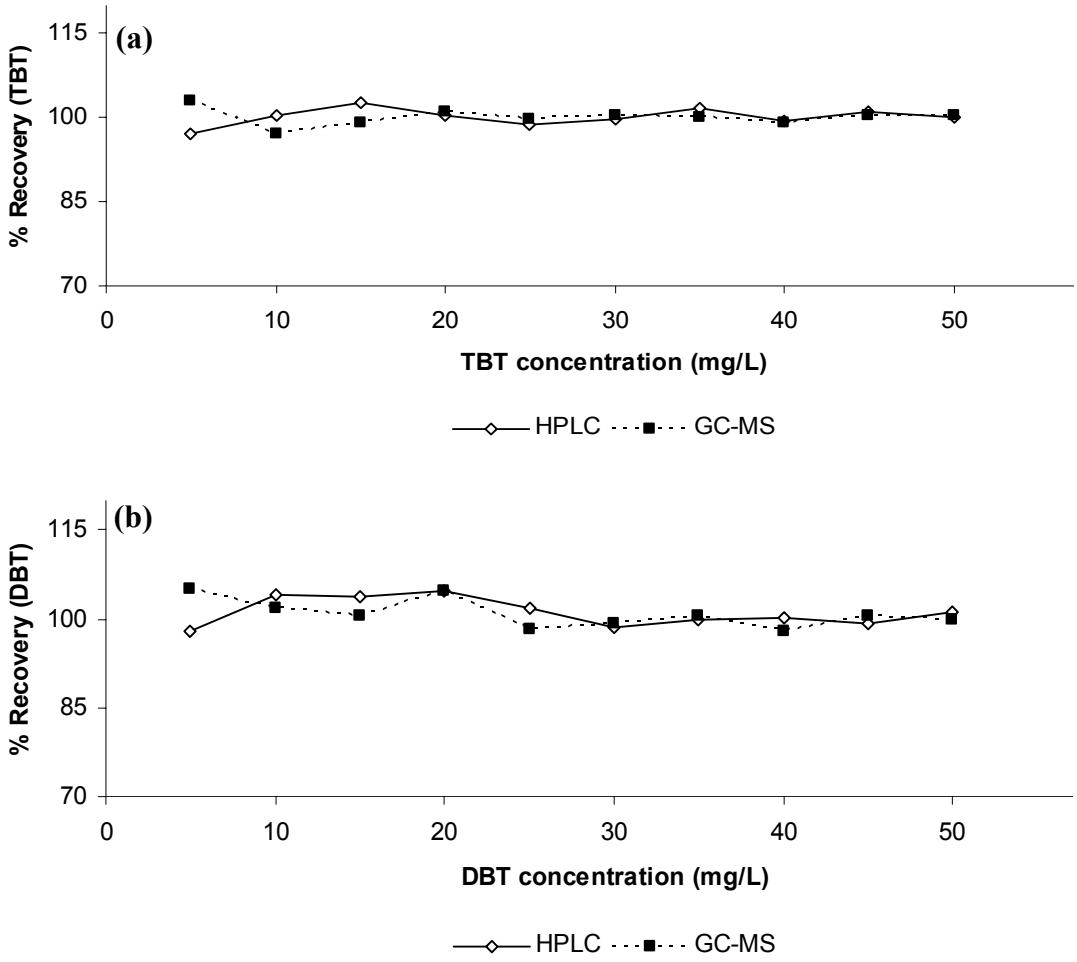

Figure 2.8 The comparison of % recovery between NPHPLC and GC-MS (a) TBT, and (b) DBT

Calculation (Appendix Table A2) showed the statistic value (0.778) to be less than the t-distribution (2.26) for TBT. Therefore, the analytical results of TBT in the samples were not significantly different between the HPLC and GC-MS. Moreover, the validation result of DBT between two techniques was successfully proved (Appendix Table A3).

From the standard GC-MS technique, the qualitative and quantitative analyses of butyltins were examined. The total ion chromatogram (TIC) and mass spectra of butyltins by GC-MS are presented in Figures 2.9 to 2.10.

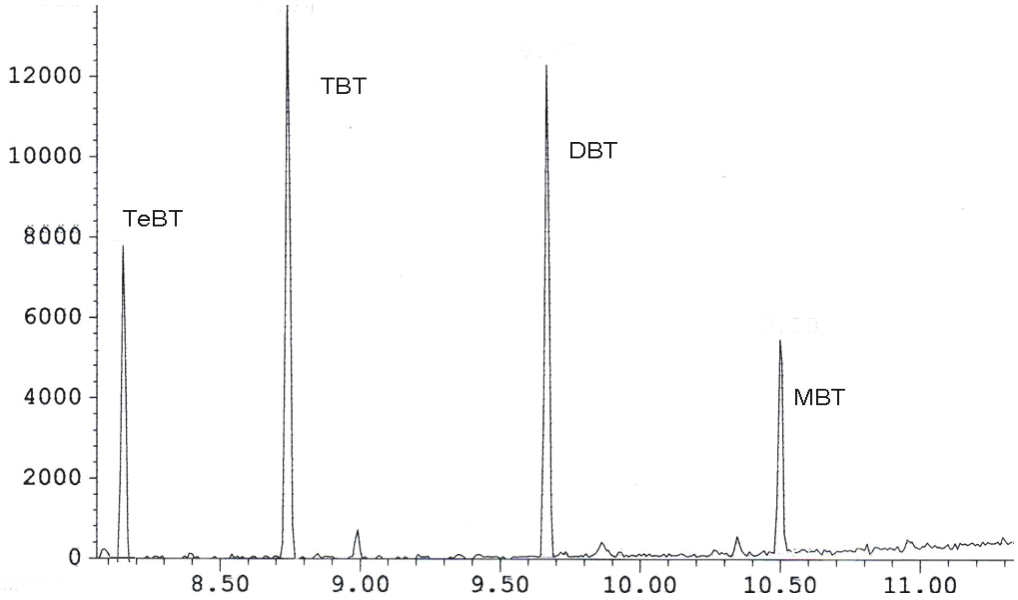

Figure 2.9 The total ion chromatogram of butyltins by GC-MS (TeBT: internal standard)

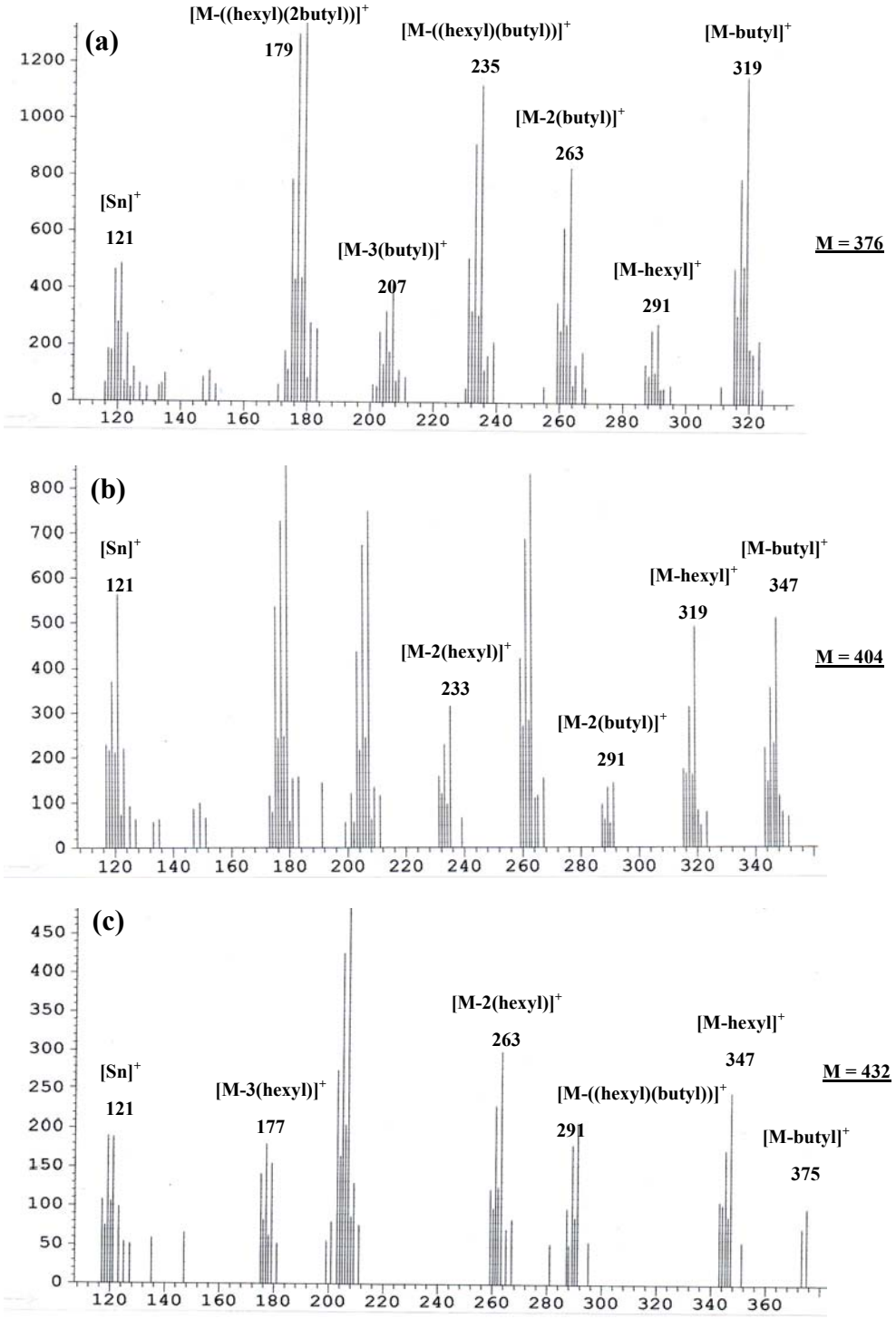

Figure 2.10 The positive EI mass spectra of butyltins by GC-MS: (a) TBT, (b) DBT and (c) MBT

From the chromatogram, the regression line and detection limit (LOD) of both techniques were produced by varying the concentration of butyltins. These are presented in Table 2.1. The calculations of the LOD for butyltins are presented in Appendix Tables A4 to A8 (Miller and Miller, 2000).

Table 2.1 The regression line and detection limit HPLC and GC-MS

Butyltins	HPLC/UV-Vis		GC-MS	
	Regression line	LOD ($\mu g\ mL^{-1}$)	Regression line	LOD ($\mu g\ mL^{-1}$)
TBT	$R^2 = 0.9998$, Y = 815.44X+ 35.999	0.71	$R^2 = 0.9977$, Y = 182908X + 148765	1.03
DBT	$R^2 = 0.997$, Y = 1531.6X+808.44	0.50	$R^2 = 0.9967$, Y = 186909X + 116133	1.24
MBT	N/A	N/A	$R^2 = 0.9932$, Y = 183376X - 41614	2.22

Table 2.1 shows that the detection limit of the developed HPLC system is slightly better than the standard GC-MS system. This developed HPLC method was then used to determine the levels of TBT and DBT in environmental samples.

2.3.2 Extraction of butyltins

The extraction of TBT and DBT in spiked samples using hexane as the extractant showed good reproducibility. Extraction gave 79.5% and 12.3% recovery for TBT and DBT, respectively. As a result of the poor DBT recovery, tropolone was added to improve the extraction. The results are shown in Figure 2.11(a).

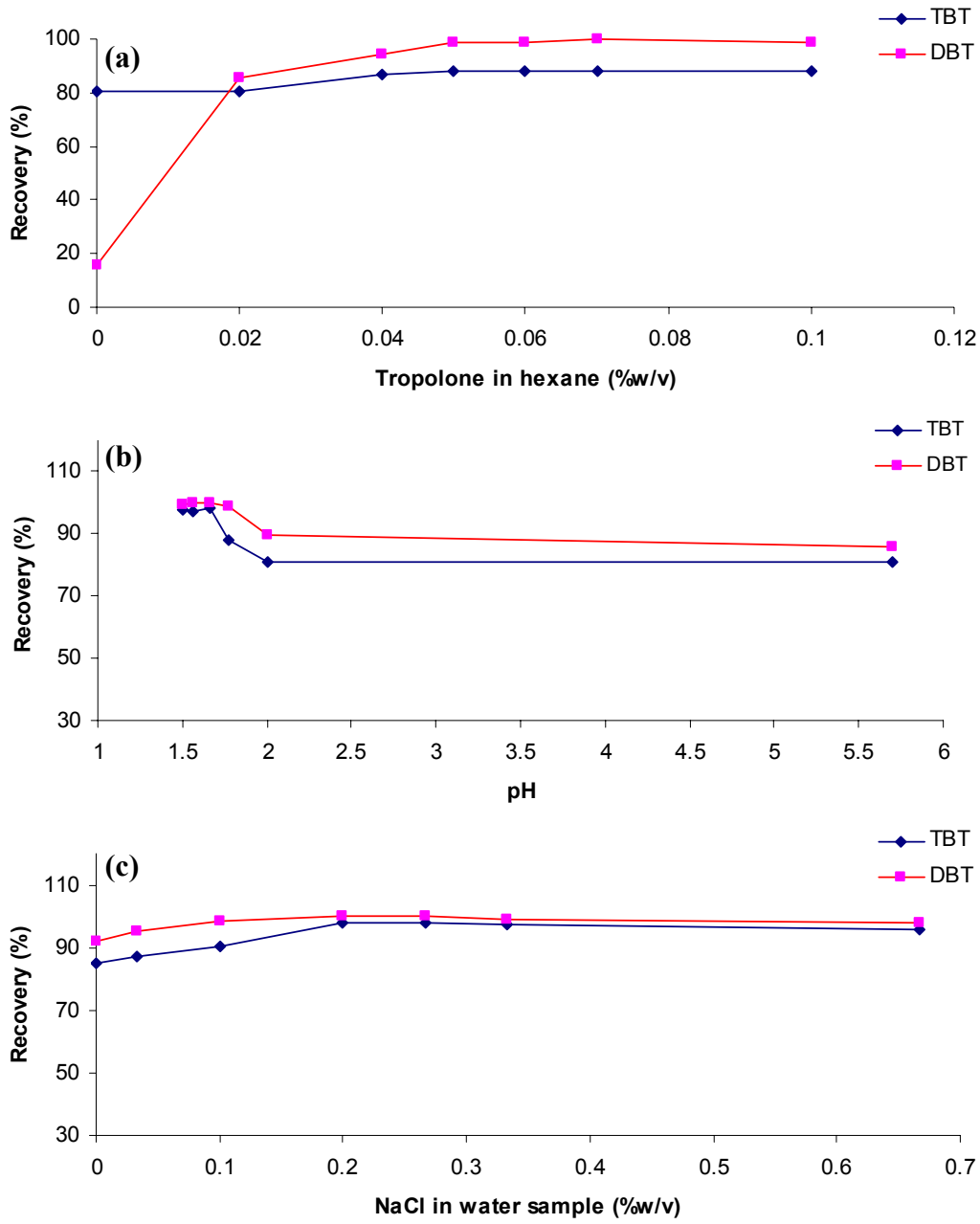

Figure 2.11 The recoveries of TBT and DBT (a) at different concentrations of tropolone in hexane, (b) at various pH, and (c) with different amounts of sodium chloride in water samples

From Figure 2.11(a), it is clear that tropolone enhanced the extraction efficiency of both compounds. Formation of butyltins-tropolone complexes could reduce the effective positive charge and water solubility of butyltin compounds thereby leading to increased preference of butyltins for the organic phase, thus increasing the recoveries of DBT in the water sample from 15.4% to 100%. Although tropolone does not form a complex with tributyltin, its recovery slightly increased from 80.3 to 88.3%. Tropolone may form an ion-dipole interaction with TBT that can increase the passage of TBT into hexane. From Figure 2.11(a), 0.05% of tropolone in hexane was found to be the optimum concentration for extraction.

Figure 2.11(b) shows the effect of pH of the water samples on extraction. pH below 1.70 improved the recovery for both TBT and DBT compared to higher pH. The addition of acid also preserved the sample by preventing hydrolysis and keeping the compounds in the cationic form. However under conditions of extremely low pH, the acid may break tin-carbon bonds and reduce the actual amount of butyltin compounds. Therefore, the pH of the samples was carefully controlled below 1.7.

Sodium chloride increases the ionic strength of water, and reduces the solubility of butyltin in water. These are salting out effects, which force butyltin compounds to transfer into the organic phase (Rydberg, 2004). From the results as shown in Figure 2.11(c), gradual improvement of extraction was found after addition of sodium chloride. At 0.2% NaCl in the water sample, the optimum extraction was obtained. Recoveries increased from 85.1% to 98.1% for TBT and from 92.2% to 98.9% for DBT.

Accordingly, the optimum conditions for the extraction of analytes from water samples had the addition of 0.2% NaCl at pH 1.7 and extraction by hexane containing 0.05% tropolone. Moreover, these extraction conditions were confirmed by GC-MS as shown in Figure 2.12.

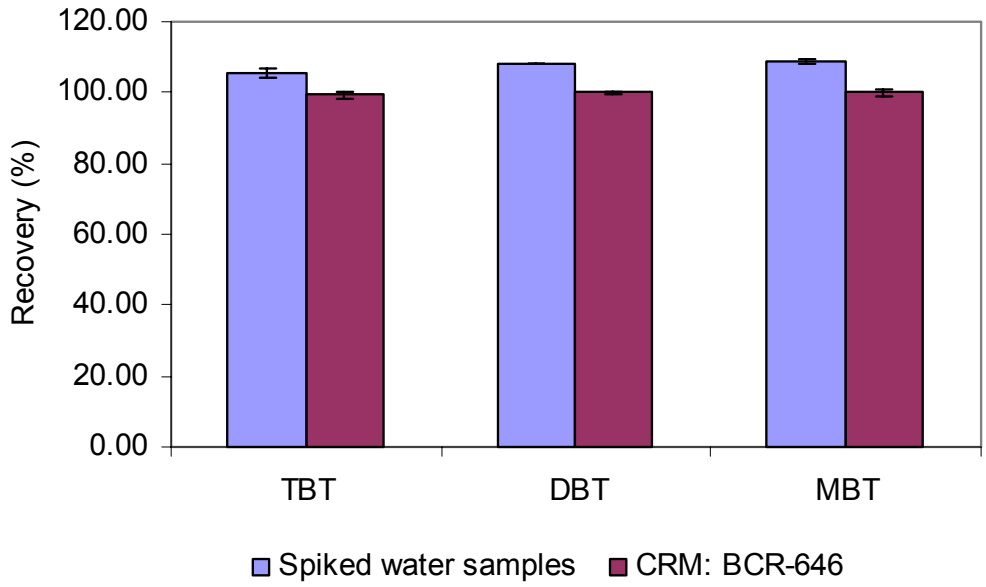

Figure 2.12 The recoveries of butyltins using GC-MS from water samples and CRM: BCR-646

The recoveries for spiked water samples ranged from 105-109% at a precision of 1.0, 0.26 and 0.46% RSD for TBT, DBT and MBT, respectively. Even though the extraction procedure for MBT in water samples has yet to be optimised the results imply the applicability of the extraction method to MBT. The optimized conditions for water extraction were slightly adapted for sediment samples. The amount of tropolone in hexane was increased to 0.5% w/v due to the more complicated matrix of the sediment. The CRM (BCR-646) containing 480 µg kg^{-1} TBT, 770 µg kg^{-1} DBT, and 610 µg kg^{-1} MBT was analyzed using the optimum conditions and the results are shown in Figure 2.12. The recoveries ranged from 99.0 to 101% at precisions of 1.17, 0.32 and 0.97% RSD for TBT, DBT and MBT, respectively.

The contamination of TBT and butyltins in the samples collected from Bowling Basin and Port Dundas in 2007 and 2008 are shown in Tables 2.2 and 2.3.

Table 2.2 Levels of TBT in samples using the optimised HPLC and extraction procedure (n=3)

Sampling site	sediment (μg kg^{-1}) ± %RSD		water (μg L^{-1}) ± %RSD	
	2007	2008	2007	2008
Bowling Basin	162 ± 0.1	125±0.8	0.85±4.8	0.31±4.1
	(35,217)*	(27,174)*	(4,250)*	(1,550)*
Port Dundas	149±0.5	75.5±0.4	0.17±1.7	0.16±2.3
	(32,391)*	(16,413)*	(850)*	(800)*

BDL: Below detection limit of determination method employed the conditions

* Number of times higher than EQS values

Table 2.3 Levels of butyltin compounds in samples (March, 2007 and 2008) using GC-MS and the optimised extraction method (n=3)

Sampling site, year	sediment (μg kg^{-1}) ± %RSD			water (μg L^{-1}) ± %RSD		
	TBT	DBT	MBT	TBT	DBT	MBT
Bowling Basin, 2007	154±0.3	BDL	BDL	0.84±5.3	1.13±5.3	2.16±1.0
Bowling Basin, 2008	123±4.4	4.56±2.3	BDL	0.29±6.4	0.19±4.9	0.83±2.1
Port Dundas, 2007	141±0.3	104±0.4	148±0.7	0.16±2.0	0.19±2.0	10.2±1.1
Port Dundas, 2008	78.4±6.9	75.7±6.2	211±0.7	0.16±6.1	0.18±7.1	0.96±4.5

BDL: Below detection limit of determination method employed

Tables 2.3 and 2.4 show the similar amount of TBT between developed HPLC and GC-MS. Comparison of the contamination by TBT (Table 2.2) to the EQS; 0.0046 μg kg^{-1} for surface sediment and 0.0002 μg L^{-1} for pelagic communities (*see Table 1.2*) (CIRCA, 2005, WFD, 2005); shows contamination by TBT of both sampling sites to be very significantly higher than the EQS values. This means that contamination by TBT can adversely affect the ecosystem, in particular living organisms present in the environment. The accumulation detected also raises the possibility of biomagnification at the top of the food chain. Moreover, Port Dundas where there has been no activity for many years is still highly contaminated,

confirming that butyltins are highly persistent organic pollutant (POP). Due to the high concentrations found in both water and sediment, it was decided to investigate the partition coefficients of TBT in order to assess the environmental fate and understand the adsorption behaviour of this toxic compound more accurately **(Chapter 3)**.

2.4 Summary

For the effective monitoring of butyltin compounds especially TBT in the environment, it was necessary to establish an economic and simple analytical method to determine levels which included an appropriate extraction method. This study developed a normal phase HPLC method with a UV/Vis detector and also optimised the extraction conditions for water and sediment samples. The advantages of the procedure are the low cost of instrumentation, shorter time consumed and the cost-saving as no derivatisation is necessary. The overall technical operation requirements are lower for HPLC than GC-MS. The developed method was optimised to separate tributyltin (TBT), dibutyltin (DBT) and monobutyltin (MBT). The separation was performed in the isocratic mode on an ultra cyanopropyl column with a mobile phase of hexane containing 5% THF and 0.03% acetic acid. This method was validated using a standard GC-MS technique and verified by the statistical paired t-test method. Under the experimental conditions used, the limit of detection (LOD) of TBT and DBT were 0.70 and 0.50 μg mL^{-1}, respectively. The optimised extraction method for butyltins in water and sediment samples used hexane containing 0.05-0.5% tropolone and 0.2% sodium chloride in water at pH 1.7. The quantitative extraction of butyltin compounds in a certified reference material (BCR-646) and in naturally contaminated samples was achieved with recoveries ranging from 95 to108% and at a % RSD 0.02-1.00%. This HPLC method and optimised extraction conditions were used to determine the contamination of butyltins in environmental samples collected from the Forth and Clyde canal, Scotland, UK. The values obtained severely exceeded the Environmental Quality Standard (EQS) values.

As shown in Table 1.2-1.4 (**Chapter 1**), TBT is a global problem, therefore low cost methods requiring less technical expertise couple with faster analysis will allow more research to be done particularly in developing countries. Moreover, this also opens the field for further research. The method developed gives detection limits similar to GC-MS and is suitable for a range of environmental samples. The procedure can be use to study partition behaviour **(Chapter 3)** which is mainly concerned with contaminated water and sediments.

CHAPTER 3

The Partition Behaviour and Prediction of Environmental Fate and Toxicity of Tributyltin

3.1 Background

3.1.1 Distribution of TBT

As previously mentioned in **Chapters 1&2**, tributyltin compounds were used for various applications such as stabilizers for polyvinyl chloride, plastic additives, insecticides, fungicides, bactericides, and wood preservatives and as constituents in antifouling paints. Consequently, the usage of TBT and its derivatives has drawn concern about the potential damage to organisms and mammals in ecosystems. The distribution of TBT considered below is therefore necessary.

3.1.1.1 TBT in aquatic systems

In natural water, TBT compounds are present predominantly as tributyltin hydroxide species or tributyltin cation depending on the pH value. At pH 8, the average pH of seawater, major species of TBT are tributyltin hydroxide and tributyltin carbonate (Champ and Seligman, 1996). The levels of TBT in aquatic systems are greater in regions with high shipping, harbours and shipyards. The release of TBT from antifouling paint raises the TBT concentration of water, sediment and biota in waterways. Besides antifouling paint, TBT has been detected in municipal waste water and sewage sludge (Fent and Muller, 1991). The degree of

tidal flushing and the turbidity of the water also influence TBT concentrations (Anderson et al., 2002).

3.1.1.2 TBT in sediments and soils

In the aquatic environment, TBT has low aqueous solubility and low mobility, thus it is easily adsorbed onto suspended particulate matter (SPM). TBT is retained on the sediment surface and persists within the sediment column over a long period of time (Quevauviller et al., 1994). The presence of TBT on suspended matter or sediment available for sediment-feeding organisms leads to biomagnification. The re-suspension of particles and remobilisation of pollutants by dredging will cause re-contamination in aquatic systems. The contamination levels of TBT are significant in sediment around the world, which affect organisms (Antizar-Ladislao, 2008). TBT can contaminate land soil by the dredging and land-filling of contaminated sediments, leaching of landfill and disposal of contaminated waste (Loch et al., 1990).

3.1.1.3 TBT in organisms

Due to the low water solubility of TBT and its lipophilic properties, it is preferentially adsorbed on particle surfaces and accumulates in organisms. TBT tends to concentrate within the liver, kidney and muscles of animals (Berge et al., 2004). Because of high concentrations of TBT in aquatic organisms, accumulation in higher predators can lead to biomagnification (Guruge et al., 1996). For humans, exposure to TBT is considerably low through the consumption of food (Takahashi et al., 1999, Forsyth et al., 1994). Direct exposure to humans is most common in workers who often have contact with the substance. The human exposure pathways of TBT are shown in Figure 3.1.

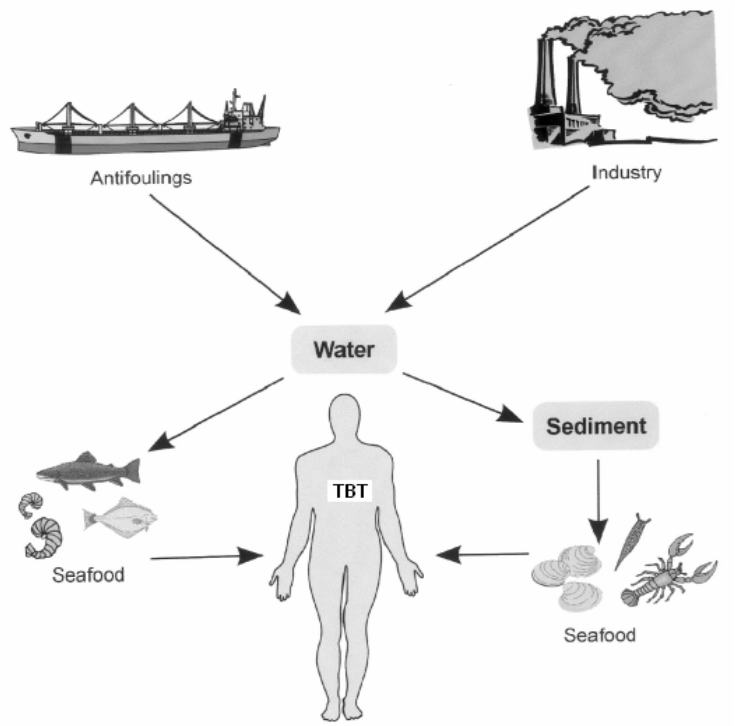

Figure 3.1 General sources of TBT for human exposure (Hoch, 2001)

3.1.1.4 TBT in air

A USEPA report presented a low Henry's law constant for butyltins, in the range of 10^{-5} to 10^{-6} atm m^3 mol^{-1} and also suggested a high boiling point (EPA, 2008). These values represent the low volatilization behaviour of these species (Baun et al., 2006). Only a few research studies in the last two decades have presented the volatilization of butyltins into the air phase (Saint-Louis and Pelletier, 2004). The results showed a considerably low rate (20-510 nmol m^{-2} $year^{-1}$) of emission to air of volatile organotins from TBT contaminated waters.

3.1.2 Fate, transport and transformation of TBT

Determination of the environmental fate of TBT gives an indication of the likely extent of environmental exposure to this chemical once it enters the environment, for example TBT exposure levels for non-target organisms. Evaluation of the data makes it practicable to determine the behaviour of a TBT in difference media (soil & sediment, water and air), the possibility for its uptake by plants or animals, and the potential for bioaccumulation in organisms. Environmental fate is considered in terms of the following.

- the partitioning of TBT between environmental media
- the transport properties of the media
- the transformation rate of TBT into other forms

The tendency of TBT to partition to a particular part of the environment can be estimated from the physical and chemical properties of the substance. The transportation of TBT depends on the transport properties of the medium into which the substance is released or partitions. It also depends on the TBT lifetime in the medium. Transformation describes the TBT lifetime in the environment with respect to degradation to less toxic forms (DBT, MBT and tin). Environmental transformation is highly dependent on the medium. In air, transformation is by abiotic chemical reactions, while in soil and water, biodegradation may predominate. TBT, which is reported to be a persistent organic pollutant, will build to higher concentrations and might become more widely distributed.

Due to low water solubility of TBT and other properties, it will bind strongly to suspended material such as organic matter or inorganic sediments (Clarkson, 1991) and precipitate to the bottom sediment (Short, 1986). Rates of sedimentation vary with location, organic content, particle size, and type of material. Reported half-lives

of the compound in freshwater are up to a month; in seawater and estuarine locations, it is 1 to 34 weeks, depending on the initial concentration (Clark et al., 1988). Because of the low levels of UV light beyond the topmost few centimetres, it is unlikely that photolysis by natural light plays a major role in degradation of TBT compounds (Clark et al., 1988). Degradation depends on temperature and the presence of microorganisms. Under aerobic conditions, TBT takes one to three months to degrade. But in anaerobic soils, this compound can persist for more than two years (Short, 1986). Previous data concerning the environmental fate have been presented on effect of TBT on the environment (Konstantinou and Albanis, 2004), biological effects (Thomas et al., 2001), environmental risks (Jacobson and Willingham, 2000) and also accumulation (Gadd, 2000).

3.1.3 Environmental modelling and adsorption behaviour

TBT is one of the most toxic anthropogenic compounds deliberately introduced into the aquatic environment. It has a relatively high affinity for particulate matter, providing a direct and potentially persistent route of entry into benthic sediments. To understand TBT behaviour in the aquatic environment, computational programs are an exceptionally helpful tool for modelling and prediction. In this work, the EPISuite program (V 4.0) was used for evaluation of the prediction data (modelling) including fate and toxicity from the partition coefficient values. Therefore, technical terms involved and supporting theory are described.

3.1.3.1 Fugacity and partition coefficients

The concept of fugacity was first introduced by G.N. Lewis in 1901 as a more convenient thermodynamic equilibrium than chemical potential (Mackay, 2001). The term fugacity comes from the Latin root *fugere*, describing a “fleeing” or “escaping” tendency. Therefore, fugacity is the measure of the escaping tendency of a chemical. It is identical to partial pressure in ideal gases and is logarithmically related to

chemical potential, the units of energy mole^{-1}. It is thus linearly or nearly linearly related to the concentration. The absolute values can be established because, at low partial pressures under ideal conditions, fugacity and partial pressure become equal. Thus, it is possible to replace the equilibrium criterion of chemical potential by that of fugacity. Fugacity has the units of pressure, Pascal (Pa), and is basically described as being the tendency for a given substance to move from one environmental compartment to another. The term is defined by thermodynamics and was originally applied to the tendency of a gas to expand or escape from a system and is related thus to the pressure of the system. It is also the subject of a book by Donald MacKay (Mackay, 2001), which gives a very in-depth explanation of the theory involved. A brief explanation of fugacity theory is presented below; other resources should be read if more in-depth explanation is needed.

From the properties of solutes (chemical substances) in solution, any chemical when at equilibrium in the environment exists at different concentrations in all the different environmental phases. It can be shown that partitioning within a system can be expressed by equating the chemical potential of the substance in each phase. The equilibrium is achieved between two phases when their "escaping tendencies" and hence fugacity exactly match one another (Mackay, 2001). For example if the five environmental compartments of atmosphere, soil, water, sediment and aquatic biota are considered as phases the following diagram represents their interactions (Figure 3.2).

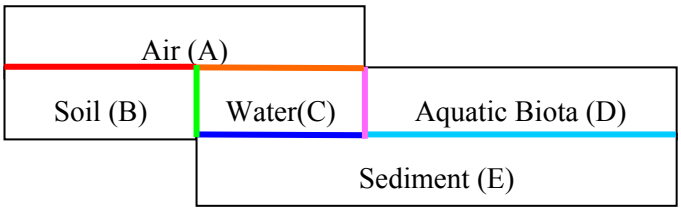

Figure 3.2 Interactions between five environmental compartments

If all 5 phases are at equilibrium it stands true that their fugacity (f) is similar. This can be expressed by the following equation (Mackay and Paterson, 1981).

$$f_A = f_B = f_C = f_D = f_E \qquad \text{(Equation 3.1)}$$

Fugacity is assumed to be linearly proportional to the concentration (C, mol m^{-3}) through a proportionality constant (Z), termed the fugacity capacity, and is measured in mol Pa^{-1} m^{-3}. The Z value is defined by the nature of the chemical and the properties of the medium it is present in, but will also vary with ambient temperature and pressure. It follows that;

$$C = Zf \qquad \text{(Equation 3.2)}$$

Hence if $f_a = f_b$ (4.1), then;

$$C_A/Z_A = C_B/Z_B \qquad \text{(Equation 3.3)}$$

Therefore,

$$C_A/C_B = Z_A/Z_B = K_{AB} \qquad \text{(Equation 3.4)}$$

Where, K_{AB} is a dimensionless partition coefficient which controls the partitioning of the chemical between the two phases (in this case A and B) and is in effect the ratio of the fugacity capacities. In Figure 3.2, each different coloured line represents a different partition coefficient between each phase. The value of Z is deduced using these partition coefficients. In the beginning, Z is first defined in the air and then progresses to other media. The definitions of Z values are shown in Table 3.1.

Table 3.1 The definitions of Z values for each compartment (Mackay, 2001)

Compartment	Definition of Z (mol m^{-3} Pa^{-1})	Definition of terms
Air	$Z_A = 1/RT$	R = 8.314 (Pa m^3 mol^{-1} K^{-1})
		T = temperature in K
		K_{AW} = air/water partition coefficient
Water	$Z_W = 1/H$ or C^S/P^S	H = Henry's law constant (Pa m^3 mol^{-1})
		C^S = aqueous solubility (mol m^{-3})
		P^S = vapor pressure (Pa)
Solid sorbent	$Z_S = K_{SW}P_S/H$	K_{SW} = partition coefficient (L kg^{-1}) = Z_S/Z_W
		P_S = phase density (kg L^{-1})

In fugacity modelling no attempt is made to determine absolute data relating to the environment. Instead an attempt is made at defining relative partitioning into each environmental phase, the dominant reactions involved, transport processes involved and overall persistence within the environment. This allows an evaluation model to be created which will allow the available environmental data to be assessed via equations which have inherent physical validity. This approach is elegant and simple to apply regardless of the complexity of the environment being considered (Mackay and Paterson, 1981). The relationship between fugacity and partition coefficients are shown in Figure 3.3.

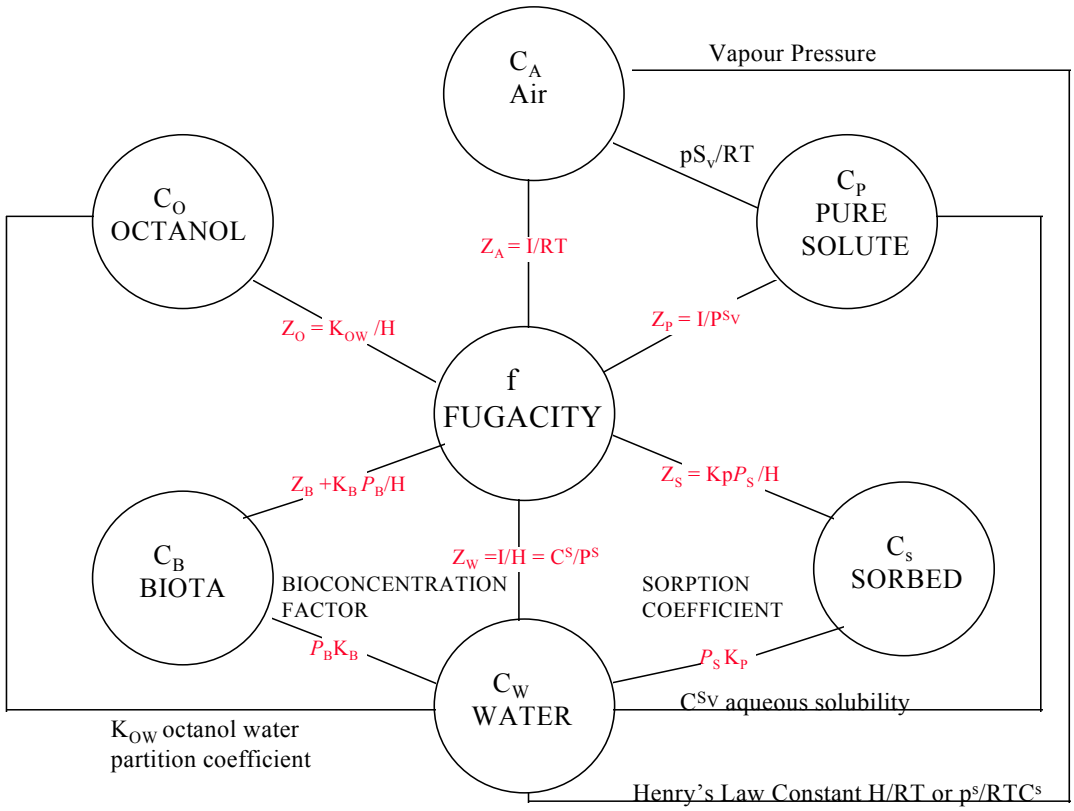

Figure 3.3 The relationship between fugacity (f), fugacity capacities (Z) and partition coefficients (K) (Samiullah, 1990, Mackay and Paterson, 1981)

Fugacity calculations can be defined into 4 levels. Each increase in level is characterised by increased complexity representing increased complexity of the environment being considered. According to the different assumptions, basic models are classified to levels (LEVEL I, II, III and IV) by following:

A Level I simulation is of the equilibrium distribution of a fixed quantity of conserved (ie. non-reacting) chemical, in a closed environment at equilibrium, with no degrading reactions, no advective processes, and no intermediate transport processes (e.g. no wet deposition, or sedimentation). The medium receiving the

emission is unimportant because the chemical is assumed to become instantaneously distributed to an equilibrium condition.

A Level II simulation describes a situation in which a chemical is continuously discharged at a constant rate and achieves a steady-state and equilibrium condition at which the input and output rates are equal. Degrading reactions are treated as loss or output processes. Intermediate transport processes (e.g. no wet deposition, or sedimentation) are not quantified. The medium receiving the emission is unimportant because the chemical is assumed to become instantaneously distributed to an equilibrium condition.

A Level III simulation describes a situation which is one step more complex and realistic than the Level II model. Like the Level II model, the chemical substance is continuously discharged at a constant rate and achieves a steady state condition in which input and output rates are equal. The loss processes are degrading reactions and advection. Unlike the Level II model, equilibrium between media is not assumed and, in general, each medium is at a different fugacity. A mass balance applies not only to the system as a whole, but to each compartment.

A Level IV simulation is a relatively straightforward means to extend the Level III model to unsteady-state conditions. Instead of writing the steady-state mass balance equations for each medium, Level IV writes a differential equation. These equations can be integrated numerically to give the fugacities as functions of time, thus quantifying the time response characteristics of the system.

In this work, a simple approach to environmental partitioning can be explained by the concept of fugacity which represents an alternative approach to environmental partitioning of a chemical and allows expected partitioning to be calculated via ratios devised from empirical values. This approach is widely used throughout the world. The powerful modelling program EPISuite (Version 4.0) which is based on fugacity

level III calculation is widely used and most comprehensive of similar program types. The program predicts environmental fate and toxicity of POP chemicals and also calculates the partition coefficients (K_{oc} and K_{ow}) from the inherent chemical and physical properties (EPA, 2009).

3.1.3.2 EPISuite program

The estimation program interface modules (EPISuite V. 4.0) used in this assessment was developed by the Syracuse Research Corporation (SRC) on behalf of the United State Environmental Protection Agency (USEPA). It comprises a suite of regression based quantitative structure activity relationship (QSAR) models and uses a variety of empirical quantitative structure property relation ships (QSPRs) with Log K (partition coefficient) as one of the most significant descriptors. In the beginning, this program was released in 2001 with EPISuite V. 1.66, and this version was only available for organic substances. By February 2009, the program had developed to version (V.4.0) which has all reactivity data in one convenient place and covers organometallic compounds such as organotin compounds (EPA, 2009). The software is a combination package that includes 14 estimation programs (Figure 4.4).

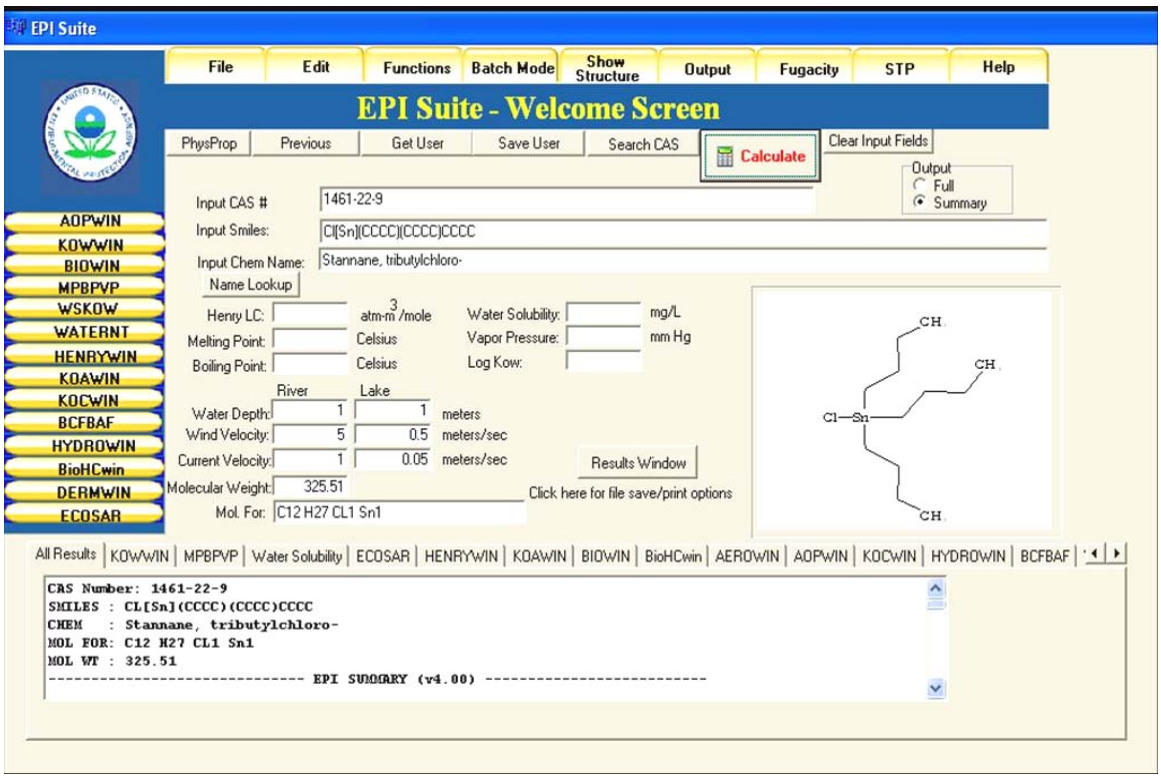

Figure 3.4 Showing the estimation programs in EPISuite V. 4.0 software (Estimation Program Interface for Windows, EPIWIN) (EPA, 2009)

Because EPIWIN estimates a wide range of physical-chemical property and reactivity data in one convenient, easy-to-use software package, EPIWIN is perceived by industrial, as well as a number of regulatory bodies, as an invaluable source of data for many chemical substances. For example, the USEPA developed the "PBT Profiler" software in 2004 for estimation of persistence (P), bioaccumulation potential (B) and toxicity (T) for large lists of chemicals. The PBT Profiler software incorporates the same SRC estimation software packages used by EPIWIN (http://www.epa.gov/oppt/pbtprofiler/) (EPA, 2009). Recent reviews suggest that EPISuite is a suitable performing software packages for prediction of K_{ow} and K_{oc} values available (Keenan, 2008, Arp et al., 2006, Dimitriou-Christidis et al., 2003). It requires simply the input of a chemical abstracts (CAS) number or simplified molecular input entry specification (SMILES) string of substances to predict a partition constant, and it is publicly accessible on line

(http://www.epa.gov/oppt/exposure/pubs/episuite.htm). Moreover, these programs are able to evaluate the prediction data including fate in terms of partitioning and toxicity within/without the experimental partition coefficient values (K_{ow} and K_{oc}). Therefore, the advantage of EPISuite program is flexible creation of an accurate prediction value for each natural site from experimental input data. In addition, other software models based on molecular structure currently available for the estimation are;

ClogP; is licensed software which is commonly used to calculate the K_{ow}, and requires only input of SMILES string (http: www.daylight.com/cgi-bin/download.cgi). It is quoted (along with EPISuite) as being able to ascertain K_{ow} values within experimental uncertainty (Arp et al., 2006).

SPARC; is another QSARs that explicitly calculates general properties such as Van der Waals force, H-bond interaction, pKa, ionisation energy, hydration, Henry constant and heat of formation etc. These values are very useful for thermodynamic study. Like EPISuite, SPARC requires only the input of a CAS number or SMILES string to predict constant values, and it is publicly accessible on the internet (http://ibmlc2.chem.uga.edu/sparc/) (Niederer and Goss, 2008).

COSMO therm C2.1; is commercial software that performs density function quantum chemical continuum salvation calculations with statistical thermodynamic in terms of three dimensional structure which can present the difference partition behaviour of isomer substances (Goss et al., 2008). Input files for COSMO therm are generated with other software packages like Turbomole or Gaussian (Arp et al., 2006).

In this work, the EPISuite program is selected because it gives an impression to evaluate the estimation for each specific site from flexible experimental input data. Moreover, this software is publicly accessible on the internet which has been widely used for estimation and modelling studies.

Although, EPISuite was used to estimate the physicochemical properties of various chemical substances in the past decade, there have been no reports on organotin compounds especially TBT. Moreover, previous reports have only presented an estimation value using the default program but do not present accurate values for modelling from experimental values. These reports miss the opportunity to improve the program output by creating more accurate data for each specific site. For example, EPISuite was used to estimate the partition behaviour of chlorophenols (Niederer and Goss, 2008), hexachlorocyclohexane (Goss et al., 2008), fluorinated compounds (Arp et al., 2006) and physicochemical properties of methylated naphthalene compounds (Dimitriou-Christidis et al., 2003). The estimation results from EPI program were compared with experimental values and also results from SPARC, ClogP and COSMO therm program, which indicated that the COSMO therm, commercial program may be a better tool for estimation and more accurate than the others. This conclusion was based on EPISuite program running with default calculation. Furthermore, EPISuite was applied to evaluate the prediction data including half-life and toxicity for PCBs (Gouin et al., 2004), pesticides (Aronson et al., 2006), toxicity of chemical warfare agents (CWAs) (Sanderson et al., 2007) and fifty types of aromatic compounds including polycyclic aromatic hydrocarbons (PAHs), benzene and its derivatives (Carlsen and Walker, 2003). The publications above all presented the EPI program under default operation without the improvement of the program by the entering of experimental data. Without experimental data, the model is useful for prediction but is essentially a default model. A site specific assessment is possible by measuring the partition coefficients and entering the experimental values obtained into the model. In this work, the experimental partition coefficient K_{ow} and K_{oc} (calculated from K_d) were used as input data into the prediction program (EPISuite) to provide accurate values for the natural samples *in-situ*. The experimental partition coefficients are based on the adsorption theory which is related to topics as following section.

3.1.3.3 Adsorption in soils and sediments

In general, the adsorption reactions usually take place at the surfaces of soil colloid. In the case of the organic colloids, e.g., organic carbon such as humic matter, adsorption is related to interaction force with their functional group at the surface of soils and sediments, for example carboxyl group, and hydroxyl groups. Adsorption reactions by inorganic soil colloids are also surface interactions attributed to charged surfaces which depend on pH (Tan, 1998). When the adsorption of substances on surfaces of soils and sediments occurs, this can be explained by adsorption forces and adsorption isotherms which can be divided as follow.

Forces of adsorption

Forces responsible for adsorption reactions can include the Van der Waals force, hydrogen bonding, protonation, hydrophobic bonding, electrostatic bonding, coordination reaction, and ligand exchange (Tan, 1998).

Van der Waals force; the most important physical force is the Van der Waals force. This force is a short-range interaction. Its role is only of importance at close distances since this type of force decreases rapidly with distance. Since Van der Waals forces decrease rapidly with distance from the colloidal surface, their effect on adsorption is greatest for ions which are in close contact with the colloid surface. Since, the small and spherically shaped ion will be in closer contact with the surface than the larger ions. They experience greater Van der Waals interaction. This force is involved in the adsorption of organic cations, anions, neutral polar and nonpolar organic ions. In addition, hydrophobic bonding, which can be regarded as a type of the Van der Waals force, is associated with adsorption of nonpolar compounds. The compounds compete with water molecules for adsorption sites, and in the process, adsorbed water is exchanged or expelled by substances, which is the reason for calling this process hydrophobic.

Protonation; this force can occur at the colloid surface, and in the solution phase, as well as in the hydration shells of cations. It is an important force for adsorption of anions and organic compounds basic in nature, because of the development of positive charge, for example NH_3 is noted to be chemisorbed by clays in the form of NH_4^+. In general, the protonation of organic compounds in the interface is affected by several factors, e.g., basicity of the adsorbate, the nature of the exchangeable cation, the negative charge of clay mineral, soil water content and surface acidicity. The surface acidicity is perhaps the most important factor in providing the protons necessary for protonation of anions and basic organic compounds.

Hydrogen bonding; the chemical force by which a hydrogen atom acts as the connecting linkage is called a hydrogen bond. It is believed that hydrogen bonding is related to protonation. Whereas protonation involves a full charge transfer from the electron donor (base) to electron acceptor (acid), hydrogen bonding is a partial charge transfer. Water, which is dipolar, may become adsorbed at the clay surface through its linkage with hydrogen bonding. Organic compounds, containing functional groups such as N-H, NH_2, OH and COOH, will be adsorbed by formation of hydrogen bonds between the functional groups and the hydrogen on the clay surface.

Electrostatic bonding; this force is the result of the electrical charge on the colloid surface. This is the reason for (i) adsorption of water, (ii) adsorption of cations, which leads to cation exchange reactions, and (iii) adsorption of organic compounds. This may develop into complex reactions, where both organic compounds and clay minerals are negatively charged, hence are expected to repel each other. However, protonation of the organic substances may convert them into positively charged ions. The protonation process is made possible by hydronium ions on the exchange sites, or dissociation of adsorbed water, or by proton transfer from water in the hydration shell of adsorbed cations.

Coordination reaction; this reaction involves covalent bonding. The latter occurs when the ligand donates electron pairs to a metal ion, usually a transition metal. The ligand, therefore, fits the definition of a Lewis base and the metal is then the Lewis acid. The compound formed is called a coordination compound, complex compound or organo-metal complex. Organo-metal complexes are substances containing a central atom, usually a metal, surrounded by a cluster of organic ligands.

Ligand Exchange; this entails the replacement of a ligand by an adsorbate molecule. The adsorbates much have a stronger binding capacity than the ligand.

Adsorption isotherm

Adsorption has been defined as the concentration of constituents at the colloidal surfaces. The curve relating the concentrations of adsorbed materials at a fixed temperature is called the adsorption isotherm. Currently two methods are available in the use of adsorption isotherms to study the behaviour of adsorption; (i) identification of shape and curvature of adsorption isotherm, and (ii) statistical formulation, known today as statistical modelling, of adsorption isotherm (Do, 1998, Tan, 1998). In the first method, four major basic types of adsorption isotherm have been recognized and used for identifying the nature of adsorption of solutes from aqueous solution (Figure 3.5).

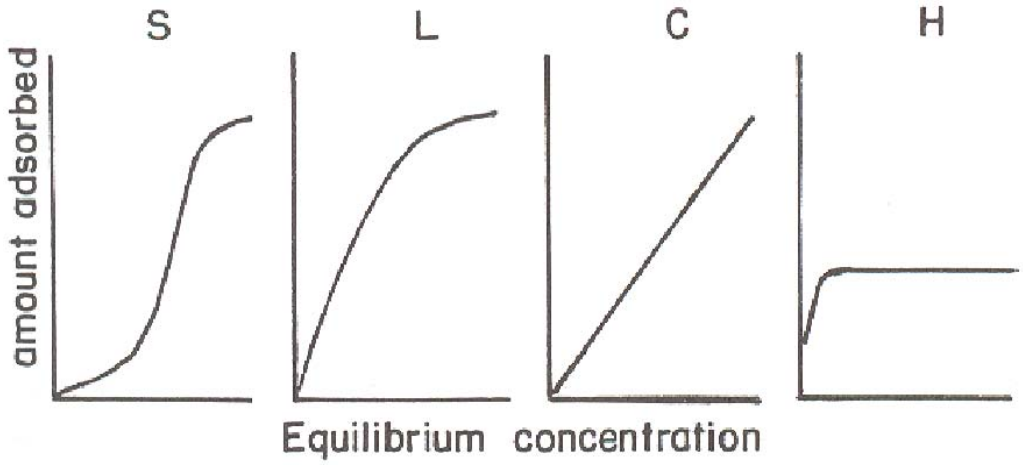

Figure 3.5 The four major types of adsorption isotherm on the basis of shape and curvature (Weber, 1970)

The S-type represents adsorption reactions when the solid has a high affinity for solvent, whereas the L-type suggests that the solid has a high affinity for the solute. Both S- and L-type adsorption curves are considered to predict similar things such as the Langmuir adsorption isotherm which normally occurs with non porous solid or tiny porous solid and similar pore size, for example activated carbon and zeolite (Machida et al., 2005, Mathias et al., 1996). The C-type curve is also known as the constant partition isotherm. The adsorption process is characterized by a constant partitioning of solute between solution and adsorbent. According to Weber (1970), this type of adsorption is common when new adsorption sites become available as the solute is adsorbed from the solution. The H-type curve, also call high affinity curve, represents adsorption reactions when the solute has affinity for solids. This type of curve is considered a special type of the L-curve. In dilute solution the solute is often completely adsorbed and no measurable amount is left in the solution.

The second method of studying the adsorption process is through statistical formulation of adsorption reactions which was applied in this study. Four major types of equations have been formulated and currently used to describe adsorption

processes; (i) the Freundlich equation, (ii) the Langmuir equation, (iii) the BET (Brunauer, Emmett, and Teller) equation, and (iv) surface concentration equation.

Freundlich equation; the adsorption isotherm in dilute solution is formulated by Freundlich as;

$$Q_e = X/m = KC_e^{1/n} \qquad \text{(Equation 3.5)}$$

Where,

X= amount of material adsorbed

m = amount of adsorbent

C_e= concentration of solute in solution at equilibrium

Q_e = amount of solute in solution at equilibrium per 1 unit of adsorbent

K and n = constant

By replacing concentration C for pressure P, the Freundlich equation can also be used to describe adsorption of gases by solids. In general, this equation was applied to the adsorption of diluted solutes on irregular surface adsorbents such as clay, and sediment (Do, 1998). Therefore the adsorption of TBT on sediment will be investigated using the Freundlich equation and subsequently presented in the experiment.

Langmuir equation; this equation, originally derived for adsorption of gases by solids and applied to monolayer adsorption of diluted solute on non porous solids or small porous solid as the previous mentioned, is formulated as follows;

$$Q_e = X/m = Q_{max}KC_e/(1+KC_e) \quad \text{(Equation 3.6)}$$

Where,

X= amount of material adsorbed

m = amount of adsorbents

C_e= concentration of solute in solution at equilibrium

Q_e = amount of solute in solution at equilibrium per 1 unit of adsorbents

Q_{max} = maximum amount of solute in solution at monolayer adsorption

K = constants

This formula states that x/m become constant at high concentrations. In other words, at high values of C, the surface of the adsorbents become saturated and adsorption reaches a maximum (Figure 3.6).

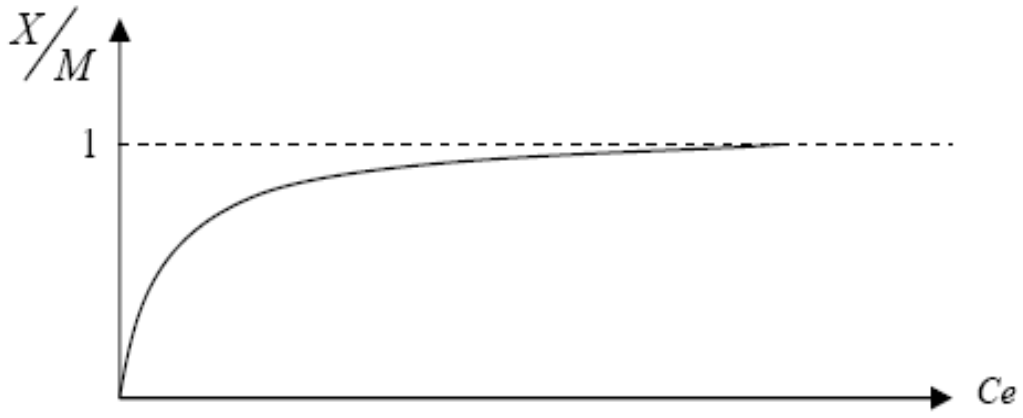

Figure 3.6 The relationship between X/m and C_e which follow the Langmuir equation (Tan, 1998)

On the other hand, at very low concentration the value of KC_e (Equation 3.6) becomes so low compared to the factor 1, that it can be neglected. Thus, the equation changes then into Equation 3.7. This equation is the Freundlich equation in which 1/n = 1.

$$Q_e = X/m = K_1C_e \qquad \text{(Equation 3.7)}$$

Where,

$K_1 = Q_{max}K$

Moreover, the partition coefficient constant value (K) for the Langmuir adsorption isotherm can be investigated by arranging the Equation 3.8 into;

$$C_e/Q_e = (1/KQ_{max}) + (C_e/Q_{max}) \qquad \text{(Equation 3.8)}$$

The intercept of linear plotting between C_e/Q_e and C_e is $1/KQ_{max}$. Then, K values can be indentified.

Brunauer, Emmett, and Teller (BET) equation; the Langmuir adsorption is useful only for simple adsorptions reaction involving monolayer adsorption (Machida et al., 2005). For multilayer adsorption which is not present in natural conditions, the use of the BET equation is suggested. In this respect the BET equation is considered an extension of the Langmuir equation. The BET equation was developed by Brunauer, Emmett, and Teller in 1983 for the adsorption of multilayer of nonpolar gases. This equation was revised again in 1946 and called BET-BDDT equation at constant pressure (Equation 3.9). Therefore, this equation is currently applied to the surface area analysis.

$$P/[V(P_o-P)] = 1/(V_mC)+[(C-1)/(V_mC)](P/P_o) \quad \text{(Equation 3.9)}$$

Where,

P = equilibrium vapour pressure

P_o = saturation vapour pressure

V = volume of gas adsorbed

V_m = volume of gas adsorbed when solid is covered with a monolayer

C = constant related to heat of adsorption

This equation assums that the first layer of gas is attracted (adsorbed) firmly to the surface, perhaps by Van der Waals forces. The second and subsequent layers are assisted by gradually weaker forces.

Surface concentration equation; was derived from the Gibbs equation. This equation describes processes in relation to surface tension and formulated as follows;

$$\Gamma= -(a/RT)(\partial\gamma/\partial a)_T \quad \text{(Equation 3.10)}$$

Where,

Γ = surface concentration of adsorbed material (moles cm^{-2})

a = activity of solute in moles

R = gas constant

T = absolute temperature (K)

γ = surface tension of adsorbents in dynes cm^{-1}

The solute is adsorbed on the surface of the adsorbents if $\partial\gamma/\partial a$ is negative when solute decreased tension. This equation is very difficult to use in the adsorption reaction at solid-liquid interface, because it is impossible to measure surface tension of solid surfaces.

3.1.3.4 Colloidal chemistry of soil and sediment

A colloid is a state of matter consisting of very fine particles that approach, but never reach, molecular sizes. The molecular size of colloid is between 5 nm and 0.2 μm. If the dispersion medium is water, colloidal systems can be divided into two groups. These are called hydrophobic and hydrophilic. A hydrophobic colloid can be flocculated, but a hydrophilic usually cannot. The colloidal system in soil and sediment can be divided into organic and inorganic constituents (Tan, 1998).

Colloidal chemistry of organic constituents

Many organic compartments in soil and sediment can exhibit both hydrophobic and hydrophilic characteristic in the same molecules. The organic colloidal phase is discussed below (Tan, 1998).

The organic components; the organic components of soils originate from the biomass that is characteristic for an active soil. Although both living organisms and the dead components are included in soil matter, only the nonliving fraction will be discussed in this section. The nonliving organic components are formed by chemical and biological decay of mainly materials. They can divide into (i) materials in which the anatomy of plant substance is still visible and (ii) completely decomposed material. The first group is of significance in soil physics (soil structure). However, from the soil chemistry perspective, the non decomposed organic fraction is chemically of minor importance for adsorption because its intact structure exhibits a relatively

small surface area rendering it inactive as an adsorbent. Of major importance in soil chemistry are decomposition products, although their nature and accumulation in soil depended on types and quantity of original material subjected to decomposition. The organic compounds, present in detectable amounts in soil, are carbohydrates, amino acids/proteins, lipids, nucleic acid, lignins, and humic compounds

Soil humus; humus refers to a mixture of organic compounds produced by decomposition as discussed above. Humus is defined as the total organic fraction in soil, exclusive of non decomposition material. Humic substrates (humic acid, fulvic acid and humin) make up the bulk of humus (Figure 3.7). However, carbohydrates are the second most abundant component of humus. The carbohydrate concentration has been estimated to range from 5 to 20% in soil humus.

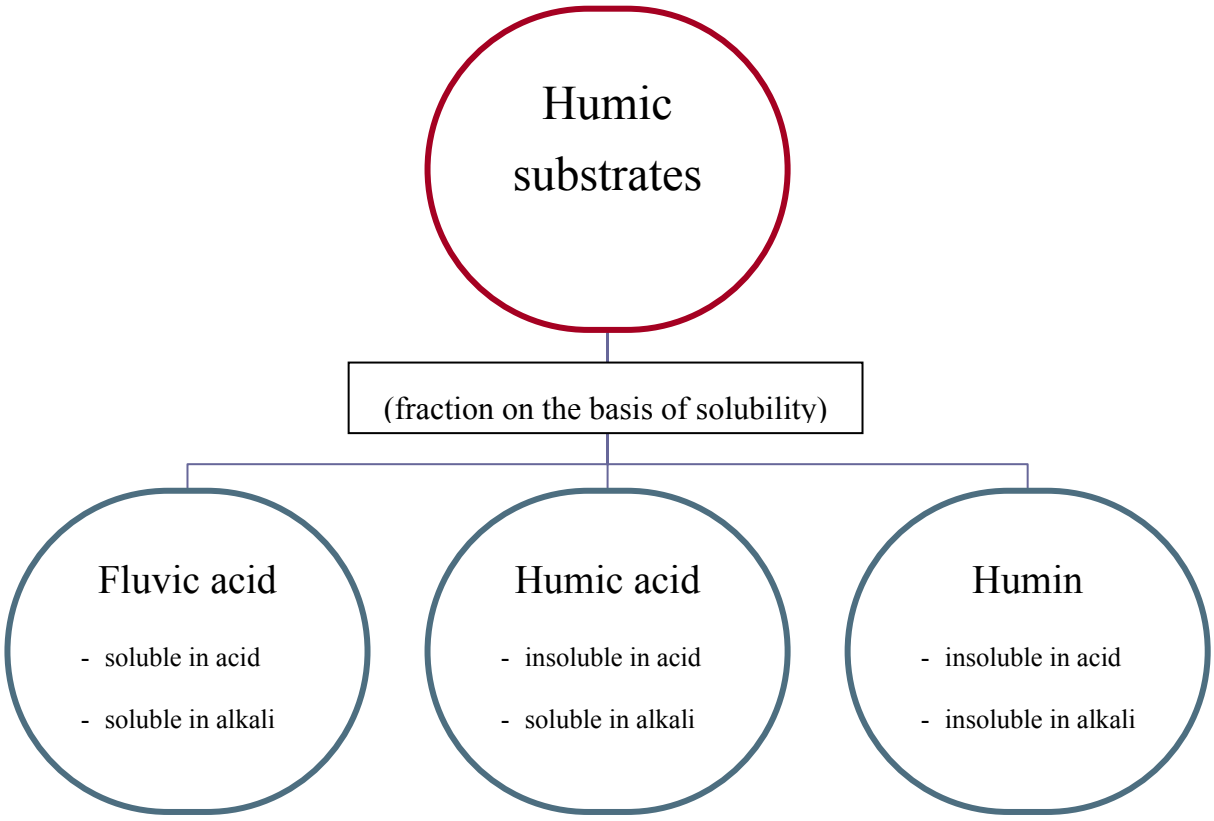

Figure 3.7 Fraction of humic substrates (Sparks, 1995)

In addition, the cation exchange capacity (CEC) of materials is defined as the capacity of materials to adsorb and exchange cations. CEC is commonly determined by extraction of the cations from soils/clays with a solution containing a known cation for exchange. The results, expressed in milliequivalents per 100 grams of soils or centi-mol equivalents of cations per kilograms of soils (cmol(+) kg^{-1}), are taken as the CEC of soil. In general, organic matters exchange cations mainly due to the presence of the carboxylate group, $-COO^-$. Humus usually has a high CEC, e.g. CEC of peat = 300-400 compared to CEC of typical soil = 10-30 (O'Neill, 1998). Therefore, the total organic carbon in soil affects the adsorption behaviour of substances, TBT in this case (Unger, 1988). The amount of total organic carbon (TOC) in the studied samples will therefore be classified by the ASTM standard method to understand the adsorption behaviour.

Colloidal chemistry of inorganic constituents

The inorganic fraction of soils is composed of rock fragments and minerals of varying size and composition. On the basis of size, three major fractions are usually recognized; (i) the coarse fraction (2-0.05 mm) called sand, (ii) the fine fraction (0.05-0.002 mm) called silt, and (iii) the very fine fraction (<0.002 mm, 2μm) referred to as clay (ASTM, 2002). In soil science, minerals in the clay fraction are usually to considering as a colloid, although only the fine clay fraction < 0.2 μm is colloidal clay. Since it has high surface area and particle size it is suitable to form colloidal systems which affect the adsorption properties. Materials coarser than sand, like rocks and gravel may also be presented in soils, but they are usually not considered as soil constituents. However, they may form sand, silt and clay upon weathering (Tan, 1998).

Clay minerals are hydrous aluminium silicates (contained Al, Si, O and OH) of small size with a layered structure. This characteristic structural feature is made up of sheets of either the tetrahedral [SiO_4] unit (Figure 3.8) or octahedral [AlO_6] unit (Figure 3.9). The [SiO_4] tetrahedral are linked together by the sharing of three basal

oxygen atoms with their apexes all pointing in the same direction. The octahedral unit contain two layers of close-packed oxygens and hydroxyls surrounding the aluminium. The relative number of oxygen and hydroxyl groups varies to satisfy the charge-balance criteria for the structure (O'Neill, 1998).

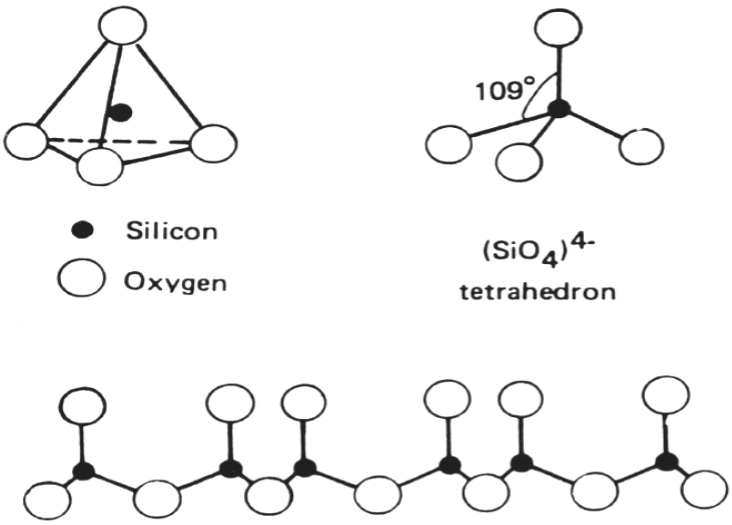

Figure 3.8 Top: The schematic structure of a single silica tetrahedral, and Bottom: The arrangement of several silica tetrahedral into a sheet by mutually sharing oxygen atoms (Tan, 1998)

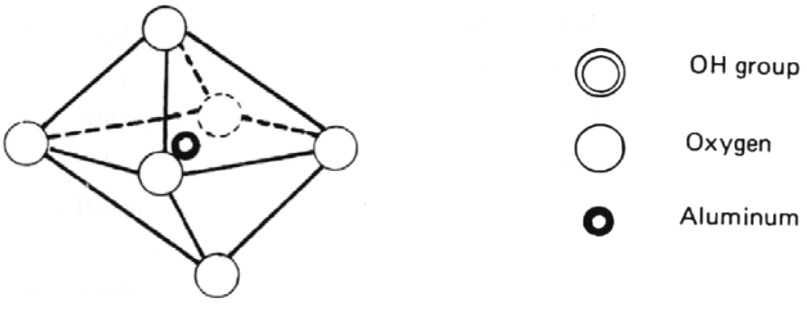

Figure 3.9 The schematic structure of a single aluminium octahedral (Tan, 1998)

Based on their structure and chemical composition, the clay minerals can be divided into three main classes i.e. kaolinite, illite and smectite which are explained as follows (O'Neill, 1998).

Kaolinite; is the simplest of clay minerals. ($Al_4Si_4O_{10}(OH)_8$), with one octahedral sheet and one tetrahedral sheet forming a 1: 1 clay mineral (Figure 3.10). A small amount of isomorphous substitution of Al for Si in the tetrahedral sheet results in a charge of < 0.005 mol negative charge per unit cell. Successive 1:1 layers are attached above each other and held together by hydrogen bonds between the oxygens in one layer and the hydroxyl group in the next layer. The hydrogen bonds prevent other groups from entering between the individual layers and keep the structure relatively rigid. These also result in a low cation exchange capacity (3-20 cmol(+) kg^{-1} and low surface area (5-100 m^2g^{-1}) and a fixed d-spacing of about 0.7 nm.

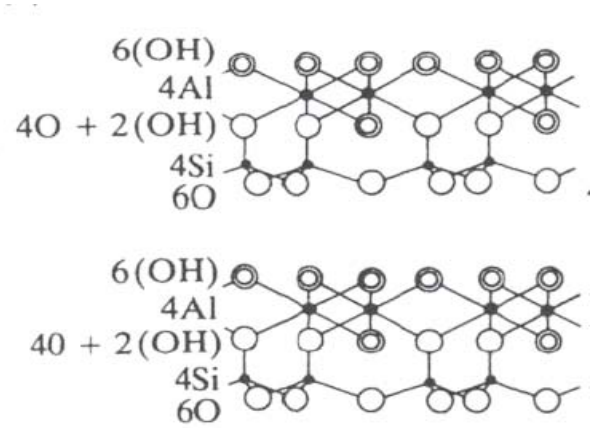

Figure 3.10 The schematic structure of kaolinite (O'Neill, 1998)

Illite (a hydrous mica); is a 2:1 clay mineral (two tetrahedral sheet and one octahedral sheet forming) with isomorphous substitution mainly in the tetrahedral sheet (Al^{3+} for Si^{4+}) resulting in a charge of 1.5 mol negative charge per unit cell. In each case the oxygens of 2:1 layer always face the oxygens of the next layer and, therefore, no hydrogen bonding can take place (Figure 3.11). The layers are not so strongly held together, and ions such as K^+ can enter between the layers. Therefore the negative charge is neutralised by K^+ ions in the interlayer space. The distribution of oxygen atoms on the tetrahedral face allows K^+ ions to sit very close to the clay

surface. The consequence of this is a low cation exchange capacity (10 – 40 cmol(+) kg^{-1}), low surface area (100 – 200 m^2 g^{-1}) and a fixed d-spacing about 1.0 nm.

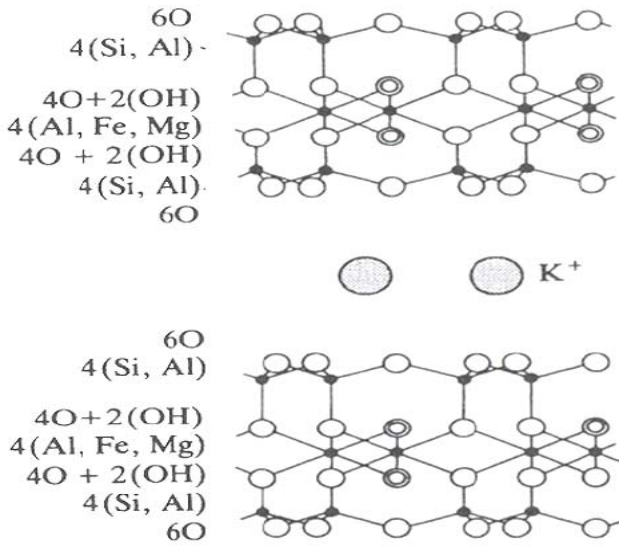

Figure 3.11 The schematic structure of illite (O'Neill, 1998)

Smectite; is a group of 2:1 clay minerals with a low degree of isomorphous substitution and low layer charge. Montmorillonite ($Al_4(Si_4O_{10})_2(OH)_4$) is the commonest smectite in which substitution occurs in the octahedral layer giving 0.7 mol negative charge per unit cell. The oxygens of one layer always face the oxygens of the next layer similar to Illite structure. Interlayer bonding is weak, with no hydrogen bonding between layers (Figure 3.12), allowing expansion of the clay lattice and easy entry of cations and water molecules into the interlayer space. The cation exchange capacity of montmorillonite (80 – 120 cmol(+) kg^{-1}) and surface area (700 – 800 m^2g^{-1}) are both high and the d-spacing variable (0.96-2.14 nm) depending on the dominant interlayer cations.

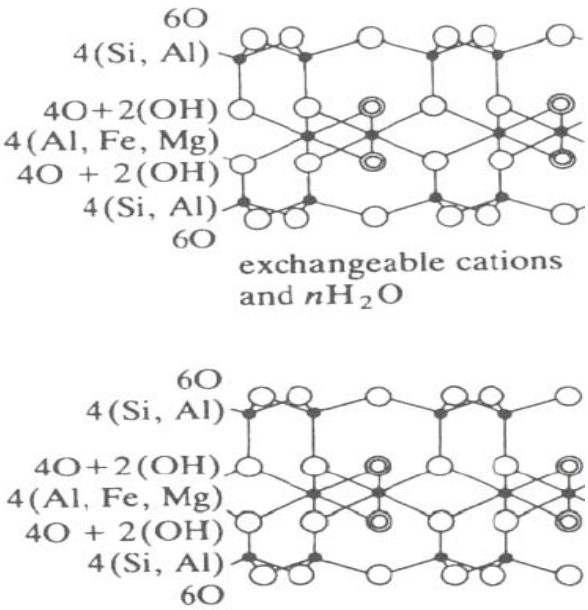

Figure 3.12 The schematic structure of montmorillonite (O'Neill, 1998)

From the CEC values, kaolinite has a relatively low CEC, which is due to the exchange of H^+ ions from the hydroxyl groups on the clay surfaces. The hydroxyl groups of montmorillonite react similarly, but the greater degree of substitution and the consequent excess negative charges lead to a higher CEC (O'Neill, 1998).

In addition, d-spacing value is an important parameter which can be used to identify clay minerals, and also the effect on the adsorption of substances into the interlayer space of clay. The X-ray diffraction (XRD) method is perhaps the most widely used technique in the identification of clays (O'Neill, 1998). It is mainly for qualitative analysis, and also frequency semi-quantitative determination of clays has been carried out. XRD is a non-destructive method. However, the method is not applicable to analysis of amorphous or noncrystalline materials. The basis for the use of x-rays in the investigation of soil clays is the systematic arrangement of atoms or ions in crystal planes. Each mineral species is characterized by a specific atomic arrangement, creating characteristic atomic planes that can diffract (reflect) x-rays. X-rays are electromagnetic radiation of short wavelength. In most crystals, the atomic spacing (d-spacing), or crystal plan, have almost the same dimension as the x-

rays wavelength. This can produce the characteristic pattern which is used as a fingerprint in the identification of mineral species.

X-rays are produced in the x-ray tube by fast-moving electrons hitting a metal target. The excited atoms in the target emit radiation with wavelength between 0.01 and 100 Å. The Cu Kα radiation was used in this work. The Cu Kα radiation beam hits a crystal plane of a mineral (Figure 3.13) and generate the scattered x-rays in a definite direction which related to d-spacing. To identification of d-spacing, Bragg's law is defined;

$$n\lambda = 2d \sin \theta \qquad \text{(Equation 3.11)}$$

Where,

d = d-spacing between atomic planes

λ = wavelength of x-rays (Cu Kα radiation source = 1.54 Å)

θ = glancing angle of diffraction

n= order of diffraction

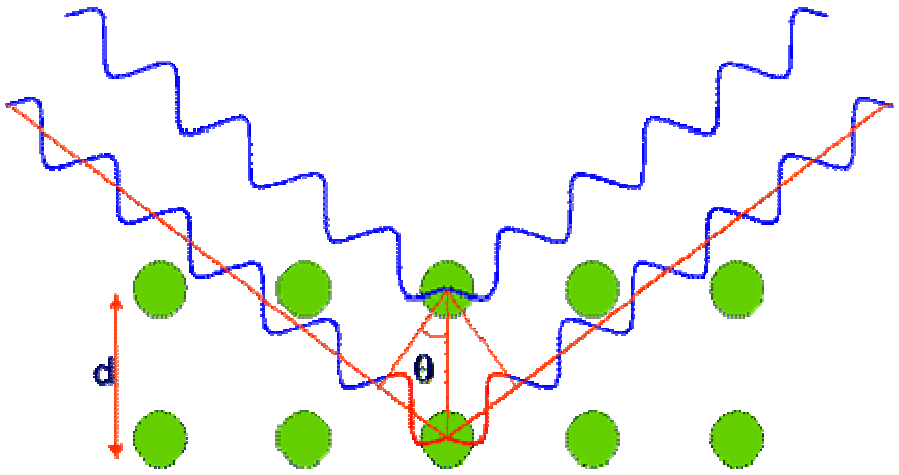

Figure 3.13 The schematic drawing of a x-rays incident beam diffraction from crystal planes, obeying Bragg's law (Tan, 1998)

The results are normally shown in terms of 2θ. However, a number of tables, and library data bases are available to convert the 2θ into d-spacing units (Appendix Table B1). Highest intensity of diffraction maxima is obtained from d(001) planes (Figure 3.14). The first-order d(001) peak, usually together with the second-order diffraction peak, are diagnostic for the identification of the mineral species.

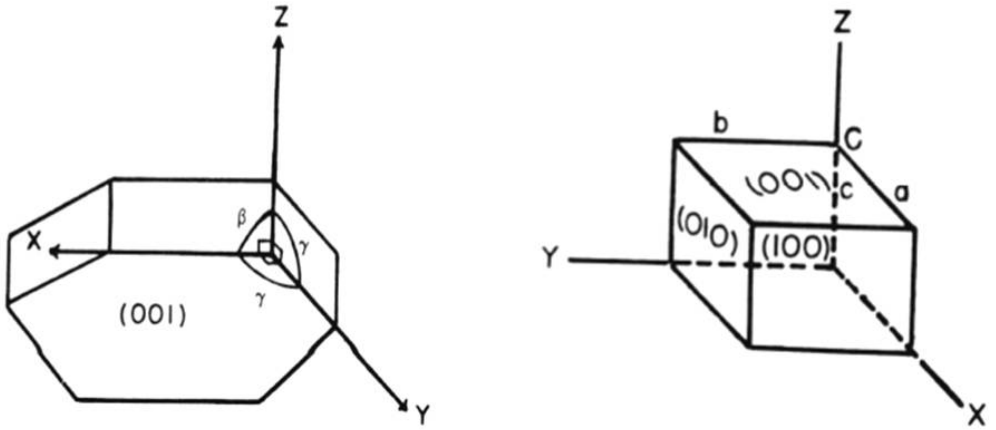

(a) (b)

Figure 3.14 The schematic drawing of d(001) plan (a), and the arrangement of d(001) plan in a unit cell (b) (Tan, 1998)

For example, kaolinite (Figure 3.15) exhibits a characteristic diffraction peak at the angle of $2\theta = 12.4^0$ This corresponds after conversion to a d(001) spacing of 7.13 Å (0.713 nm) which corresponded with the characteristic of kaolinite as previous mentioned. Therefore, d-spacing of illite and montmorillonite are also investigated using the same approach (Appendix Figure B1) and the results presented are as previous mentioned. These values will be used to discuss the parameters influencing the adsorption of TBT in experiments.

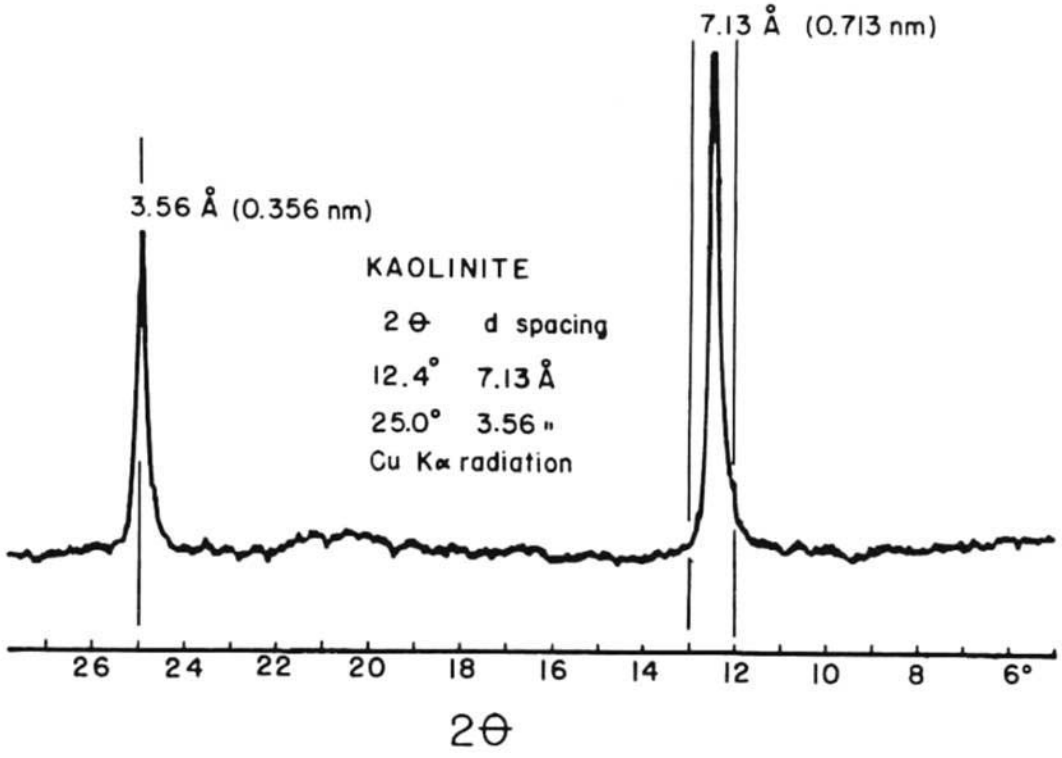

Figure 3.15 The interpretation and identification of kaolinite using XRD pattern. A first order diffraction peak at $2\theta = 12.4^o$, together with second order peak at $2\theta = 25^o$, is diagnostic for the presence of kaolinite (Tan, 1998).

3.1.3.5 Molecular size of TBT

The size of the adsorbed molecule is considered to play an important role in the adsorption. The effect of molecular size can be summarised as follow.

- The adsorption of nonelectrolytes by nonpolar adsorbents increases as molecular weight, size and diameter of the substances increase.
- The adsorption decreases because of steric hindrance

There are the guidelines to estimate the adsorption tendency of substances. For the adsorption of TBT compounds on the clay minerals, TBT compounds are large molecules which present a high steric hindrance. Therefore, the program called Chem3D pro 11.0 were used to investigate the orientation of TBT compounds in aqueous phase (CambridgeSolf, 2009). The dissimilarity of molecular size might be considered influential on the dissimilar adsorption behaviour of TBT in different types of clay mineral. The program presented the molecular size in terms of molecular diameter and the orientation of TBT compounds such as TBTCl and TBT positive ion (Figure 3.16).

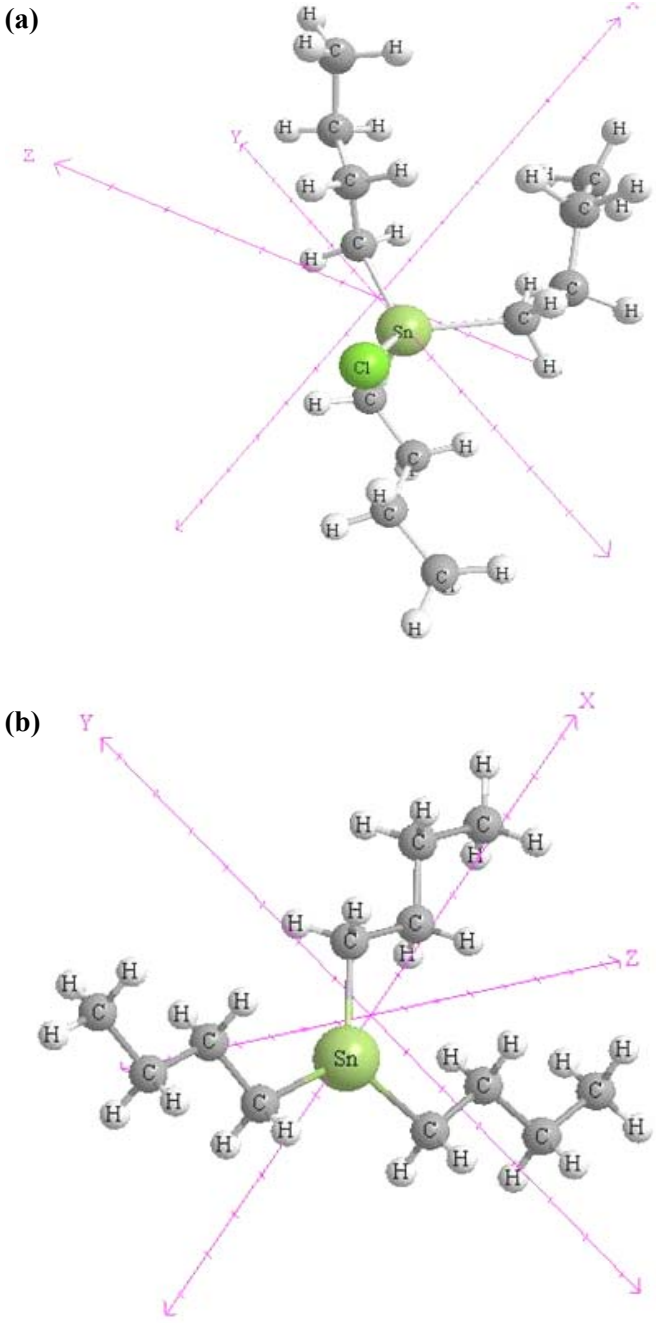

Figure 3.16 (a) orientation of tetrahedral TBTCl, and (b) planar TBT^{+} ion using Chem3D pro 11.0 program based on MM2 XYZ Cartesian calculation (CambridgeSolf, 2009)

Figure 3.16, the molecular geometry of TBTCl is tetrahedral which presents higher steric hindrance than the geometry of TBT positive ion, trigonal planar. These can affect the adsorption on clay minerals which is discussed following the experiment. The program can also calculate the molecular size of molecules using MM2 XYZ Cartesian calculation, as presented in Table 3.2

Table 3.2 The molecular diameter of TBTCl and TBT^+ on XYZ axis

Substances	Molecular diameter (nm)		
	X-axis	Y-axis	Z-axis
TBTCl	1.20	0.85	0.62
TBT^+	1.05	1.04	0.18

Table 3.2, both TBTCl and TBT ion are considered as large molecular sizes compared with aliphatic hydrocarbon especially TBTCl which present higher steric hindrance on adsorption than TBT ion. From comparison between molecular diameter and d-spacing of clay minerals (*see section Colloidal chemistry of inorganic constituents*), it can be shown that molecular sizes of TBT compounds (TBTCl and TBT^+) are similar to the interlayer space of clay minerals. This result might affect the adsorption ability on clay minerals.

However, in this study, the structure of TBT positive ion (TBT^+) was used to represent TBT species to consider and discuss adsorption behaviour in the aquatic environment. This is justified since TBT^+ is present as the major species when butyltin compounds pollute in the aquatic system as regarding to the dissociation of butyltin compounds in water. This can be shown by Equation 3.12 (Antizar-Ladislao, 2008).

$$Bu_3SnX + H_2O \rightarrow Bu_3Sn(H_2O)^+ + X^- \qquad \text{(Equation 3.12)}$$

Thus, TBT^+ is the dominance species which can adsorb on the surface of soils and sediments. Moreover, toxicity of TBT compounds is attributed to the cation (TBT^+), and not to the anion associated with the biocide in the natural compound (Antizar-Ladislao, 2008). Therefore, the effects of structure and molecular size of TBT^+ on adsorption behaviour will be investigated in subsequent experiments.

3.2 Experimental

According to a recommendation by the International Maritime Organization (IMO, 2002), TBT's application as an antifouling paints is now regulated in most countries. Nevertheless, non-regulated countries entering to waterways and also illegal used could be found. TBT is still present in many aquatic systems at concentrations that cause adverse physiological effects on both organisms and mammals (Antizar-Ladislao, 2008). Therefore, the determination of partition coefficients and also the adsorption behaviour are vital to verify the environmental fate and toxicity of TBT. According to its low volatization and high boiling point (*see section 3.1.1.4*), the distribution and partition of TBT can simplified, as presented in Figure 3.17.

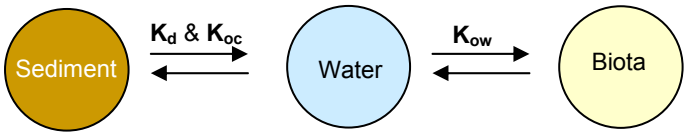

Figure 3.17 The partition coefficients between three mediums

The adsorption behaviour of TBT in solid:water systems has been investigated in terms of the solid:water partition coefficient, K_d (ASTM, 2001, Mackay, 2001). The partition coefficient K_d is found to fit the Freundlich equation depending on TBT concentration (Langston and Pope, 1995). The K_d values reported vary from 10^{-1} to

10^6 L kg^{-1} depending on the conditions and method used to determine the value (Dowson et al., 1993, Langston and Pope, 1995, Burton et al., 2004, Burton et al., 2006). The most comprehensive standard method published that was found suitable for this work in determining K_d is ASTM E1195-01. Quantification of the partition coefficient in the previous reports was not carried out precisely according to this standard method. Variations included, for example, the use of dried or frozen sediment, the degree of water purity used, the ratio of solid: water for the experiments or the equilibrium time used. Moreover difference in the partition behaviour of TBT reported in the literature indicates variation of the partition coefficient as a function of salinity (Hoch, 2004). Previous studies on the effect of salinity have not covered the full salinity range and therefore interpretation may be erroneous as the effect of salinity is a parabolic curve (Unger, 1988, Harris, 1987). Thus when the complete range is observed it leads to a contradiction of findings of relationships between K_d and salinity.

The influence of pH on K_{ow} is extensively reported (Tsuda et al., 1990, Avery et al., 1993, Arnold et al., 1998, White et al., 1999, Looser et al., 2000) but only one report from Burton also described the effect of salinity on K_{ow}. However, again, the complete salinity range was not studied (Burton et al., 2004). In addition, partition coefficients of TBT are often only presented without the prediction of environmental fate and toxicity using the experimental partition coefficient values obtained to create accurate prediction values for each natural site.

Therefore, in this study, the experimental partition coefficients were derived based on standard methods. The variations of partition coefficients were investigated as a function of TBT concentration, time, solid:water ratio, pH, salinity, sediment type and temperature. Subsequently, the coefficients obtained from the experiments and program calculations from EPISuite (V4.0) were compared (EPA, 2009). Also the environmental fate and toxicity were predicted using the experimental partition coefficients as the input for the program to create a more accurate model for specific contaminated sites.

3.2.1 Materials and equipments

The analytical standards and all reagents for butyltins analysis were used similar to the **Chapter 2**. The developed HPLC method was also used to identify amount of TBT in the samples for this section (*see section 2.2.1*).

The powder X-ray Diffractometer (XRD) was carried on a Philips PW 1830 system (Almelo, Netherlands). X-ray diffractometer operated at 40 kV and 30 mA which used Cu Kα radiation source at λ of 1.54 Å. XRD data were collected from 2θ of 5-40 degrees. The crystalline phases of all samples were identified by comparison with the joint committee on powder diffraction standards (JCPDS) files.

3.2.2 Sample collection

Sediment and water samples were collected from potentially polluted areas (Bowling Basin and Port Dundas). The samples were collected in March 2008. In this study, samples collected from Bowling Basin were used to determine the partition coefficients and subsequently predict the behaviour of TBT in the natural environment. Potentially uncontaminated sandy samples were collected from the Clyde River (Bothwell area, taken 6 miles upstream from Glasgow) to study and compare the adsorption behaviour of TBT. A Map and the environment of the sampling sites are presented in Figures 3.18 and 3.19. All sediment samples were collected from the surface layer at the top 15 cm of the solid profile using a dredge sampler and passed through a 2 mm sieve before storage in polyethylene bags. Surface water samples were collected and stored in polypropylene bottles.

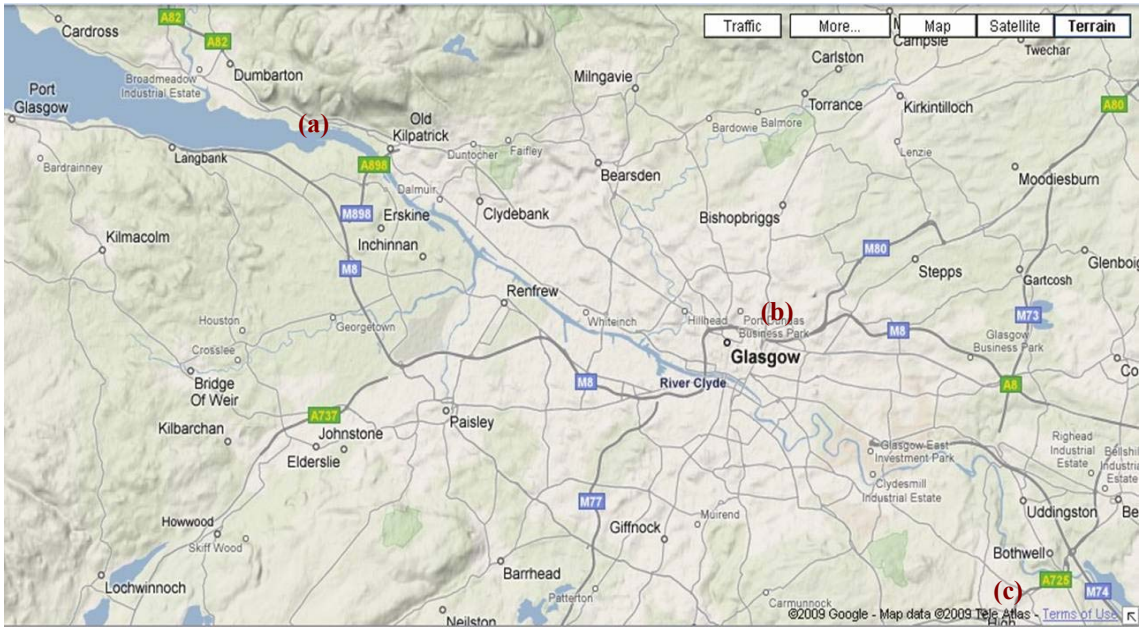

Figure 3.18 Map showing sampling sites in the Forth and Clyde canal; (a) Bowling Basin, (b) Port Dundas, (c) Clyde River

Figure 3.19 Showing of the environment of sampling sites in the Forth and Clyde canal; (a) Bowling Basin, (b) Port Dundas, (c) Clyde River

3.2.3 Octanol-water partition coefficient (K_{ow}) of TBT

The K_{ow} was determined by following the OECD guideline 107 (shaking flask method) at constant temperature, 20 °C (OECD, 1995). The method allows the user to select the TBT concentration in octanol and the ratios of octanol-water; however, a balance between these parameters is strictly required. The volume ratios between octanol and water studied were 1:1, 1:2 and 2:1. The Log K_{ow} value was obtained from the average results (n=3) of each ratio, where the results varied by less than ± 0.3 units, which was achieved by maintaining the amount of TBT dissolved in the octanol at less than 300 μg mL^{-1}. The effect of salinity on K_{ow} was studied. The salinity of the water was estimated using standard methods for the examination of water and wastewater which converts the conductivity measured into salinity (practical salinity units: psu or parts per thousand: ppt) (APHA, 1999). Freshwater salinity is usually less than 0.5 psu, brackish or estuarine water is between 0.5 psu and 17 psu, and ocean salinity is between 32-37 psu (APHA, 1999). In the experiment, the salinity of water was adjusted by adding KCl because potassium is absorbed in water better than NaCl. This method is based on electrical conductivity measurement in which salinity is dependent the conductivity ratio (R_t) as a function of temperature (t, °C). The software used for calculation is publicly accessible online (http://www.es.flinders.edu.au/) and was used to convert from conductivity (μS cm^{-1}) to salinity (psu) (APHA, 1999). In addition, the K_{ow} value of the canal water sample from Bowling Basin was investigated.

For TBT analysis, a 10 mL aliquot of the aqueous phase was withdrawn and TBT was quantified using normal phase HPLC **(Chapter 2)** (Bangkedphol et al., 2008). The amounts of TBT in organic phases were determined by subtraction from the total amount of TBT in the system (300 μg mL^{-1}) of the amount of TBT in water measured. Then the results were compared to the K_{ow} value from the computational program (default value).

3.2.4 Sediment characterization and TBT contamination

The sediment was characterized by pH, total organic carbon (TOC), moisture content, and particle size distribution. Moisture content and TOC of the sediments were determined based on ASTM standard D2974-87 (ASTM, 2000). Moisture was determined by drying a peat (an accumulation of decayed vegetation matter) or organic soil sample after air drying at 105 °C. TOC was determined by igniting the oven-dried sample from the moisture content determination in a muffle furnace at 440 °C due to the prevention of weight loss from carbonate. The carbonate minerals are inorganic carbon which can be destroyed at temperature higher than 800 °C (Santisteban et al., 2004). Therefore, the total weight loss at temperature 440 °C represented TOC in sample. Particle size distribution of the sediment was carried out using specific gravity measurements by hydrometer based on ASTM standard D422-63 (ASTM, 2002). A hydrometer measures the specific gravity (specific density or relative density) of a liquid or suspension. Specific gravity is defined as the mass of a liquid relative to the mass of an equal volume of water. In pure distilled water at 20 °C, the hydrometer reading will be 1.00. When soil is suspended in the water, the specific gravity and the hydrometer reading are increased. In order to measure the specific gravity of the soil/water suspension, the dispersion solution for soil is the solution of sodium hexametaphosphate and sodium carbonate mixture. When a mixture of particle sizes is suspended in a column of water (using a cylinder) containing dispersion agents, the heavy large particles settle first. When a soil sample is stirred or shaken, sand particles will settle to the bottom of cylinder after 2 minutes, while the clay and silt size particle will stay in suspension. After 24 hours, the silt particle will settle, leaving only clay in suspension. By using tables and charts (Appendix Table B2), the exact percentage of sand, silt and clay can be investigated. Moreover, minerals in the clay fraction were identified by XRD technique. The initial TBT concentration in sediments was determined from 5 g sample, on a dry weight basis. In water samples the initial concentration was determined from a 500 mL sample. The samples were extracted and analysed using a NPHPLC method (Bangkedphol et al., 2008).

3.2.5 Solid:water partition coefficient (K_d) of TBT

The adsorption of pollutants from water to sediment is based on the Freundlich equation (McKay, 2001, ASTM, 2001, EPA, 1999). K_d values of TBT were determined by ASTM standard E1195-01 to measure TBT adsorption behaviour (ASTM, 2001). This involves 4 main steps. Firstly, in accordance with the standard method, ratios between the solid:water were optimized when the volume of water was fixed at 20 mL. The amounts of sediment used were 0.1, 0.2 and 0.4 g on a dried weight basis which represent 1:200, 1:100 and 1:50 sediment to water ratio, respectively. The concentrations of TBT in water were 40, 80, 120, 160, 200, 240 and 300 μg mL^{-1}. Secondly, the working range and the highest concentration of TBT in water that was considered to follow the Freundlich adsorption isotherm was determined. This enabled the effective range of TBT concentrations in water to be defined and the maximum suitable TBT concentration. Then, the adsorption times were varied from 15 minutes to 24 hours at 20 °C using the highest concentration of TBT to achieve the equilibrium time, which was then set for the subsequent experiments. Finally, the K_d value was investigated by varying the TBT concentration in water and shaking at the equilibrium time. In addition, the standard method for K_d determination also requires specific Type IV reagent water, that is water of conductivity less than 5 μS cm^{-1}, electro resistivity less than 0.2 Mcm, and pH range from 5.0 to 8.0 (ASTM, 2008). The K_d value using natural water from Bowling basin was also examined and compared with the K_d value from Type IV water.

The major parameters that influence K_d studied in this work indicate TBT adsorption behaviour and fate in the natural environment. This understanding leads to more efficient modelling and remediation processes. The parameters studied were sediment type, pH, salinity and temperature in the range where they practically occur in natural conditions. The sediment from Bowling Basin was used for case study. The sediments from the other two areas were also considered as sediment composition will affect the adsorption behaviour of TBT, compared to Bowling

Basin sediment. The salinities were studied at 0, 15, 32, 50 and 100 psu which represented the range of salinities from freshwater to greater than full strength seawater. The salinity of Type IV water was adjusted by adding KCl because potassium is absorbed in water better than NaCl (APHA, 1999). Various pH of water (4, 5, 6, 7 and 8) were adjusted with 0.1M HCl or 0.1 M NaOH. The pH of water was measured before and after the experiment. The study temperatures were varied from 20 to 50 ^{o}C using an incubator shaker.

K_{oc} the organic carbon partition coefficient, was calculated from the obtained K_d value as presented in Equation 3.13 (ASTM, 2001, McKay, 2001). Therefore, the experimental K_d values were re-calculated to K_{oc} values. Then, the results were compared to the K_{oc} value from the computational program (i.e. the default value).

$$K_{oc} = \frac{K_d}{\%OC} \times 100 \qquad \text{(Equation 3.13)}$$

3.2.6 Prediction of environmental fate and toxicity of TBT

Many different models have been used in an attempt to predict the environmental fate of chemical substances (Samiullah, 1990). A simple approach to environmental partitioning can be explained by the concept of fugacity. The powerful modelling program EPISuite program (Version 4.0) is widely used and the most comprehensive of its type. The program predicts environmental fate and toxicity of POP chemicals and also calculates the partition coefficients (K_{oc} and K_{ow}) from inherent chemical and physical properties (EPA, 2009).

Without experimental data, the model is useful for prediction but is essentially a default model. A site specific assessment is possible by measuring the partition coefficients and entering the experimental values obtained into the model as opposed

to the default values (Keenan, 2008). Therefore, production of K_d, K_{oc} and K_{ow} values from the experiment were entered into the program to determine the environmental fate and toxicity in natural conditions at the specific site.

3.2.7 Desorption of TBT

The sediment from Bowling Basin was studied. A 0.1 gram of sediment (on a dried weight basis) was added to 20 mL of 240 mg L^{-1} TBT dissolved in water and shaken overnight at 20 ^{o}C. The supernatant was poured off after centrifugation and the sorbent was rinsed twice with deionized water before the vial was refilled with 20 ml of study water. The study conditions for water were type IV water, Bowling Basin water (pH 8.2, salinity 0.2 psu) and artificial seawater (pH 8, salinity 32 psu). The desorption study was performed from 30 minutes to 24 hours.

3.3 Results and discussion

3.3.1 Octanol-water partition coefficient (K_{ow})

TBT contamination in the environment has the potential for bioaccumulation. To predict the possible accumulation of TBT in organisms, the dimensionless octanol-water partition coefficient (K_{ow}) is used. Octanol represents lipids because of its similar carbon to oxygen ratio. The octanol-water partition coefficient is a measurement of the hydrophobicity and hydrophilicity of a substance. K_{ow} value is defined by Equation 3.14 (OECD, 1995). The comparison of Log K_{ow} values obtained between the experimental and default values are presented in Table 3.3.

$$K_{ow} = \frac{\text{Concentration in octanol, } (\mu g\ mL^{-1})}{\text{Concentration in water, } (\mu g\ mL^{-1})} \qquad \text{(Equation 3.14)}$$

Table 3.3 Comparison between the experimental and default Log K_{ow} values

Ratio of volume (octanol:water)	Log K_{ow}
1:1	3.96
1:2	3.90
2:1	4.01
Experimental value, average ($\bar{x}$)	3.95±0.05
Water from natural site	4.15
EPISuite (V4.0) program	4.70

Table 3.3 shows a disparity in the experimental values and the values given from the computational model. Because the default values were estimated from the

properties of TBT without accounting for local environmental conditions, the potentially influencing parameters were studied in an attempt to explain the difference in Log K_{ow}. Salinity affects water solubility and causes "salting out", which can change the K_{ow} value (Rydberg, 2004). Therefore, the K_{ow} value was examined in artificial water at various salinities, and also in the natural water from the site. The results are presented in Figure 3.20.

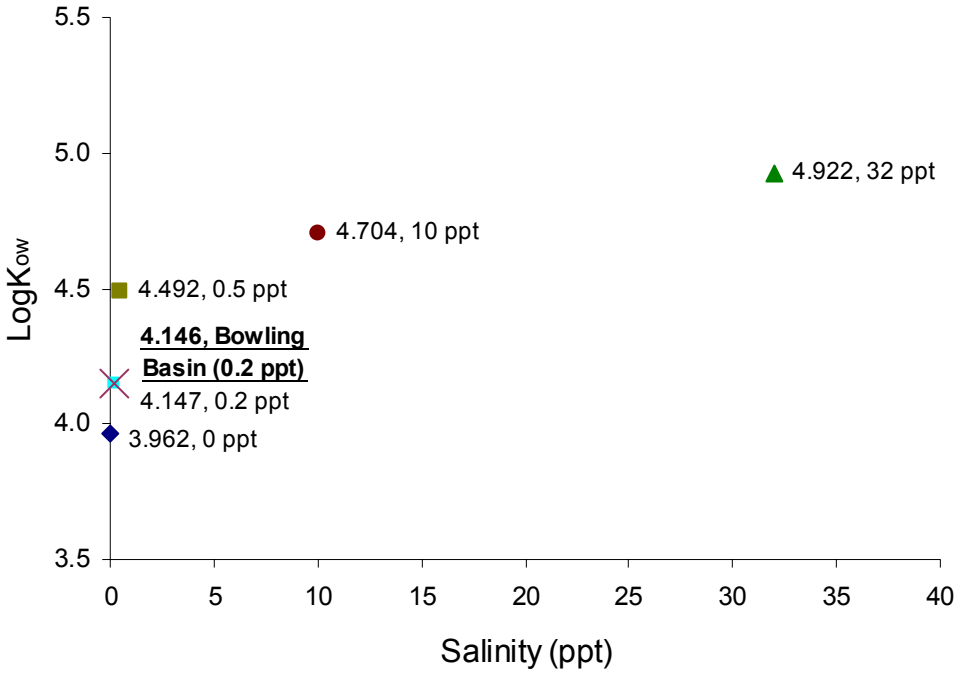

Figure 3.20 Log K_{ow} of TBT in water of various salinities

The results show the relationship between salinity of water and Log K_{ow}. Increased salinity resulted in higher Log K_{ow} values. Greater salinity is therefore likely to lead to higher accumulation of TBT within the lipid of organisms. The water from Bowling Basin, the salinity of which was 0.2 psu gave a similar Log K_{ow} value to synthetic water at 0.2 psu.

3.3.2 Solid:water partition coefficient (K_d)

The solid (soil and sediment):water partition coefficient (K_d) is of paramount importance in order to predict the behaviour and mobility of pollutants within the environment. The K_d value is determined as a plot of the Freundlich equation and yields the following linear relationship:

$$Q_e = K_d C_e^{1/n} \quad \text{(Equation 3.15)}$$

$$\text{Log } Q_e = 1/n \text{ Log } C_e + \text{Log } K_d \quad \text{(Equation 3.16)}$$

Where Q_e(mg kg^{-1}) and C_e(mg L^{-1}) denote the sorbed and aqueous concentration at equilibrium, respectively. The Equation 3.16 is the Log plot of Equation 3.15. A single point K_d value (calculated from Equation 3.15) has been used and reported but this results in poor accuracy (Langston and Pope, 1995). The K_d value obtained from a slope is also used as presented in Equation 3.15 this assumes that n is equal to 1 (Langston and Pope, 1995, Hoch et al., 2002, Hoch et al., 2003, Burton et al., 2004, Keenan, 2008) which can not be used to present the actual adsorption of TBT on the sediment surfaces. Therefore, the K_d value in the current study was obtained from intercept of a log plot of the Freundlich equation to improve the correlation coefficient and assess the actual adsorption behaviour of TBT.

The appropriate sediment-water ratio was investigated in accordance with the standard procedure to obtain the maximum adsorption of TBT concentration that fitted the Freundlich equation (ASTM, 2001). The sediments from Bowling Basin were selected because the site is still active, with contamination present (Bangkedphol et al., 2008) and therefore the prediction will be applicable. Following Equation 3.16, the working concentration range of TBT in water was decided for K_d

identification (ASTM, 2001). At 20 °C, the samples were shaken for 24 h to reach the equilibrium and the results are presented in Figure 3.21.

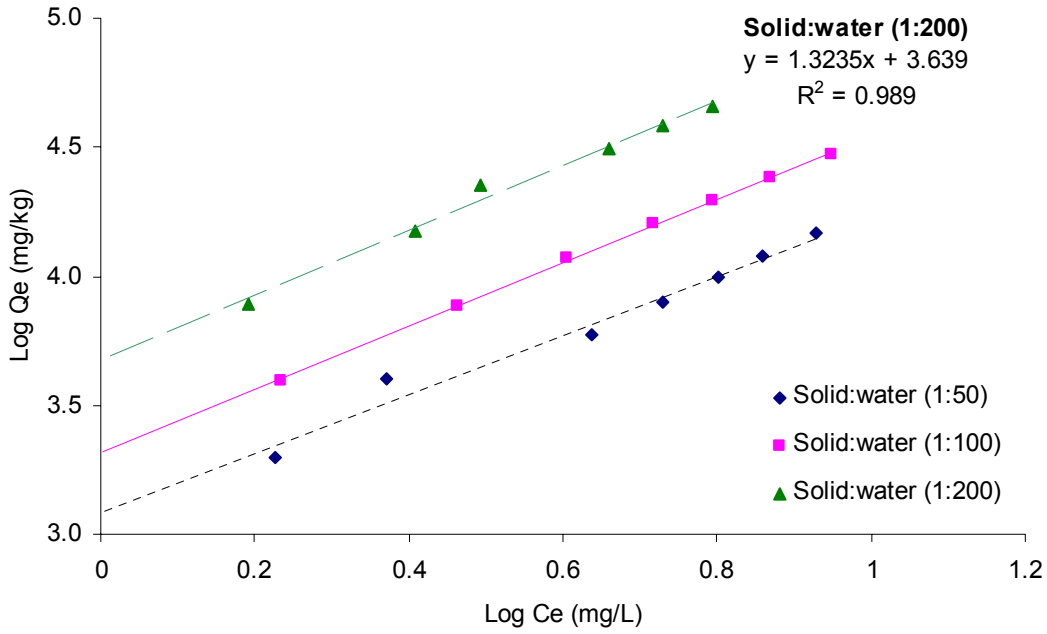

Figure 3.21 Freundlich adsorption isotherm of TBT on sediment from Bowling Basin at various sediment-water ratios

Figure 3.21 shows that the sediment-water ratio at 1:200 gave the maximum capacity of TBT on the sediments, Log K_d can be identified by the intercept on the y-axis of the Log plot in Figure 3.21. Under these conditions, the Log K_d of TBT for the Bowling sediments was 3.64. The maximum TBT concentration in water (240 µg mL^{-1}) from the experiment with sediment-water (1:200) was used to determine the equilibrium time. Time scales were varied from 15 minutes to 24 hours. The results are presented in Figure 3.22.

In addition to the sediment-water ratio at 1:200, the concentration of TBT in water higher than 300 µg mL^{-1} was ignored due to the adsorption behaviour not fitting the Freundlich adsorption isotherm. The surfaces of the adsorbents become

saturated and adsorption reaches a maximum (type L adsorption curve) at concentration higher than 300 μg mL^{-1}. Therefore, at this ratio, the working range of TBT concentrations in water at 40-240 μg mL^{-1} was studied.

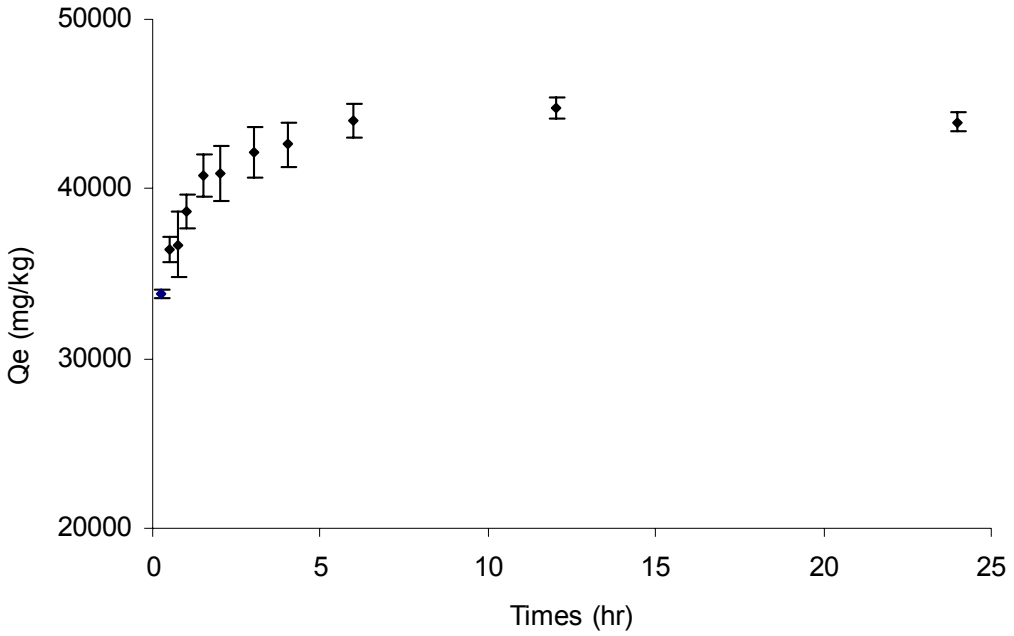

Figure 3.22 Adsorption of TBT on the Bowling sediment at various times

Figure 3.22 shows that the adsorption of TBT on the sediment was almost steady after 6 hours. Therefore, the shaking time was fixed at 12 h for the subsequently experiments to complete the steady state on the adsorption. The optimum conditions obtained were used in subsequent studies of the influence of other parameters on the partition coefficient K_d.

3.3.3 The effect of sediment properties, salinity, pH and temperature on K_d

The quality of water affects the adsorption of TBT on sediment. The Log K_d values were 3.64 for Type IV water and 3.34 L kg^{-1} for water taken from the Bowling Basin (Figure 3.23).

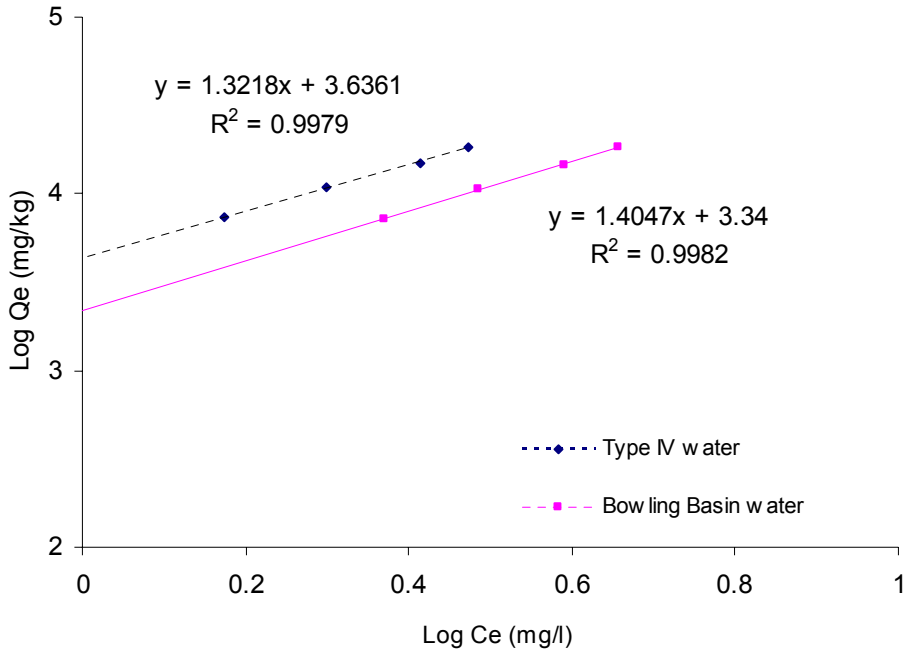

Figure 3.23 Freundlich adsorption isotherm of TBT on sediment from Bowling Basin for difference types of water (type IV and Bowling Basin water)

The lower Log K_d in the natural water is possibly due to the pH (pH 8) and salinity (0.2 psu) which were different from the Type IV water at pH 7.0 and zero salinity. Therefore, the effects of these parameters on the adsorption behaviour were studied. The results were input into the modelling program with the new values obtained providing a more accurate assessment for the natural conditions in terms of the toxicity and fate of TBT.

3.3.3.1 Effect of sediment properties

The characteristics of the sediments collected are presented in Table 3.4. The sediment samples were also tested for carbonate, which proved negative. Therefore, the total organic carbon is considered similar to the organic matter in sediment (ASTM, 2000).

Table 3.4 Properties of the sediment from the three study sites

Sediment sample	pH	* Moisture content (%)	TOC (%)	Particle size analysis (%)		
				sand	silt	clay
Bowling Basin	8.0	3.23	12.1	7.67	63.5	28.8
Port Dundas	8.0	2.85	17.4	17.4	53.0	29.6
Clyde River	7.5	0.37	1.21	79.5	0.97	19.5

* Wet sample moisture content required for recalculation to dry basis.

The isotherms of TBT on sediments were obtained at the optimum condition for the adsorption i.e. a sediment-water ratio of 1:200 and 12 h shaking time (Figure 3.24).

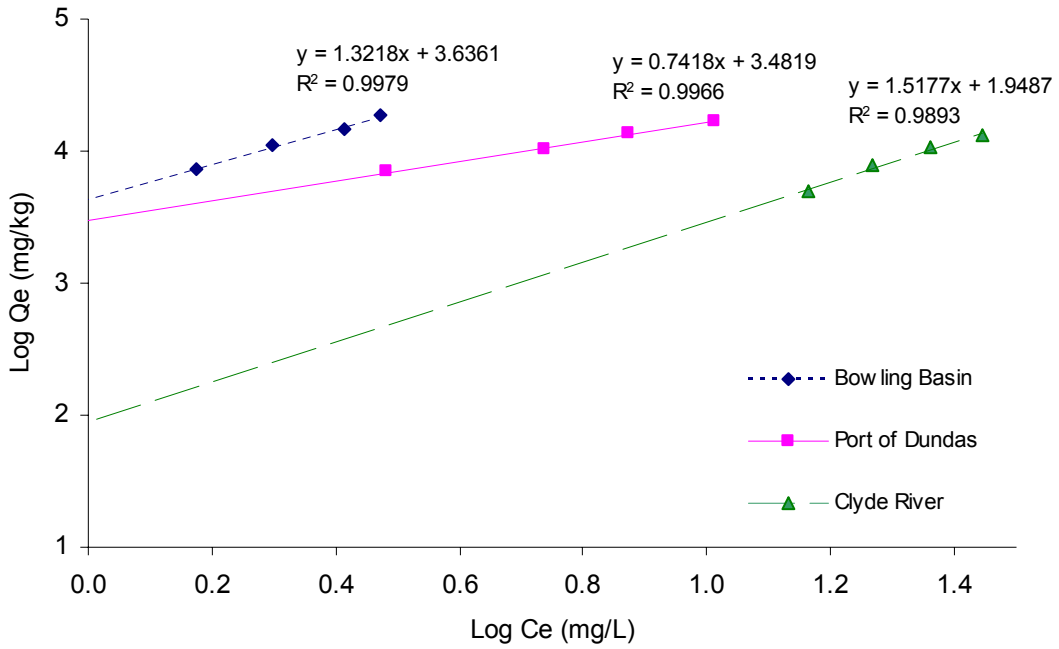

Figure 3.24 Freundlich adsorption isotherm of TBT on sediment from Bowling Basin, Port Dundas and Clyde River using the optimum conditions

The Log K_d of sediments from Bowling Basin, Port Dundas and the Clyde River were 3.64, 3.48 and 1.95, respectively. The sediment from Clyde River which contains considerably less organic carbon than the other sites had the lowest Log K_d. The result supports previous reports that organic matter in sediment increases the adsorption of TBT (Unger, 1988). Conversely, even though the organic carbon content in Bowling Basin sediments was lower than in Port Dundas, a higher Log K_d was found. It is possible that this phenomenon could be explained by the types and proportions of clay minerals present (see *Table 3.5*). Therefore the clay minerals in the three sediment samples were identified by XRD (Figure 3.25).

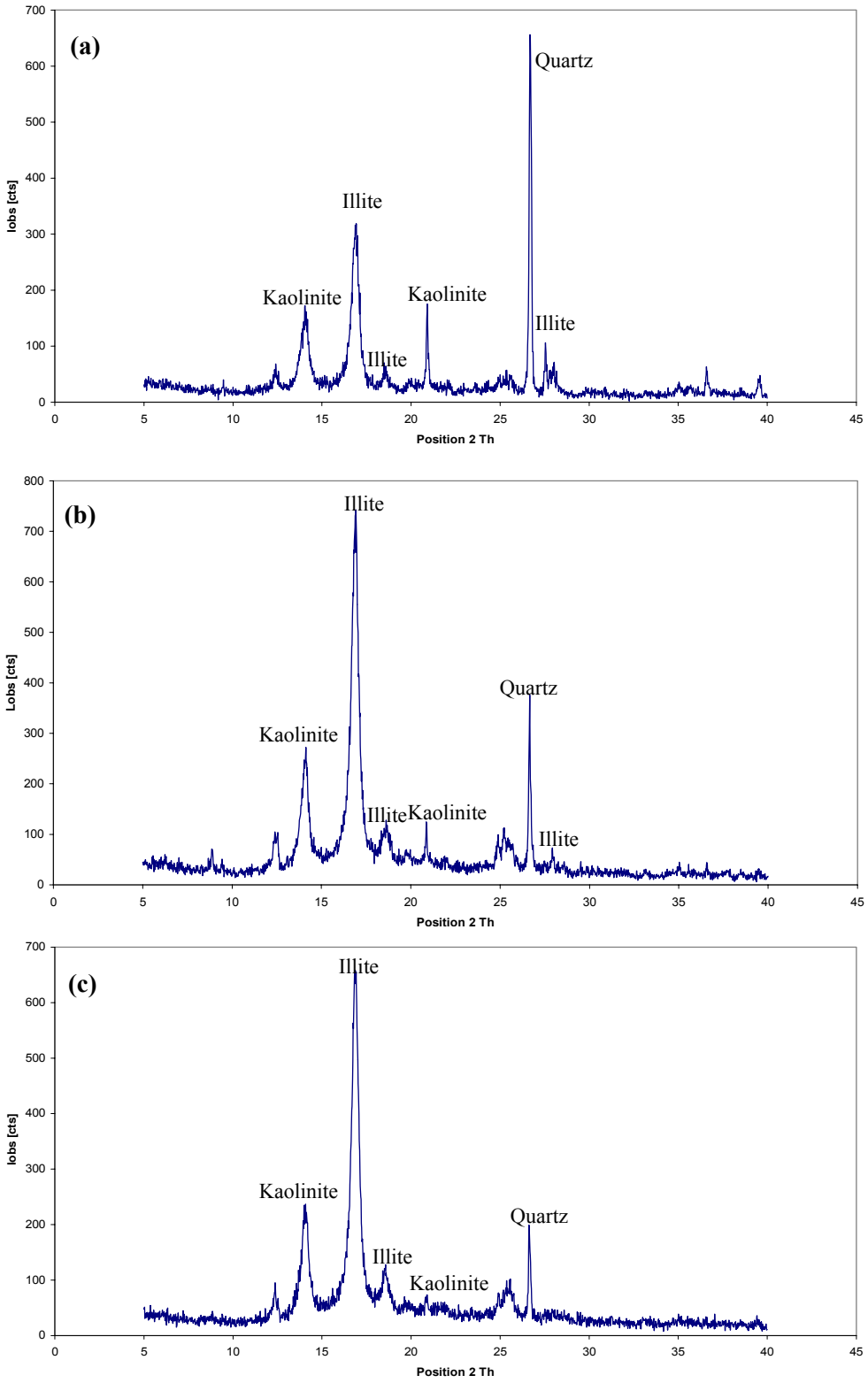

Figure 3.25 The XRD patterns of sediments from (a) Clyde river, (b) Bowling Basin, and (c) Port Dundas

Results of semi-quantitative analysis of the clay minerals are presented as relative intensity ratios of kaolinite:illite:quartz. The 2θ of the main peak of montmorillonite, kaolinite, illite, quartz are 5.89, 14.1, 16.9 and 26.7 respectively. Montmorillonite in the Forth and Clyde Canal samples was below the limit of detection. Generally, the affinities of the sorbents for TBT at pH 8 are reported to be in the order of kaolinite < kaolinite-illite mixture < montmorillonite ≈ illite (Hoch et al., 2002). In addition, the low adsorption affinity of kaolinite was supported by hydrogen bonding in the structure. Hydrogen bonds keep the structure relatively rigid and prevent the entering atom or molecule being adsorbed on the kaolinite structure (O'Neill, 1998). Thus, TBT which presents steric hindrance structure could not enter into the kaolinite. The Bowling Basin sediment appears to contain the highest proportion of illite, therefore this can explain why it showed a greater Log K_d even though it contained lower organic carbon content than the sediment from Port Dundas. In addition, the d-spacing of illite is bigger than kaolinite (*see section Colloidal chemistry of inorganic constituents)* which supported the higher adsorption of TBT in illite.

Table 3.5 The relative intensity ratio of clay minerals in sediments as determined by semi quantitative XRD spectroscopy

Sediment sample	Intensity Ratio kaolinite/illite/quartz
Clyde River	1/1.8/3.8
Bowling Basin	1/3.0/1.5
Port of Dundas	1/2.8/0.8

In general, organic carbon is believed to be a major factor to predict the adsorption behaviour of TBT on sediment. However, this study demonstrates that the clay minerals are also important, particularly in samples with similar organic carbon content, where the types of the clay minerals present may strongly affect TBT sorption behaviour.

3.3.3.2 Effect of salinity

The effect of salinity was studied on the Bowling Basin sediments with Type IV water. The salinity range was varied from 0 to 100 psu. The results are shown in Figure 3.26.

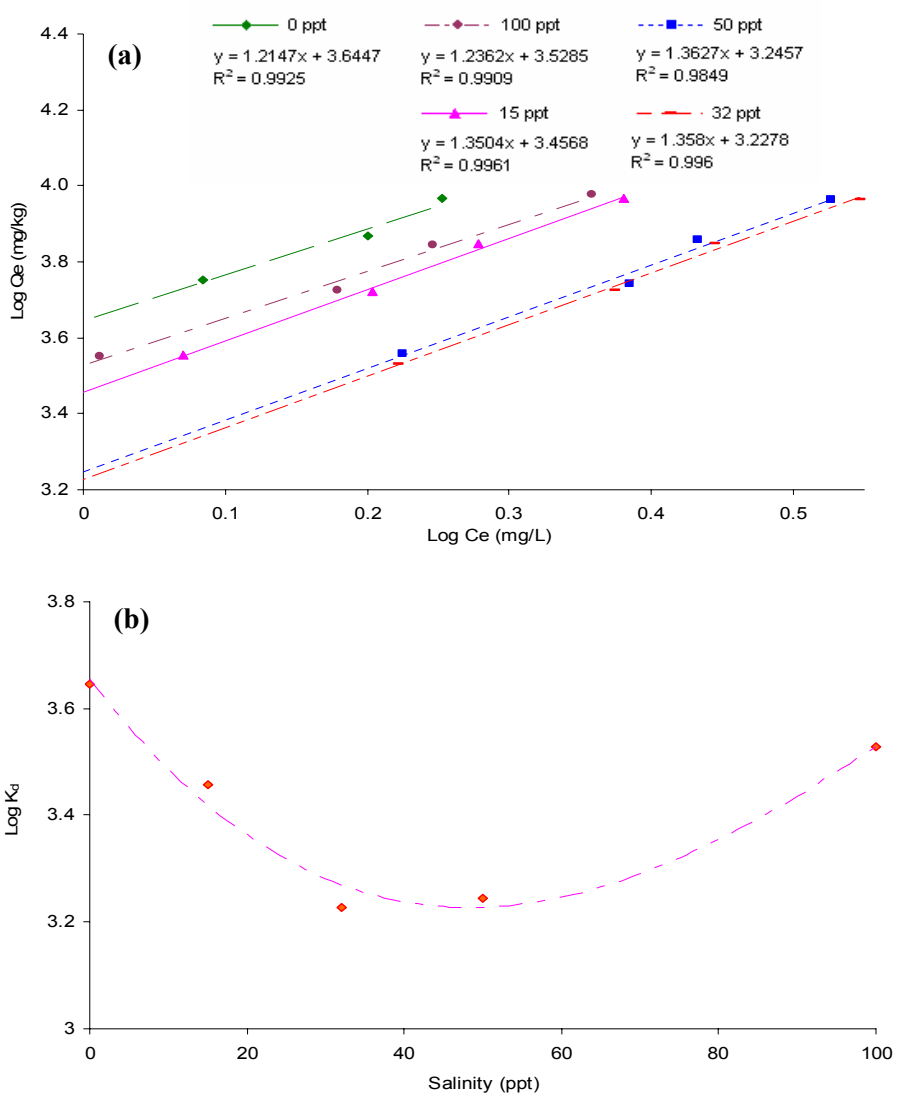

Figure 3.26 (a) Freundlich adsorption isotherm of TBT on Bowling Basin sediment at various salinities of water (n=3, SD < 0.0023%), and (b) relationship between Log K_d and salinity of water

Figure 3.26 shows the effect of salinity on TBT adsorption for the Bowling Basin sediments with Type IV water. The results show that adsorption was greatest in freshwater and began to decrease at low and intermediate salinities. Then the Log K_d increased again at high salinities. This could be explained by the capacity of TBT to show characteristics of both metal ions and hydrophobic properties with respect to partitioning. It is typical of hydrophobic compounds that the adsorption of TBT increases with salinity because of "salting out" (Harris, 1987). However, at low salinity the decreasing of TBT adsorption is more consistent with the behaviour of metal cations (Unger, 1988). At higher salinities, more competition for adsorption sites by cations, in this case K^+, led to less negatively charged particulate matter and resulted in decreased adsorption.

3.3.3.3 Effect of pH

The pH is an important factor in controlling the partitioning of butyltin compounds, since this parameter not only affects the surface properties of the clays but also the aquatic chemistry of the organotin species (Hoch et al., 2002). Varying the pH of the system was achieved by addition of acid or base (0.1M) (Burton et al., 2004). The pH of water was measured before and after the experiment (Table 3.6).

Table 3.6 pH of water before and after the adsorption experiment

pH	Before adsorption	After adsorption
4	4.07	4.32
5	5.08	5.20
6	6.01	6.17
7	7.05	7.16
8	8.07	7.89

The effect of pH on K_d was studied for the Bowling Basin sediments with Type IV water. The pH of water was measured before and after the adsorption experiment to confirm that it was constant. The variation of Log K_d values are presented in Figure 3.27.

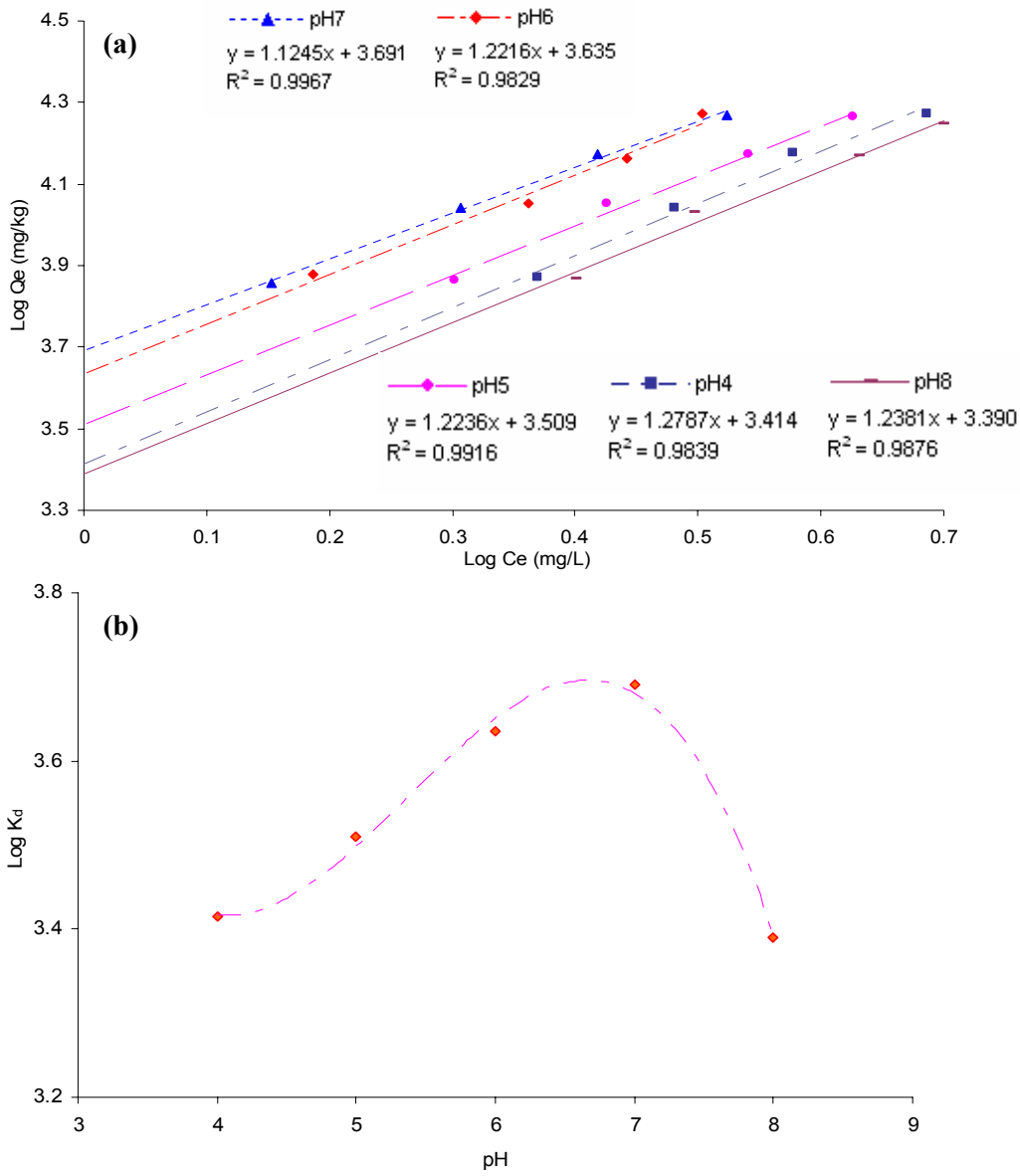

Figure 3.27 (a) Freundlich adsorption isotherm of TBT on Bowling Basin sediment at various pH of water (n=3, SD < 0.0013%), and (b) relationship between Log K_d and pH of water

The results show the highest adsorption of TBT occurs at pH 7. There are 2 main reasons as to why this should occur;

(i) The pKa of TBT is approximately 6.51 depending on the experimental conditions (Fent and Looser, 1995). At pH < pKa, cations are formed as the predominant species in water, when pH > pKa the neutral hydroxo-complex TBTOH dominates as shown in Equation 3.17.

$$TBT^{+}.nH_2O \leftrightarrow TBTOH + H^{+} \qquad pKa = 6.51 \qquad \text{(Equation 3.17)}$$

(ii) The zero point of charge (pHzpc) is the pH at which the surface exhibits a neutral net electrical charge. The pHzpc of clay minerals including kaolinite, illite, montmorillonite is approximately 4 (Hoch et al., 2003). Thus, raising the pH over 4 increases the negative charge on the surface of the clay minerals. In contrast, these clays exhibit a positive charge at pH < 4. Therefore, the adsorption zone is at pH 6.5 and this gives the highest adsorption of TBT on sediment surface. At pH 6.5 the TBT cation is the main species, therefore this suggests that electrostatic attraction is the driving force for adsorption between the negative charged clay surface and the positive charged TBT molecules.

3.3.3.4 Effect of temperature

The effect of temperature was studied on the Bowling Basin sediments with Type IV water. The study temperatures were varied from 20 to 50 ^{o}C using an incubator shaker. The results are shown in Figure 3.28.

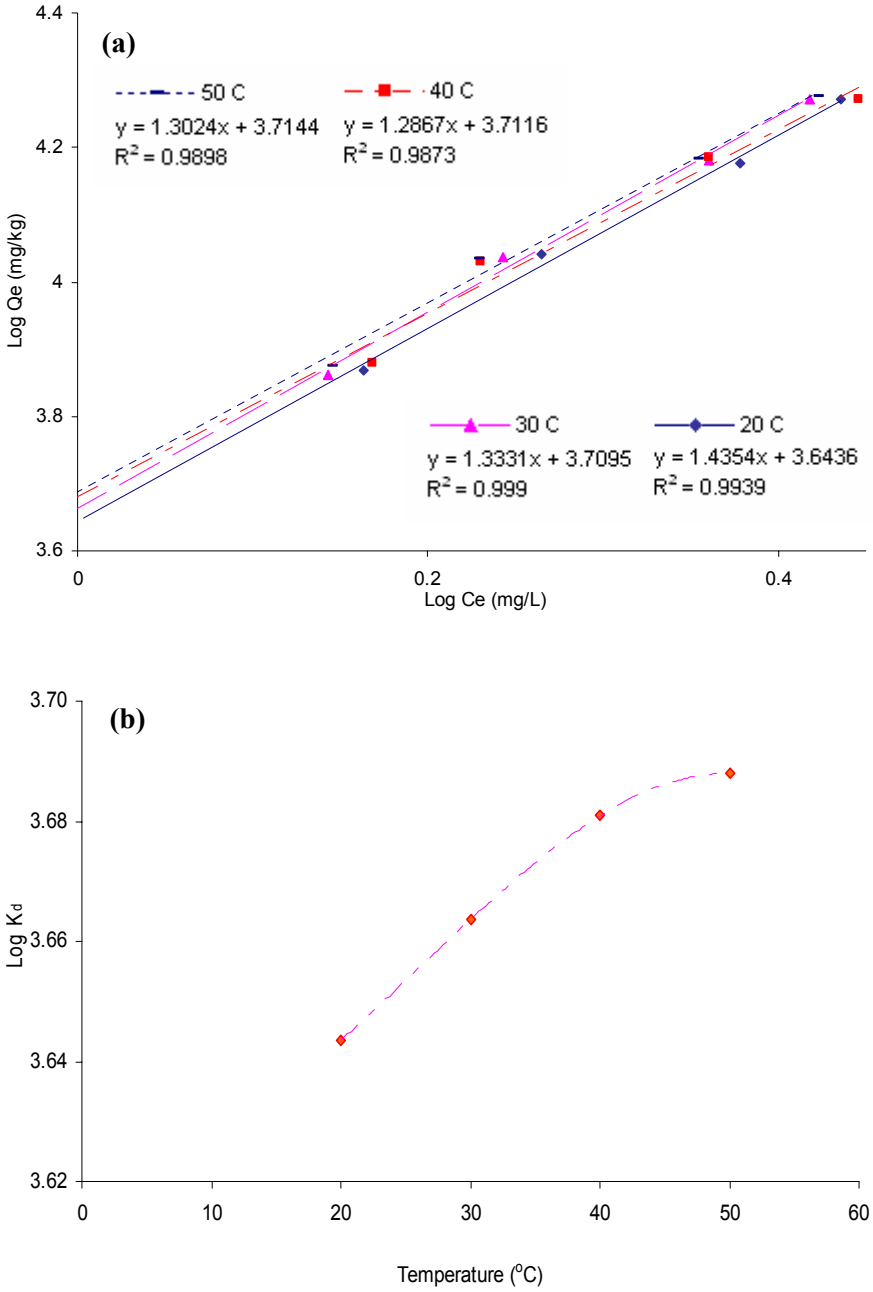

Figure 3.28 (a) Freundlich adsorption isotherm of TBT on Bowling Basin sediment at various temperatures (n=3, SD < 0.0004%), and (b) relationship between Log K_d and temperature of water

From Figure 3.28(b), the adsorption of TBT on sediment slightly increases at higher temperature. This can be clarified in that the adsorption of atoms/molecules on surfaces and interlayers of sorbents is related to the Gibb's surface concentration

equation as previous mentioned (*see section Adsorption isotherm*) (Bajpai and Vishwakarma, 2003, Ip and Toguri, 1994, Tan, 1998). Increasing temperatures reduce the surface tension of water (Rinker, 1994), which then produce a higher Gibb's surface concentration (Γ) (*see Equation 3.10*). These lead to increase in adsorption on the sediment surface.

3.3.4 Prediction of environmental fate and toxicity

The experimental values of Log K_{oc} and Log K_{ow} calculated by the Equations 3.13 and 3.14 respectively were compared to calculation values from EPISuite, as presented in Table 3.7.

Table 3.7 Comparison of experimental and calculation partition coefficients

Parameter	Log K_d ($L\ kg^{-1}$)	$K_{oc} = K_d$ X100/%OC ($L\ kg^{-1}$)	Log K_{oc} ($L\ kg^{-1}$)	Log K_{ow}
Bowling Basin (water from site): Experimental	3.34	18,087 (%OC = 12.10)	4.26 (K_{oc} = 18,197)	4.15 (K_{ow} = 14,125)
EPISuite program :Default	N/A	12,023	4.08 (K_{oc} = 12,023)	4.70 (K_{ow} = 50,118)

N/A: not available

Table 3.7 shows the considerable difference between experimental values obtained and the values given from the computational model. The EPISuite program underestimates K_{oc} but overestimates K_{ow} values. The program calculation uses only the inherent chemical and physical properties of TBT and does not account for local environmental conditions. The different coefficients lead to dissimilar predictions of environmental fate and toxicity. Subsequently, the experimental values of K_{oc} and K_{ow} were entered into the program to create a more accurate prediction based on

natural conditions. A comparison of the prediction data between using the input from the experiment and default values is presented in Table 3.8.

Table 3.8 Comparison of the predictions obtained using experiment and default values as the input for the EPISuite program

Input values [a] (K_{oc} and K_{ow})	Partitioning (%)			Toxicity in fish ($\mu g\ mL^{-1}$)	
	Air	Water	Solid	LC_{50} [b] (14 Day)	ChV [c] (30 day)
Experimental values	1.98	22.3	75.7	3.37	0.39
Default values	3.65	33.9	62.4	1.11	0.13

[a]Input values are the K_{oc} and K_{ow} values from Table 3.7

[b]Lethal concentration 50 is the concentration of a material that will kill 50% of the test subjects

[c]Chronic value is the geometric mean of the lower and upper chronic limits

Table 3.8 indicates considerable differences between predicted experimental fate and toxicity of TBT depending on whether experimental or default input values were used. The experimental prediction showed lower toxicity than the default model for Bowling Basin but this represents the actual toxicity and accumulation at the natural site. Moreover, the environmental fate in term of partitioning for TBT was very different for the experimental values compared to the default values obtained. The percent partitioning to solid was increased, therefore, bioaccumulation might be greater in mud dwelling bottom feeding fish. Also higher bioaccumulation may occur for all fish as contaminated suspended solids are ingested.

The default model is useful as a general indicator of environmental fate and toxicity. However, results based on experimental data differ greatly from those

predicted by EPISuite. Therefore, experimentally-derived parameters (K_{oc} and K_{ow}) are necessary for site-specific investigations. This can help with an understanding of real behaviour of TBT in a local area and provide more effective remediation solutions.

One of the most significant findings of this work is the underestimate of K_{oc} in the computational model as presented in Table 3.7. If only the computational calculation is used in decision-making, there will be a danger that the solids are not properly treated and remediated. This could lead to more widespread contamination through environmental transport pathways, risk may be magnified, and subsequent costs of remediation may be increased. It is thus clear that the default model, although useful as a general indicator of TBT behaviour, is imprecise when applied to a specific site and thus cannot replace experimentation.

3.3.5 Desorption of TBT

Nanopure water (representing type IV water), Bowling Basin water (pH 8.2, salinity 0.2 psu) and artificial seawater (pH 8, salinity 32 psu) were used to desorb TBT from the sediment surface. Desorption study was performed from 30 minutes to 24 hours. The % desorption of TBT are presented in Figure 3.29.

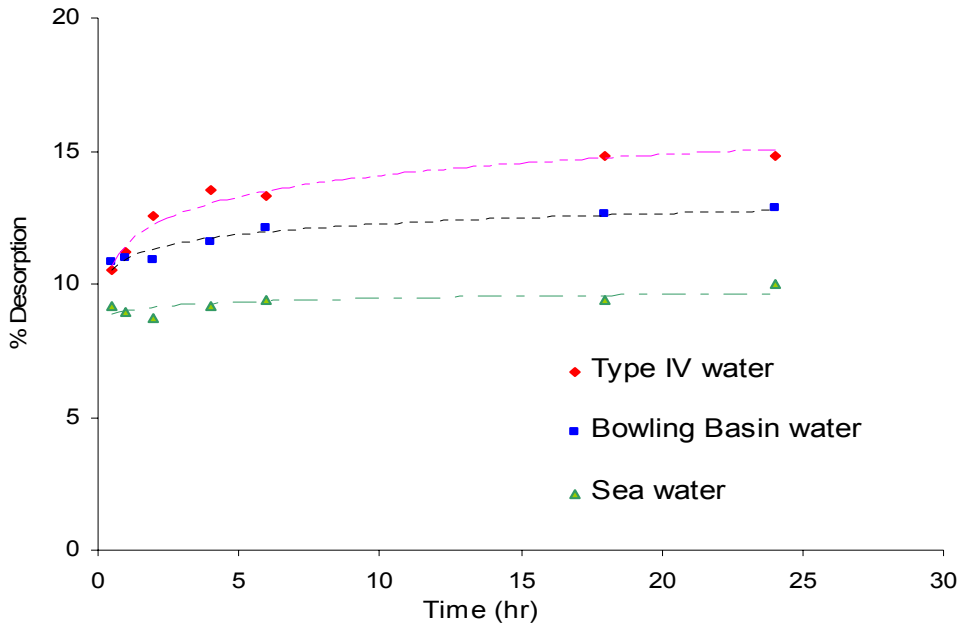

Figure 3.29 % desorption of TBT from Bowling Basin sediment in various type of waters

Figure 3.29 shows that % desorption of TBT in type IV water is the highest. This is because desorption of TBT is related to solubility, where the solubility is depending on water composition such as salinity. Salinity affect the increasing of ionic strength of water which reduce the solubility of TBT in water (Rydberg, 2004). Thus, less salinity of type IV water can increases desorption of TBT from sediment surfaces.

For the natural condition, desorption using water from Bowling Basin, % desorption is presented 12.9% in 24 hours. Moreover, a previous study from Landmeyer indicated that the adsorption of TBT on sediment is a reversible process: the compound can desorb back to the aqueous phase until the equilibrium point is reached. At equilibrium TBT is present both in water and sediment (Landmeyer et al., 2004). These finding infer that sediment could represent a continuing source for TBT. Contamination of TBT in water could then become considerable. It is therefore necessary to study the remediation process of TBT in water. In this study, catalytic

photo-degradation of TBT in water was studied and the degradation efficiency improved **(Chapter 4)**.

3.4 Summary

The K_{ow} and K_{oc} (calculated from K_d) were used as input values for the EPISuite program to predict the fate and toxicity of TBT. For the default prediction, the partitioning coefficients were calculated from only the inherent chemical and physical properties of TBT but did not account for the site-specific environmental conditions. Therefore, K_{ow}, K_d and K_{oc} were derived by experiment. Experimental values can estimate the actual toxicity and potential for accumulation at a specific site which leads to more appropriate decision-making for remediation.

The variations of partition coefficients were studied as a function of TBT concentration, time, solid:water ratio, pH, salinity, sediment type and temperature to understand and explain the adsorption behaviour of TBT in the natural environment. The log octanol-water partition coefficient (K_{ow}) of values obtained for TBT ranged from 3.9 to 4.9 depending on salinity. These values presented the potential for bioaccumulation and biomagnification through the food chain which may attain levels dangerous for the consumer even if they are safe for the species itself (Keenan, 2008). The sediment-water partition coefficient (K_d) was determined by Freundlich adsorption isotherms, the optimised parameters which fitted the equation were solid:water ratio; 1:200, TBT concentration in water; lower than 240 $\mu g\ mL^{-1}$, the equilibrium time; 12 hours. The K_d values obtained ranged from 88 to 4,909 $L\ kg^{-1}$ depending on the following.

(i) Sediment organic carbon and clay mineral content which were also an important factor to forecast the sorption behaviour.

(ii) Salinity, as TBT showed characteristics of both metal ions and hydrophobic properties with respect to partitioning. Therefore, sorption was greatest in freshwater, then began to decrease at low and intermediate salinities. This could indicate that bioavailability is enhanced in the marine environment, then increased again at high salinities but at values not typically experienced in the environment (100 psu).

(iii) pH, as the highest adsorption of TBT is at pH 7 due to the charge contained on clay surfaces and dominant species of TBT (TBT^{+}).

(iv) Temperature, where the adsorption of TBT on sediment slightly increases at higher temperature due to the reduction of surface tension which increases the Gibb's surface concentration (Γ).

It could be concluded that modelling based on chemical and physical properties although a useful tool should never replace realistic experimentation. In this instance it is inappropriate for scientists to move entirely away from laboratory testing toward computational models.

CHAPTER 4

Photo-degradation of Tributyltin by N-doped TiO_2 Photocatalyst

4.1 Background

As mentioned in previous chapters, TBT still contaminates many aquatic systems at concentrations that cause adverse physiological effects on organisms and mammals (Antizar-Ladislao, 2008). TBT is initially released into water, partitioned and accumulated in soil and sediments (Burton et al., 2004). From **Chapter 3**, the partitioning ratios of TBT in solid-water system were indicated and the % desorption of TBT were approximately 10-15% in 24 hours. The partitioning ratio of TBT in solid-water system is approximately 3:1 (Bangkedphol et al., 2009). At equilibrium TBT is present in both in water and sediment (Landmeyer et al., 2004). This infers that sediment could represent a continuing source for TBT, resulting in ongoing contamination of water. This contamination of TBT by water could become considerable. The contaminant also accumulates in aquatic organisms due to the bioavailability of TBT in water media (Extoxnet, 1996). Accordingly, many researchers have focused on the impacts of TBT on living organisms and plants, and also on effective options for TBT degradation. Therefore, the remediation process of TBT in water is important to study.

Remediation is a procedure to treat a contaminated site by reducing the amount of the substances below safety levels for health protection. Degradation of pollutants is one of the processes that reduce toxicity. Generally, remediation technologies can be classified as *in situ* or *ex situ*. *In situ* remediation involves treating the contaminated material at the site while *ex situ* involves the excavation and removal

of the contaminated material to be treated elsewhere. *In situ* techniques have the advantage of treating the contamination in place so that large quantities of soil, sediment or water do not have to be dug up or pumped out of the ground for treatment. Several approaches to remediation exist which can largely be divided into chemical, physical and biological classes. These methods are separated by the different action used to degrade the hazardous contaminants into less toxic or non-toxic substances (Maguire and Tkacz, 1985).

Bioremediation is defined as any process that uses microorganisms, fungi, green plants or their enzymes to return the environment altered by contaminants to safe levels. The disadvantages of this process are the limitation of an initial concentration of pollutant, time consuming and complicated to control the process. For example, Harino presented the degradation of TBT in water by microorganisms within 18-42 days depending on the condition (Harino et al., 1997a).

Chemical remediation is a treatment technology that relies on a range of chemicals to initiate reaction to destroy, transform or immobilise contaminants. This process is a potential method for clean up of contaminated sections of the environment because this process can be completed within short time scales, typically weeks or months. A disadvantage of this process is the high running costs and also the need to introduce the chemical effectively into the environment. This may cause contamination by the remaining chemical (Hoch, 2001).

Physical remediation is an environmental friendly method used to clean up the environment. A disadvantage of this process is its poor degradation efficiency. The degradation level of contaminations is normally slow; typically months or years. However, this process can be improved by the optimisation of effective parameters, for example addition of an effective catalyst into the water, specific design of the reactor etc. Photo-degradation is one of the techniques of interest for removing TBT from surface water and sediment utilising UV and solar light radiation (Maguire and Tkacz, 1985, Navio et al., 1993, Navio et al., 1996, Saeki et al., 2007).

Previous work indicates that neither volatilization nor degradation of TBT species dissolved in water occurs over a period of 2 months in the dark at room temperature. In sunlight, the compound undergoes slow photolytic decomposition in water, with a half-life ($t_{1/2}$) > 89 days in water and about 120-150 days in water-sediment mixture (Maguire and Tkacz, 1985). Navio and colleagues reported the improvement of photo-degradation in a UV reactor that showed approximately an 80% reduction of TBT concentration in water within 30 h (Navio et al., 1993). However, this efficient process is limited in the natural environment by the relatively lower intensity of UV in natural light (Maguire and Tkacz, 1985, Chen et al., 2005). Photocatalytic degradation is an alternative approach to enhance TBT degradation without the need for intense UV irradiation. Titanium dioxide (TiO_2) is frequently used as a photocatalyst because of its availability, stability and low toxicity. TiO_2 is naturally found in mineral sources such as anatase, rutile and brookite. In particular, the anatase form of TiO_2 has been utilized in many photo-degradation reactions. Generally, both anatase and rutile forms of TiO_2 are used as photocatalysts and some research stated that anatase had higher photo-activity than rutile (Linsebigler et al., 1995). There are also other studies which claimed that a mixture phase between anatase and rutile provided higher efficiency than the pure phase (Muggli and Ding, 2001, Jie et al., 2009). All these different results depend on the intervening effect of several factors such as specific surface areas, crystallite sizes, and recombination process.

The photocatalytic mechanism of TiO_2 catalyst involves irradiation of electron-hole pairs in the valence band of TiO_2 catalyst by light of energy higher than that of the band gap (Choi et al., 2006). Overall, photocatalytic reactions can be generally summarized as displayed in Figure 4.1. Initially, e^- and positive holes (h^+) are generated by using photon energy (hν) which has equal or higher energy than the band gap energy of TiO_2. Some electrons (e_{cb}^-) are excited into the conduction band whilst holes (h_{vb}^+) still stay in the valence band and then both of them will move to the TiO_2 surface with a view to reducing or oxidizing. In most studies on photocatalysts, oxygen (O_2) plays a vital role as the primary electron acceptor. In this step, electrons will transfer to oxygen molecules to form superoxide radicals ($O_2^{\cdot -}$),

which subsequently react with protons (H^+) to produce hydroxyl radicals ($^{\cdot}OH$). Meanwhile, h_{vb}^+ reacts with adsorbed water molecules on the surface or surface titanol group (>TiOH), and finally hydroxyl radicals, which initiate photo-degradation are also formed. On the other hand, e^- and h^+ are able to recombine, which can occur in the bulk and at the surface. The recombination process is usually considered as the deactivation process in photocatalytic reaction (Maness et al., 1999, Sirisaksoontorn et al., 2009).

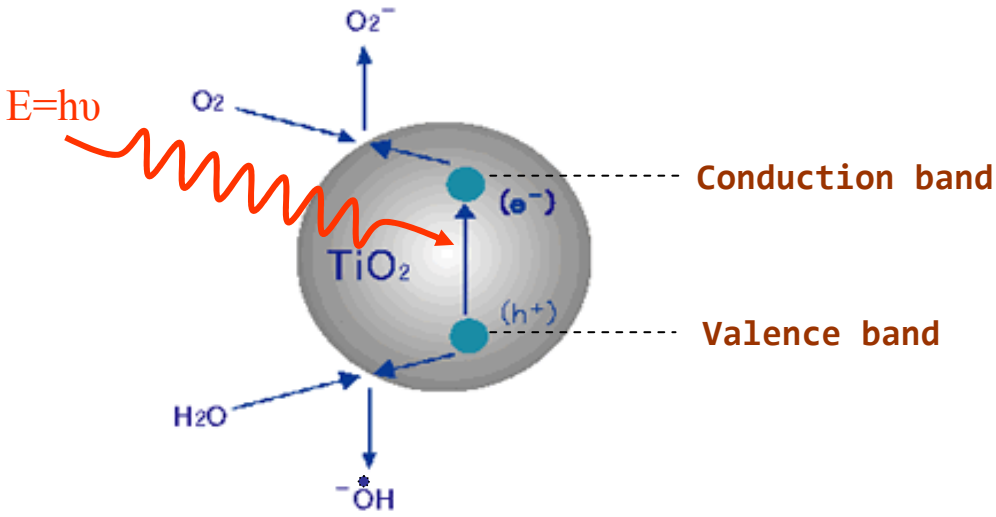

Figure 4.1 Principal processes on the TiO_2 particles

Previous studies discussed degradation of toxic compounds, such as bisphenol A, volatile organics and polycyclic aromatic hydrocarbons (Horikoshi et al., 2007, Tsoukleris et al., 2007, Zhang et al., 2008). However, there is only one reported attempt at the photo-assisted degradation of butyltin in aqueous TiO_2 suspensions (Degussa P25, 1-5 μm) calcined at 500 ºC in an UV reactor. This achieved a 30% reduction in TBT concentration within 30 h (Navio et al., 1996). The lower degradation rate than that without catalyst might be caused by the specific energy of the UV used in the reactor not matching sufficiently well the catalyst's band gap energy, and the slightly large particle size of catalyst used. Navio also concluded that

butyltins are highly resistant to photo-degradation by both UV-photolytic and TiO_2 photo-assisted oxidation (Navio et al., 2009).

The band gap energy of TiO_2 corresponds to a wavelength of UV light < 400 nm (Navio et al., 1996, Nakamura et al., 2004). Since sunlight consists mainly of visible wavelengths, these do not fit with TiO_2 band gap. Moreover, there is only 3-4% of an ultraviolet part in the natural light that transmits through to the earth's surface (Chen et al., 2005). This reduces the ability of TiO_2 to degrade toxic compounds under natural illumination. Consequently, the present study substituted some oxygen atoms of the TiO_2 with nitrogen atoms to improve the photo-degradation ability of the catalyst under natural conditions. Although there are several kinds of anion dopants such as B, C, N, S, F as well as co-dopants, N anion dopants seem to be the most popular anions because its anion size is closest to that of the oxygen anion in TiO_2 lattice (Wang et al., 2005). The resulting mixed state of N_{2p} and O_{2p} lowers the band gap of TiO_2 so that irritations with sunlight can excite electrons from the valence band to the conduction band (Asahi et al., 2001). The modified band structure of N-doped TiO_2 is shown in Figure 4.2.

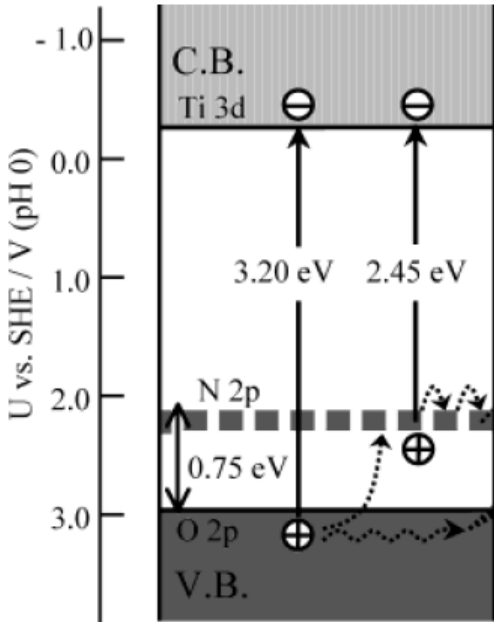

Figure 4.2 Schematic illustration of the expected energy bands for N-doped TiO_2 (anatase) together with some photoinduced electronic process (Nakamura et al., 2004)

In this work, catalysts were prepared in the laboratory using a sol-gel method. This method is efficient for tailoring nanostructured materials with increased surface area of catalyst and that are simple to handle at room temperature (Shioji et al., 2004). This can improve the degradation ability of the catalyst under visible and natural light (Ksibi et al., 2008). The sol-gel method is composed of four key steps as follows;

Wet solution; This step focuses on gel formation, which is a diphasic material with a solid encapsulating solvent. Before gel formation occurs, a starting material is hydrolyzed and partially condensed in order to form a sol, which is liquid suspension in solid particles. After that, further condensation in a three-dimension network is conducive to gel formation. In the case of metal alkoxide precursors, all reactions involved are shown below.

Hydrolysis reaction: $\equiv M\text{-}O\text{-}R + H\text{-}O\text{-}H \rightarrow \equiv M\text{-}O\text{-}H + R\text{-}O\text{-}H$

Condensation reaction: $\equiv M\text{-}O\text{-}X + H\text{-}O\text{-}M\equiv \rightarrow \equiv M\text{-}O\text{-}M\equiv + X\text{-}O\text{-}H$

Where X is an alkyl group(R) or H.

Aging; To further complete the reaction, the gel is left to continue constructing more networks causing stronger cross-linkage. Moreover, some solvent molecules are expelled by the extensive condensation of gel. This step mainly depends on aging time and temperature, as well as pH.

Drying; In order to remove organic solvent or hydrolyzed molecules, the metal oxide needs to be heated at the sufficient temperature to dispel them. Additionally, this step is involved in the capillary pressure that has an effect on the pore size of the metal oxide. Therefore, many factors, such as heating rate, pressure rate and time, are taken into serious consideration with a view to controlling the pore structure of the metal oxide.

Calcination; This final step controls the crystallization of the metal oxide. Calcination is used to remove the dormant organic residues and to crystallize the metal oxide. However, it will inevitably cause a decrease in surface area, loss of surface hydroxyl groups and even phase transformation.

Photocatalytic degradation of TBT upon N-doped TiO_2 under visible or natural light irradiation has not previously been reported in literature. Therefore, the main objective of this work was to study the enhancement of degradation of TBT, in visible and natural light, by nanoparticles of N-doped TiO_2 which have been prepared by the sol-gel method. The photo-activity of the synthesized catalyst was compared with those of undoped-TiO_2 and P25-TiO_2, a standard commercial material

for photocatalytic reactions, consists of 75% anatase and 25% rutile (Ohno et al., 2001).

4.2 Experimental

4.2.1 Materials and equipments

The analytical standards and all reagents for butyltins analysis used were similar to **Chapter 2** (*see section 2.2.1*). Titanium (IV) tetraisopropoxide (AR grade) was obtained from ACROS (New Jersey, USA). Degussa P25-TiO_2 was obtained from S.M. chemical (Bangkok, Thailand). Samples for X-ray powder diffraction (XRD) analysis were deposited on a silicon wafer sample holder and characterized using a Philips Pw 1830 X-ray diffractometer (Cu Kα, 1.5418 Å). The morphology and particle size of all catalysts were investigated by transmission electron microscopy (TEM) recorded on a JEOL 1200 EX, 120 keV electron microscope fitted with a standard tungsten filament and operated at 80 keV. Images were recorded digitally using a Mega View II digital camera with Soft Imaging System GmbH analysis 3.0 image analysis software and/or on KODAK Electron Image Film SO-163. Samples for TEM were diluted in ethanol solution, then deposited onto Formvar-coated, carbon-reinforced, 3-mm-diameter copper electron microscope grids and left to air-dry prior to analysis. The morphology of all N-doped TiO_2 catalysts was also determined by scanning electron microscopy (SEM) recorded on a JEOL JSM-5600Lv scanning electron microscope fitted with tungsten filament. Each of the powdered samples for SEM was spread on a carbon tape mounted on a SEM stub and needed to be coated with Pt/Pd prior to SEM operation. The percentage of nitrogen in the photocatalyst was determined by LECO CHNS-932 Elemental Analyzer using sulfamethazine as a standard material. About 2.000 mg standard reference, sulfamethazine, was required, in order to check the instrumental accuracy which shows that the percentages of C, H, N and S were congruent with the standard values, that is, C 51.78%, H 5.07%, N 20.13% and S 11.52%. Then three-replicated

samples weighted in tin capsules about 2.000 mg in each replica were analysed. The amount of butyltins was identified by GC-MS systems, which were a Hewlett-Packard 5980 gas chromatograph/quadrupole mass spectrometer (Ramsey, Minnesota, USA) and a Thermo Scientific DSQ™ II single quadrupole GC-MS system (Loughborough, Leicestershire, UK).

4.2.2 Catalyst preparation

N-doped TiO_2 catalyst was prepared following the sol-gel method (Wang et al., 2005, Sirisaksoontorn et al., 2009) by the addition of 5 mL of 25% ammonia solution to 10 mL of titania precursor. In this work, Titanium (IV) tetraisopropoxide was chosen as the main starting material because it is generally used for TiO_2 synthesis (Qourzal et al., 2004, Jie et al., 2009) and for commercial P25-TiO_2 (Sivalingam et al., 2003, Nagaveni et al., 2004). After the reactions, the mixture was incubated at 30 ºC for 1 h and the temperature then raised to 105 ºC for a further hour to obtain a pale yellow solid. Subsequently, the solid was calcined at temperatures between 300–600 ºC for 1 h to provide catalysts for further characterization. The colour of catalysts varied depending on the calcination temperature, from brown at low temperature to white and light yellow at high temperature. Undoped TiO_2 was prepared under the same conditions as N-doped TiO_2 except that nanopure water was added into the titania precursor instead of ammonia solution.

4.2.3 Photo-degradation activity

Photocatalytic activity was assessed by the photo-degradation of TBT under artificial visible light and under natural light (in June 2009, Glasgow, UK). A stock solution of TBT 1,000 μg mL^{-1} was prepared in methanol. From the stock solution, 10 μg mL^{-1} working solutions in nanopure water were freshly prepared prior to undertaking the reaction. The photocatalytic degradation was carried out in 250 mL

beaker containing 150 mL working solution and 0.10 g of catalyst at room temperature (25-30 ºC). For the visible irradiation, the photo-degradation reaction of TBT was studied by using the developed photoreactor (Figure 4.3). The current adaptor has necessarily been used for the adjustment of AC 220V to DC 12V. The reactor contained a set of magnetic stirrers, and included a 250 mL foil-covered beaker equipped with a cut off filter. This reactor can maintain the inside temperature to 30 ºC during the reaction.

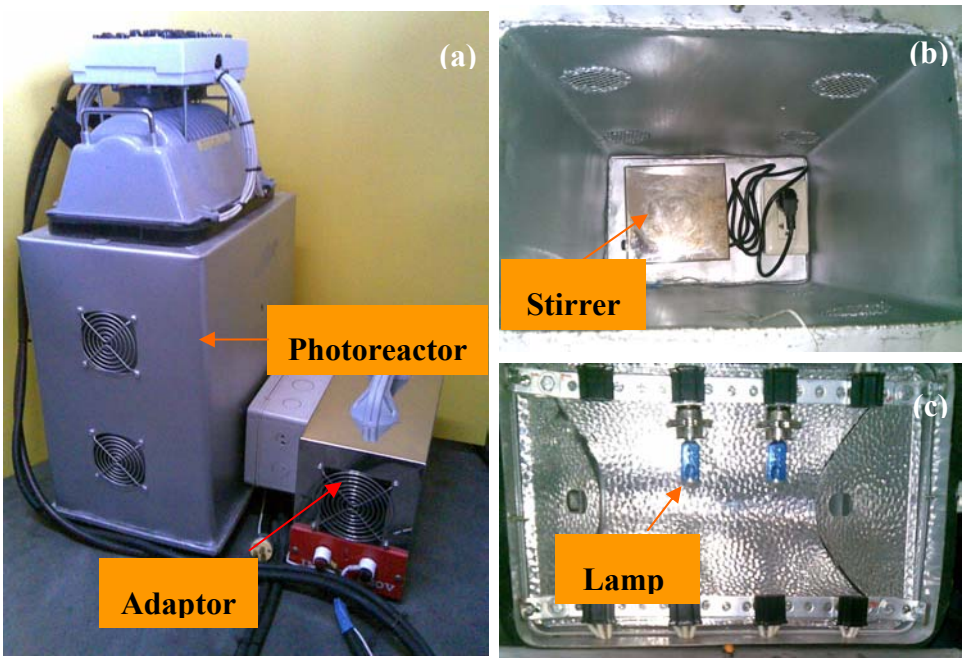

Figure 4.3 The picture of the developed photoreactor; (a) the photoreactor set, (b) the stirrer, and (c) the Xe-lamp set.

For the visible irradiation, the reaction mixture was stirred for 30 min in the dark then stirred under visible light using a 190 W, Xe-lamp equipped with a HOYA UV 385 cut off filter at an average distance of 30 cm between water surface and lamp. Samples were collected between 30 min and 3 h. For the natural light, the reaction mixture was stirred in the dark for 30 min then stirred with direct exposure to sunlight. The experiments were carried out between 11:00 am and 5.00 pm during the months of June (summer season) in Glasgow (latitude: 55.8618N, longitude: -

4.2401W). Samples were collected between 30 min and 5 h. Concentration of TBT and degradation products were determined in all samples using GC-MS. Dark control samples were covered with aluminum foil and stirred under the same condition.

4.2.4 Sample collection and determination of TBT

The extraction was optimized as previously described (*see section 2.2.3*). A 15 mL aliquot of the sample solution was withdrawn from the beaker after switching off the stirrer for 5 min to allow settlement of catalyst. In triplicate, each 5 mL aliquot was adjusted to pH 1.7 and sodium chloride was added to 0.2% w/v. Butyltins were extracted three times into hexane containing 0.05% tropolone, 10 mL of hexane in total, by shaking at 350 rpm for 30 minutes. All organic phases collected from each step were mixed and then evaporated until close to dryness on a heating block (20 ^{o}C) over N_2. A 0.25 mL internal standard, tetrabutyltin (1 μg mL^{-1}) in hexane was added into the samples and volume was adjusted to 1 mL. Butyltins were derivatised with 0.5 mL 2M *n*-hexylmagnesium bromide for 30 min under an inert atmosphere. 2M HCl was then added to stop the reaction. Anhydrous ammonium sulfate was added to remove moisture. A 1 μL aliquot of solution was injected into the GC-MS with HP5-MS column (30m x 0.25mm i.d. x 0.25 μm). The carrier gas was helium at a flow rate of 1 mL min^{-1}. The injector and detector temperatures were held at 280 °C and 300 °C, respectively. The column oven temperature was programmed from an initial temperature of 100 °C, hold for 2 min, to a final temperature of 300 °C at the rate of 15 °C min^{-1}, and hold for 10 min. The peak areas and mass spectrum (Total Ion Chromatogram, TIC) were recorded. The calibration graph was performed in the range of 0.5-50 μg mL^{-1} for each butyltins.

4.3 Results and discussion

4.3.1 Characterisation of catalyst

The X-ray diffractograms of N-doped TiO_2 calcined at differences temperature and P25-TiO_2 are presented in Figure 4.4.

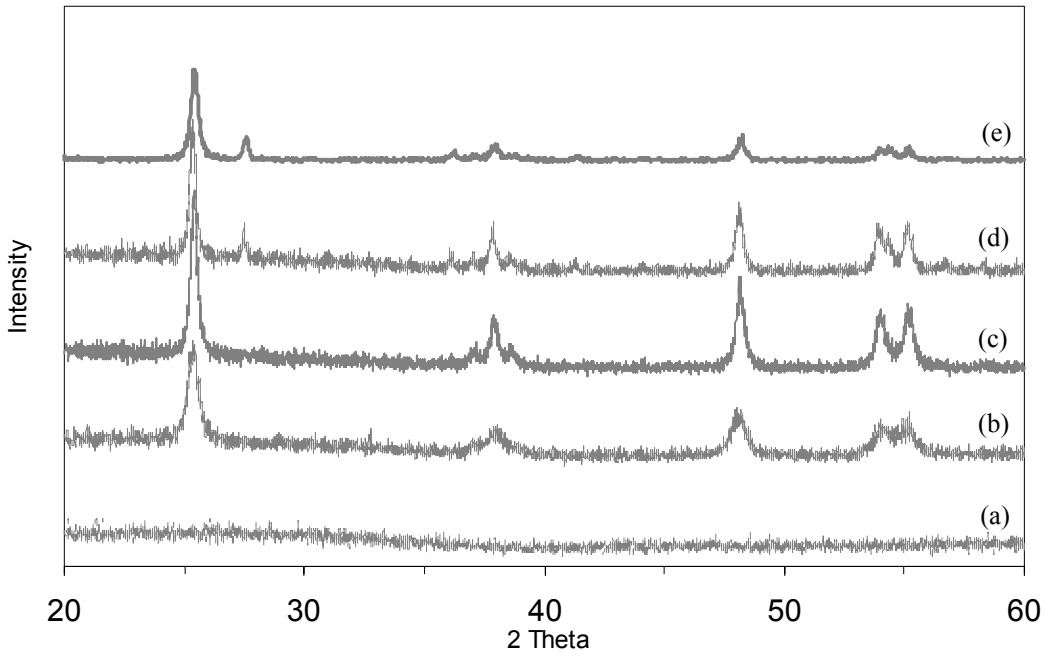

Figure 4.4 XRD patterns of N-doped TiO_2 calcined at different temperatures (a) 300°C (b) 400°C (c) 500°C (d) 600°C and (e) P25-TiO_2.

The XRD patterns in Figure 4.4 exhibit amorphous, anatase and rutile phases, depending on the calcination temperature. At 300°C (*see* (a)), no peaks occurred in the diffraction pattern, which indicates that the amorphous phase of N-doped TiO_2 was present. When the calcination temperature was raised to 400°C, all peaks (2θ = 25.4°, 38.1°, 48.4°, 53.9°, 55.2°) which are regarded as an indicator of the anatase phase of titania (JCPDS files No. 21-1272) were clearly observed. The crystalline anatase phase at a 2θ of 25.40° corresponding to the (101) reflection (Nakano et al.,

2007) started to appear at 400°C and increased in intensity with increasing calcination temperature. When the calcination temperature was elevated to 600°C, the transition to rutile phase could be observed. The characteristic peaks of rutile at a 2θ of 27.60° corresponding to the (110) reflection (Nakano et al., 2007) and at 36.1° (JCPDS files No. 21-1276) (Wang et al., 2005, Sirisaksoontorn et al., 2009) emerged.

The average particle size was calculated by applying Scherrer's equation (Equation 4.1) to the anatase (101) and rutile (110) diffraction peaks which represented the highest intensity peak for each pure phase (Vomvas et al., 2007, Patterson, 1939).

$$d = \frac{k\lambda}{\beta \cos\theta_B} \qquad \text{(Equation 4.1)}$$

where, d is crystallite size (nm); k is shape factor, a constant value of approximately 0.9; λ is wavelength of the X-ray radiation source (0.154 nm for Cu Kα); β is full width at half maximum intensity (radians); and θ_B is Bragg angle at the position of peak maximum.

The percentage of anatase was calculated in accordance with the Spurr-Myers equation (equation 2) (Spurr and Myers, 1957).

$$w_A = \frac{1}{(1+1.26\frac{I_R}{I_A})} \qquad \text{(Equation 4.2)}$$

where, w_A is weight fraction of anatase in the mixture; and I_R and I_A are intensities of the diffraction peak of rutile and anatase, respectively.

Unit cell volume was calculated from the product among three lattice parameters (a, b and c), which can be equated for the tetragonal system (a≠b=c) as in equation 3 (Sirisaksoontorn et al., 2009).

$$\frac{1}{d^2} = \frac{h^2 + k^2}{a^2} + \frac{l^2}{c^2} \qquad \text{(Equation 4.3)}$$

Where d is the lattice spacing between the planes in the atomic lattice; h, k, l are Miller indices; and a, b, c are lattice parameters. The characterization results are shown in Tables 4.1 and 4.2.

Table 4.1 The effect of calcination temperature on the crystallite size, the content of anatase phase and rutile of N-doped TiO_2 and P25- TiO_2

Titania precursor	Calcination temperature (°C)	Phase[a]	2θ (degree)	Cosθ	β (degree)	β (radian)	Crystallite size (nm)[b]	Intensity (A)	Intensity (R)	% A[c]	% R[d]
Titanium(IV) tetraisopropoxide	400	A	25.355	0.976	0.50	0.00873	16.3	426	-	100	0
	500	A	25.395	0.976	0.33	0.00576	24.7	610	-	100	0
	600	A	25.365	0.976	0.29	0.00506	28.1	538	202	67.9	32.1
		R	27.495	0.971	0.16	0.00541	51.1				
P25-TiO_2	-	A	25.430	0.975	0.36	0.00628	22.6	296	79	74.9	25.1
		R	27.610	0.971	0.18	0.00314	45.5				

[a]A and R are stand for anatase and rutile, respectively

[b]The crystallite size was calculated by using Scherrer's equation.

[c]The relative anatase content was calculated by applying Spurr-Myers equation.

[d]The relative rutile content was calculated by 100% - Anatase%.

(**Note**: The example of the calculation is shown in the Appendix C.)

Table 4.2 The effect of calcination temperature on the unit cell volume of N-doped TiO_2 and P25-TiO_2

Titania precursor	Calcination temperature (°C)	Phase	Lattice parameters (nm)			Unit cell volume (nm^3)
			a	b	c	
Titanium(IV) tetraisopropoxide	400	A	0.9452	0.3780	0.3780	0.1350
	500	A	0.9496	0.3769	0.3769	0.1349
	600	A	0.9496	0.3774	0.3774	0.1352
		R	0.2976	0.4564	0.4564	0.0619
P25-TiO_2	-	A	0.9588	0.3758	0.3758	0.1354
		R	0.2984	0.4569	0.4569	0.0623

(**Note**: The example of the calculation is shown in the Appendix C.)

TiO_2 nanoparticles can be synthesised by the sol-gel process. Anatase has a smaller crystallite size than rutile (Table 4.1). The crystallite size represented specific surface area (m^2 g^{-1}) of catalyst which affects the photo-catalytic activity. A small crystallite size has higher specific surface area than a larger crystallite. More surface area promotes greater efficiency on light and substance absorption on the surface, which increases the decomposition area and degradation activity of the catalyst (Ohno et al., 2001). The higher specific surface area of anatase compared to rutile was also confirmed by a larger unit cell volume (Table 4.2). This finding was supported by previous studies on photo-degradation of phenol and phenanthrene using difference particle sizes of N-doped TiO_2 (Sirisaksoontorn et al., 2009). The results showed that the smallest crystallite size of N-doped TiO_2 gave the greatest degradation. Moreover, N-doped TiO_2 calcined at 400 ºC contains only anatase, which was reported to have higher photo-activity than rutile. The slow movement of electron in rutile provides more chances for electron-hole recombination and might cause this lower activity (Sun et al., 2003).

Therefore, N-doped TiO_2 calcined at 400 ºC was chosen for the subsequent TBT degradation study. The photocatalytic efficiency of N-doped TiO_2 was compared to that in the absence of catalyst, and with those of commercial P25-TiO_2 and undoped TiO_2 synthesized by sol-gel method and calcined at 400 ºC. The undoped TiO_2 crystalline was in anatase phase with a particle size of 11.3 nm and a unit cell volume of 0.1332 nm^3. Relevant calculations are presented in Appendix C. Additionally, the percentage of nitrogen in N-doped TiO_2 was determined using an elemental analyzer (Table 4.3).

Table 4.3 The amount of nitrogen of N-doped TiO_2 with various temperatures

Titania precursor	Calcination temperature (ºC)	Nitrogen content (%)			Average nitrogen content (%)
		N_1	N_2	N_3	N_{ave}
Titanium(IV) tetraiso-propoxide	300	0.060	0.060	0.080	0.066
	400	0.059	0.054	0.048	0.054
	500	0.086	0.054	0.059	0.067
	600	0.084	0.094	0.078	0.085

The percentage of nitrogen in N-doped TiO_2 calcined at 400 ºC was 0.054 % ± 0.006 (n=3) which is similar to previous studies, depending on the titania precursor (Ksibi et al., 2008, Sirisaksoontorn et al., 2009).

4.3.2 Scanning electron microscopy (SEM) and transmission electron microscopy (TEM)

SEM and TEM photomicrographs of the N-doped TiO2 show morphology of nano-sized particles (Figures 4.5 to 4.7).

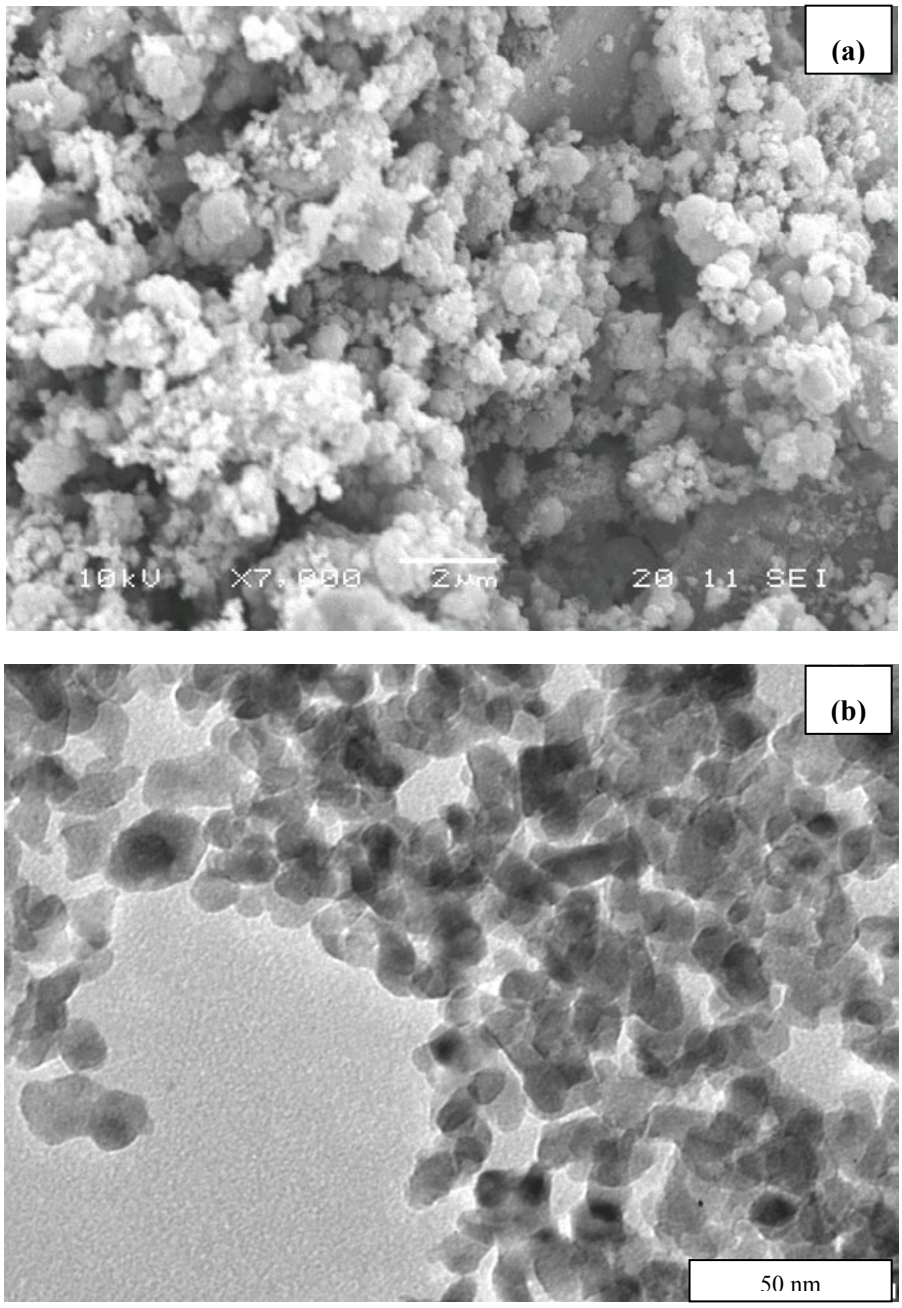

Figure 4.5 (a) SEM and (b) TEM images of N-doped TiO_2 calcined at 400 ºC.

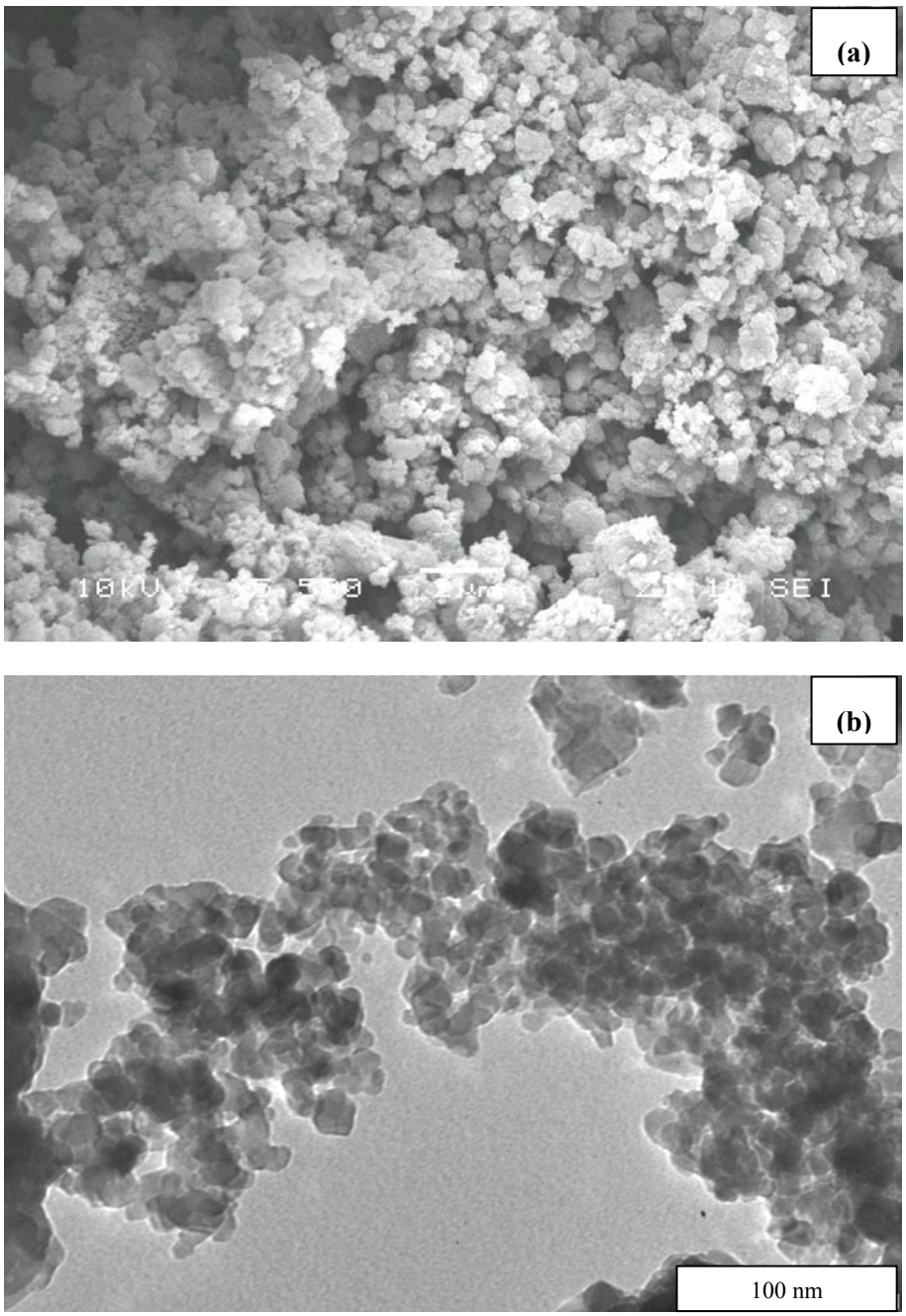

Figure 4.6 (a) SEM and (b) TEM images of N-doped TiO_2 calcined at 500 ºC.

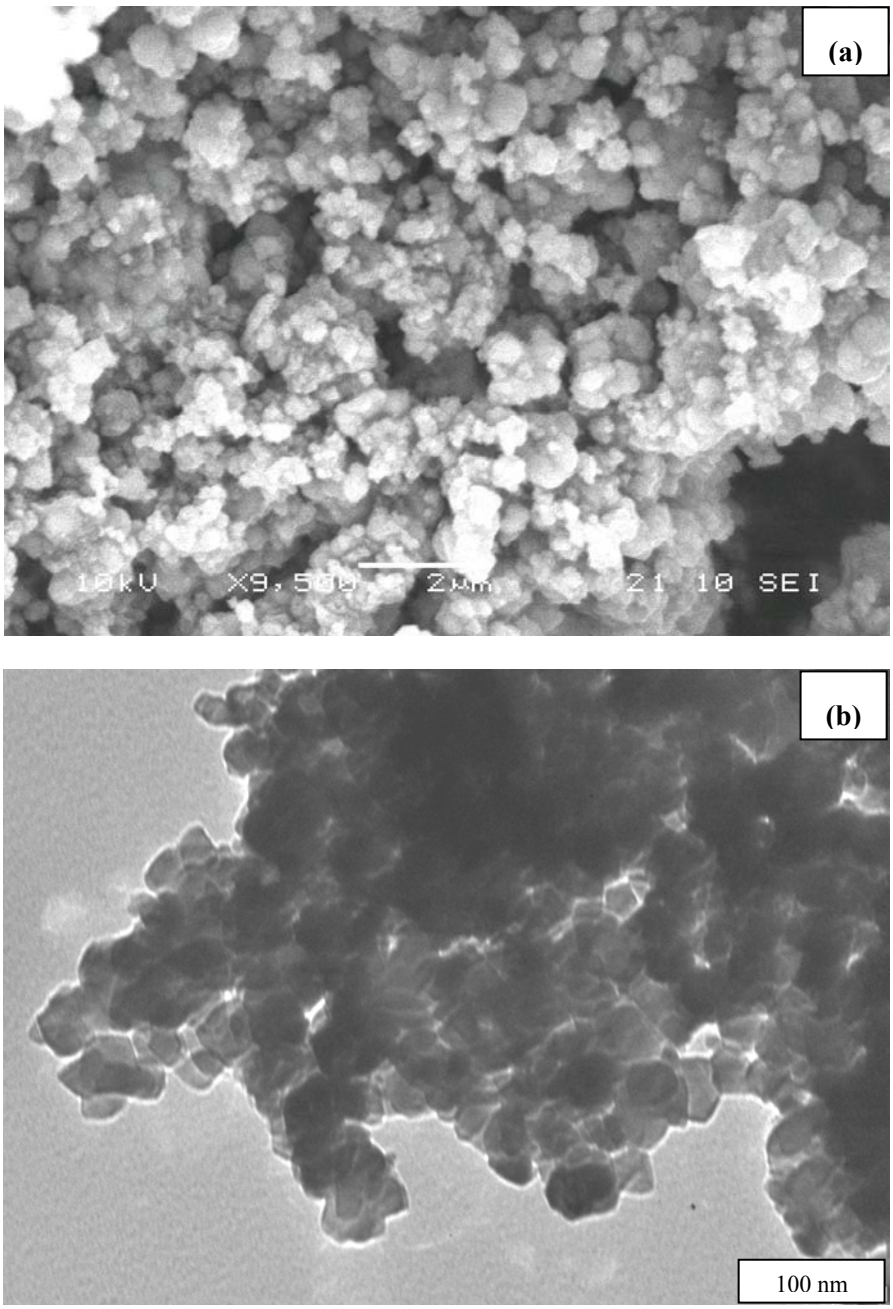

Figure 4.7 (a) SEM and (b) TEM images of N-doped TiO_2 calcined at 600 ºC.

The SEM images (Figure 4.5(a), 4.6(a) and 4.7(a)) show that the surface morphology of N-doped TiO_2 using titanium(IV) tetraisopropoxide is mainly like fluffy powders. These results are consistent with TEM images (Figure 4.5(b), 4.6(b) and 4.7(b)) for the N-doped TiO_2 samples that show the particle morphology is rather spherical in both the analysis. Furthermore, the average sizes of N-doped TiO_2 calcined at 400ºC and 500 ºC by TEM are 15.0 nm and 21.1 nm, respectively, based on the diameter calculation of randomly selected 50 particles. A densification phenomenon occurred when the N-doped TiO_2 sample was calcined at 600 ºC as clearly displayed in the TEM image. This effect brings about an increase in particle size (30-59 nm), as determined from a randomly selected 30 particles by TEM. These average sizes of mono-disperse particles which was identified by TEM correspond with the values calculated from the Scherrer's equation.

From SEM and TEM images it can be concluded that the surface morphology of N-doped TiO_2 using titanium(IV) tetraisopropoxide produced a morphology like fluffy powders for all calcination temperatures. Moreover, N-doped TiO_2 has bigger particle sizes with increasing calcination temperature. In each calcination temperature, the particle size from the TEM analysis is equivalent to that from the XRD results. The SEM and TEM images of P25-TiO_2 are presented in Figure 4.8. The surface morphology of P25-TiO_2 is spherical. However, P25-TiO_2 has the polydispersed round particles which can be clearly seen in the TEM image.

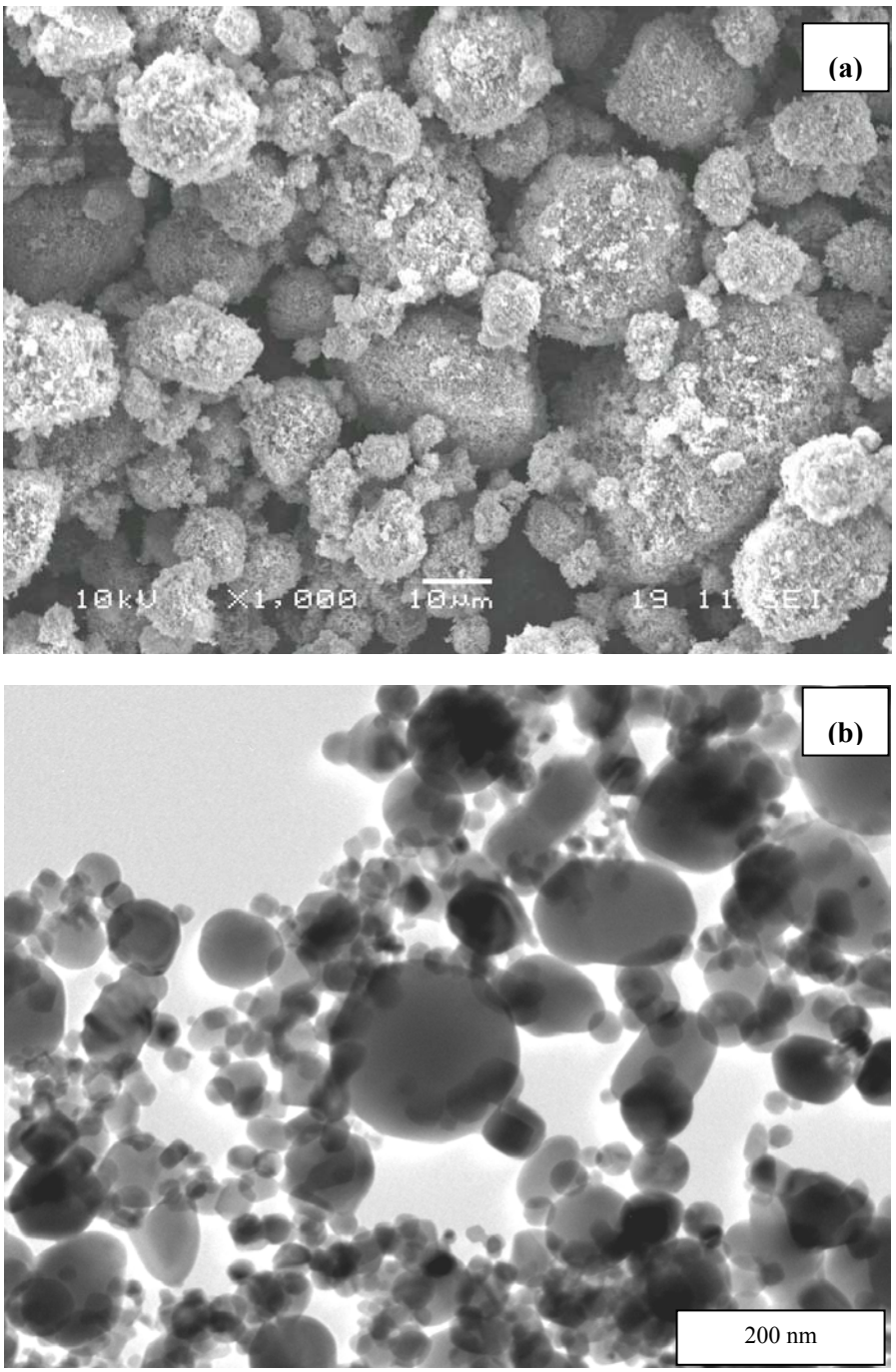

Figure 4.8 (a) SEM and (b) TEM images of P25-TiO_2.

4.3.3 Photo-degradation activity

Investigation of photocatalytic TBT degradation by the catalysts was performed under artificial visible light and natural light (Figure 4.9). The photocatalytic efficiency was determined by calculating the relative concentration (C/C_0), where C is the concentration at the sampling time and C_0 is the initial concentration.

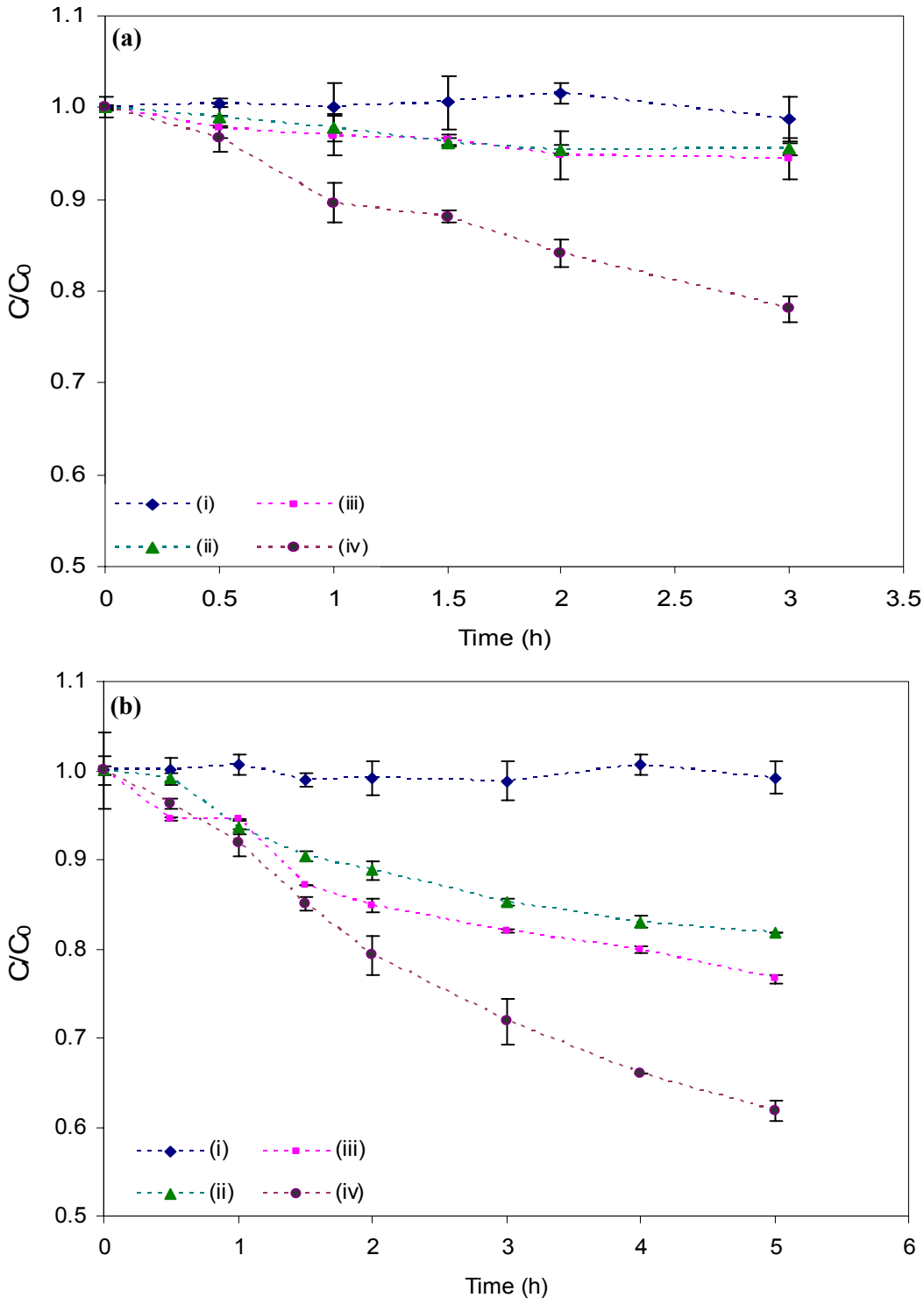

Figure 4.9 Photo-degradation of TBT under visible light (a) and natural light (b) by (i) no catalyst, (ii) undoped TiO_2 calcined at 400 °C, (iii) P25-TiO_2 and (iv) N-doped TiO_2 calcined at 400 °C. Error bars represent one standard deviation for n = 3. (**Note**: raw data are shown in Appendix D.)

The N-doped TiO_2 calcined at 400 °C shows the highest efficiency whereas TBT concentration was not significantly changed in the absence of catalyst in both situations. Under visible light (Figure 4.9(a)), undoped TiO_2 and P25-TiO_2 unsurprisingly demonstrated low degradation activity which corresponded with a previous study (Navio et al., 1996). Since the band gaps energy of undoped TiO_2 and P25-TiO_2 are high (anatase and rutile are 3.2 and 3.0 eV, respectively), electrons in the valence band cannot be excited to the conduction band by the low energy protons of the visible light (Nakamura et al., 2004). In natural light (Figure 4.9(b)), the existence of UV wavelengths causes the degradation of TBT by undoped TiO_2 and P25-TiO_2. The higher degradation activity of P25-TiO_2 than undoped TiO_2 resulted from the developed crystallinity containing anatase and rutile (75:25). This prevents the recombination of holes and electrons after "the line up of Fermi levels of anatase and rutile" (Appendix Figure D1) (Sun et al., 2003). Furthermore, the N-doped TiO_2 proved that successful degradation activity in natural light, as a result of "band gap narrowing" (Asahi et al., 2001, Morikawa et al., 2001). The band gap narrowing after doping TiO_2 with nitrogen was confirmed by absorption spectra (Figure 4.10).

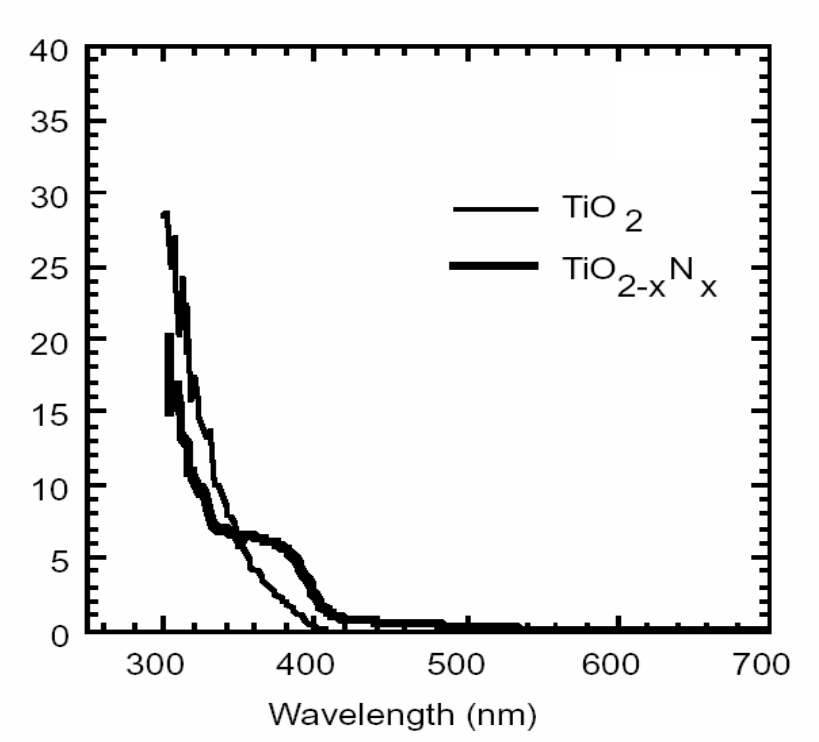

Figure 4.10 The absorption spectra of $TiO_{2-x}N_x$ compared with those of TiO_2 (Morikawa et al., 2001)

The degradation curves of TBT obtained by plotting ln C/C_0 against time (h) were well fitted by first order decay kinetics as presented in Figure 4.11. The TBT degradation products, DBT and MBT could not be found in the reaction solution after irradiation. A high conversion rate of DBT and MBT to final products such as carbon dioxide, water and inorganic tin species might explain this finding (Navio et al., 1996). Navio et al. also proposed a mechanism for the TiO_2-photocatalytic degradation of butyltin (Appendix Figure D2). They also reported that the degradation products in the photolysis process by TiO_2 were at trace concentrations in the solution. However, inorganic tin, after the degradation process, was found to remain on the TiO_2 surface both as metallic tin and/or SnO_x, which was detected by X-ray Photoelectron Spectroscopy (XPS) (Navio et al., 2009). The rate constant of photocatalytic reaction was calculated from the slope of the first order reaction graph and also the % conversion of TBT after 3 h under visible light and natural light (Table 4.4).

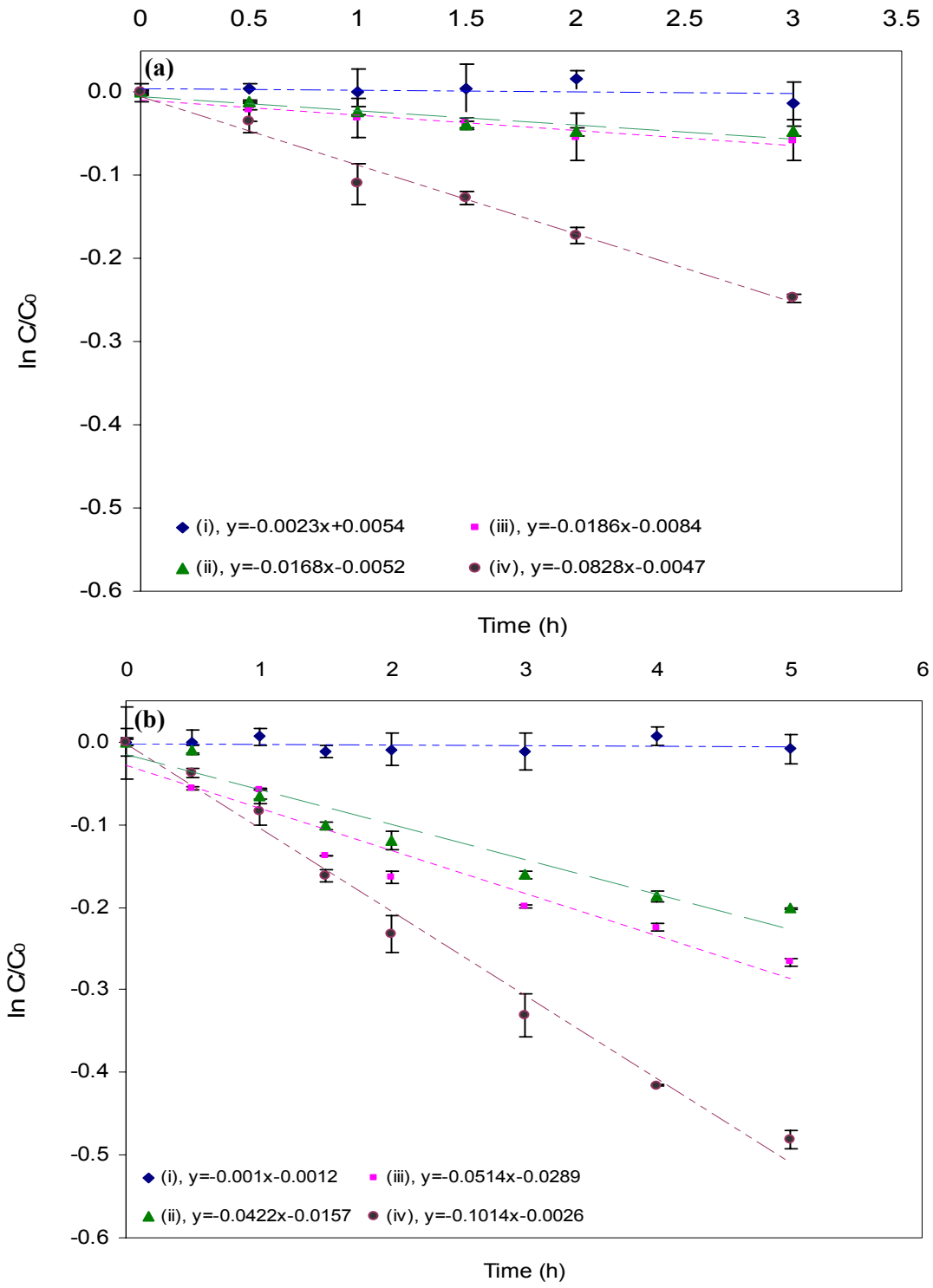

Figure 4.11 The relation between ln C/C_0 and time (h) of TBT photo-degradation reaction under visible light (a) and natural light (b) by (i) no catalyst, (ii) undoped TiO_2 calcined at 400 °C, (iii) P25-TiO_2 and (iv) N-doped TiO_2 calcined at 400 °C. Error bars represent one standard deviation for n = 3.

Table 4.4 Reaction rate constants and % conversion of photocatalyst under artificial visible light and natural light. (**Note**: raw data are shown in Appendix D.)

Photocatalyst	Visible light			Natural light		
	% Conversion[a] (3h)	R^2	Rate constant, k[b] (h^{-1})	% Conversion (3h)	R^2	Rate constant, k (h^{-1})
No catalyst	1.20	0.07	ND[c]	1.16	0.05	ND
TiO_2	4.52	0.86	0.017	14.8	0.93	0.042
P25-TiO_2	5.54	0.91	0.019	18.0	0.93	0.051
N-doped TiO_2	21.9	0.98	0.083	28.2	0.99	0.101

[a]% Conversion was calculated from ($C_{initial} - C_{final} / C_{initial}$) x 100%

[b]Rate constant was identified from slope of graph which presented the relation between ln C/C_0 and time (h), slope = -k

[c] ND, non detectable

Table 4.4, clearly confirms that N-doped TiO_2 has the highest photocatalytic ability to degrade TBT in water. Under natural light, 28% of TBT initially present is degraded in 3 h by the N-doped catalyst, and complete conversion would occur in 4-5 days (Appendix D) depending on the weather. The advantages of catalytic photo-degradation of TBT in aqueous media when compare with biological process (Harino et al., 1997b, Bernat and Dlugonski, 2006) are shorter degradation period, independence from microorganism behaviours and, especially, applicability at high TBT contamination levels. TBT has been reported to exist at significantly higher concentrations in sediment than in water (e.g. at a 3:1 ratio in the solid-water system (Bangkedphol et al., 2009)). However, contaminated sediment may exist at too great a depth for light to penetrate and would require to be treated *ex-situ.* A simple approach is to remove the TBT from water, which will continually be resupplied with pollutant from the sediment, until contamination levels in the entire system are reduce to acceptable values (<EQSs). Therefore, this process is an economical

method in terms of catalyst preparation and natural light requirement which can be applied for an effective remediation of TBT in water.

4.4 Summary

A simple and economical sol-gel method was successfully applied for the synthesis of nanoparticle N-doped TiO_2, visible and natural light-active photocatalyst. According to XRD analysis, the N-doped TiO_2 transformed from anatase to rutile phase at calcination temperature ranging from 400 to 600 ºC. Calcination of the doping catalyst at 400 ºC was chosen. The N-doped catalyst enhanced the degradation of TBT in water under natural light, giving a 28% reduction in initial TBT concentration in 3 h. The process can now move forward to application on a larger scale for TBT remediation in water.

CHAPTER 5

Conclusions and Recommendations for Future Work

TBT, which is widely used in antifouling paints and which is consequently released in large quantities to the aquatic environment, has marked biocidal properties and is considered to be a priority pollutant. This thesis describes novel contributions to the measurement of TBT, the understanding of the partitioning behaviour of the compound in sediment-water systems, and the remediation of pollution by TBT. The aims of this thesis were:

- To develop a rapid, straightforward and inexpensive method of analysis for TBT in polluted waters and sediments. Then, optimise the extraction of TBT from the matrices and use to study a real environment by monitoring TBT contamination as selected sites in the Forth and Clyde canal
- To study the adsorption behaviour of TBT and the parameters that influences its environmental fate and toxicity in the aquatic environment. The experimental partition coefficients were then investigated and compared to a default model which was generated from EPISuite program.
- To study and enhance the photodegradation process for TBT in aqueous samples under natural light with a view to remediation of contaminated sites.

These aims were all successfully achieved as described in the relevant chapters. For the extraction method it was found that if the pH of the matrix is first adjusted to 1.7, all the TBT may be extracted by 0.05-0.5% of tropolone in 0.2% aqueous sodium chloride. This is the first achievement noted in the thesis **(Chapter**

2). The optimum concentration of tropolone depends on the nature of the matrix and future work should systematise this by considering a wider range of matrices and correlating their properties with the optimum tropolone concentrations. In this way future extractions of TBT could become more routine. The TBT and DBT in the extracts have to be separated and their concentrations determined. The thesis describes the development of a straightforward, novel, rapid and inexpensive method of achieving this using simple instrumentation that could be adopted universally. Separation was accomplished by NPHPLC in the isocratic mode on an ultracyano column using hexane containing 5% THF and 0.03% of acetic acid as the mobile phase **(Chapter 2)**. Quantification of the concentrations is readily achieved using a UV/Vis absorption detector. The optimised extraction and analysis method was employed in the monitoring of samples from the Forth and Clyde Canal. The sites studied were at Bowling Basin and Port Dundas. Both were found to be highly contaminated areas and to grossly exceed the EQS values. This was true even though one of the areas has experienced many years of inactivity showing that TBT is highly persistent in the aquatic environment.

The partition studies showed that TBT is mainly to be found in the sediments (3:1 ratio in solid-water system) and although this means that it is less bioavailable or mobile it does increase environmental persistence. There is also a danger to pelagic species as they will be in direct contact with the contamination. Understanding of the behaviour of TBT in the environment was enhanced by measurements of K_d and K_{ow} **(Chapter 3)**. K_d values were high, consistent with the preferential ad/absorption of TBT onto sediments. K_{ow} values were also high indicating the ability of TBT to partition into organisms, indicating significant biomagnification of TBT in the food chain. The experimental values of K_d and K_{ow} differed markedly (Table 3.7) from the default values generated by the EPISuite modelling program. Accordingly, the experimental variation of K_d with environmental properties, namely salinity, pH, temperature and the nature of the sediment **(Chapter 3)** which could be sensitively affected by climate change. Therefore, this study provides future workers with data that should facilitate the improved prediction and interpretation of the behaviour of

TBT in a variety of environments. Future examination of the variation of absorption behaviour of TBT at different depths in the sediment column would be worthwhile.

Finally it has been shown for the first time that the considerable contamination of waters by TBT can be cleaned up photochemically **(Chapter 4)**. It has been shown that solar light will degrade TBT in 5 days in the presence of nitrogen-doped titanium dioxide. The catalyst can be re-used several times and the method of remediation is cheap and straightforward. The approach has the potential for widespread adoption. Whereas the conditions for the maximum rate of photochemical degradation were readily found, future research should establish the mechanism of the degradation and optimise the catalyst, for example by increasing its surface area and optimising the nitrogen doping.

Accordingly, the thesis contributes new knowledge on the measurement, chemistry and degradation of TBT and, thereby, to the goal of sustainable management of the global aquatic environment.

References

AGUILAR-MARTINEZ, R., GREENWOOD, R., MILLS, G. A., VRANA, B., PALACIOS-CORVILLO, M. A. & GOMEZ-GOMEZ, M. M. (2008) Assessment of Chemcatcher passive sampler for the monitoring of inorganic mercury and organotin compounds in water. *International Journal of Environmental Analytical Chemistry,* 88**,** 75-90.

ANDERSON, B. A., UNGER, M. A. & MOORE, K. A. (2002) Fate of tributyltin in a created tidal wetland. *Environmental Toxicology and Chemistry,* 21**,** 1176-1183.

ANDERSON, C. D. & DALLEY, R. (1986) *Use of the organotins in antifouling paints,* Washington DC, USA, Marine Technology Society.

ANTIZAR-LADISLAO, B. (2008) Environmental levels, toxicity and human exposure to tributyltin (TBT)-contaminated marine environment. A review. *Environment International,* 34**,** 292-308.

APHA (1999) *Standard methods for the examination of water and waste water (APHA: 2520B)* NW Washington, DC, USA, American Public Health Association, Water Environment Federation.

ARONSON, D., BOETHLING, R., HOWARD, P. & STITELER, W. (2006) Estimating biodegradation half-lives for use in chemical screening. *Chemosphere,* 63**,** 1953-1960.

ARP, H. P. H., NIEDERER, C. & GOSS, K. U. (2006) Predicting the partitioning behavior of various highly fluorinated compounds. *Environmental Science & Technology,* 40**,** 7298-7304.

ARTHUR, C. L. & PAWLISZYN, J. (1990) Solid-phase microextraction with thermal-desorption using fused-silica optical fibers. *Analytical Chemistry,* 62**,** 2145-2148.

ASAHI, R., MORIKAWA, T., OHWAKI, T., AOKI, K. & TAGA, Y. (2001) Visible-light photocatalysis in nitrogen-doped titanium oxides. *Science,* 293**,** 269-271.

ASTM (2000) *Standard test methods for moisture, ash, and organic matter of peat and other organic soils (ASTM: D 2974-87)* Race Street, Philadelphia, ASTM international publisher.

ASTM (2001) *Standard test methods for determining a sorption constant (Koc) for an organic chemical in soil and sediments (ASTM: E 1195-01),* West Conshohocken, ASTM international publisher.

ASTM (2002) *Standard test methods for particle-size analysis of soils (ASTM: D 422-63),* West Conshohocken, ASTM international publisher.

ASTM (2008) *Standard specification for reagent water (ASTM: D 1193-99)* West Conshohocken, ASTM international publisher.

ASTRUC, A., ASTRUC, M., PINEL, R. & POTINGAUTIER, M. (1992) Speciation of butyltin compounds by online Hplc Etaa of tropolone complexes in environmental-samples. *Applied Organometallic Chemistry,* 6**,** 39-47.

BAJPAI, A. K. & VISHWAKARMA, N. (2003) Adsorption of polyvinylalcohol onto Fuller's earth surfaces. *Colloids and Surfaces a-Physicochemical and Engineering Aspects,* 220**,** 117-130.

BANGKEDPHOL, S., KEENAN, H., DAVIDSON, C., SAKULTANTIMETHA, S. & SONGSASEN, A. (2008) Development of a low-cost method of analysis for the qualitative and quantitative analysis of butyltins in environmental samples. *Journal of Environmental Science and Health Part A,* 43**,** 1744-1751.

BANGKEDPHOL, S., KEENAN, H., DAVIDSON, C., SAKULTANTIMETHA, S. & SONGSASEN, A. (2009) The partition behavior of tributyltin and prediction of environmental fate, persistence and toxixity in aquatic environments. *Chemosphere,* 77**,** 1326-1332.

BAUN, A., ERIKSSON, E., LEDIN, A. & MIKKELSEN, P. S. (2006) A methodology for ranking and hazard identification of xenobiotic organic compounds in urban stormwater. *Science of the Total Environment,* 370**,** 29-38.

BENNETT, R. F. (1996) *Industrial manufacture and applications of tributyltin compounds, Tributyltin: case study of an environmental contaminant,* UK, Cambridge University Press.

BERGE, J. A., BREVIK, E. M., BJORGE, A., FOLSVIK, N., GABRIELSEN, G. W. & WOLKERS, H. (2004) Organotins in marine mammals and seabirds from Norwegian territory. *Journal of Environmental Monitoring,* 6**,** 108-112.

BERNAT, P. & DLUGONSKI, J. (2006) Acceleration of tributyltin chloride (TBT) degradation in liquid cultures of the filamentous fungus Cunninghamella elegans. *Chemosphere,* 62**,** 3-8.

BOND, A. M., TUROCZY, N. J. & CARTER, R. J. (1995) The electrochemistry of monobutyltin and mixtures of butyltin compounds at mercury-electrodes in aqueous-media. *Analytica Chimica Acta,* 310**,** 109-119.

BOTANA, J. C., PEREIRO, I. R. & TORRIJOS, R. C. (2002) Rapid determination of butyltin species in water samples by multicapillary gas chromatography with atomic emission detection following headspace solid-phase microextraction. *Journal of Chromatography A,* 963**,** 195-203.

BOWLES, K. C. (2004) Determination of butyltins in environmental samples using sodium tetraethylborate derivatization: characterization and minimization of interferences. *Analytica Chimica Acta,* 509**,** 127-135.

BOYER, I. J. (1989) Toxicity of dibutyltin, tributyltin and other organotin compounds to humans and to experimental-animals. *Toxicology,* 55**,** 253-298.

BURTON, E. D., PHILLIPS, I. R. & HAWKER, D. W. (2004) Sorption and desorption behavior of tributyltin with natural sediments. *Environmental Science & Technology,* 38**,** 6694-6700.

CAMBRIDGESOLF (2009): ChemDRAW Ultra 11 (Chem3D Pro 11.0); http://cambridgesolf.com/Default.aspx. Cambridge, USA.

CARDWELL, R. D., KEITHLY, J. C. & SIMMONDS, J. (1999) Tributyltin in US market-bought seafood and assessment of human health risks. *Human and Ecological Risk Assessment,* 5**,** 317-335.

CARICCHIA, A. M., CHIAVARINI, S., CREMISINI, C., MORABITO, R. & SCERBO, R. (1994) Influence of storage-conditions on the determination of organotin in mussels. *Analytica Chimica Acta,* 286**,** 329-334.

CARLSEN, L. & WALKER, J. D. (2003) QSARs for prioritizing PBT substances to promote pollution prevention. *Qsar & Combinatorial Science,* 22**,** 49-57.

CEFAS (2006) Toxicity database. *Centre for Environment, Fisheries & Aquaculture Science.*

CENTINEO, G., GONZALEZ, E. B. & SANZ-MEDEL, A. (2004) Multielemental speciation analysis of organometallic compounds of mercury, lead and tin in natural water samples by headspace-solid phase microextraction followed by gas chromatography-mass spectrometry. *Journal of Chromatography A,* 1034**,** 191-197.

CEULEMANS, M., WITTE, C., LOBINSKI, R. & ADAMS, F. C. (1994) Simplified sample preparation for GC speciation analysis of organotin in marine biomaterials. *Applied Organometallic Chemistry,* 8**,** 451-461.

CHAMP, M. A. & SELIGMAN, P. F. (1996) *An introduction to organotin compounds and their use in antifouling coatings,* London, Chapman and Hall.

CHEN, H., LONG, M. C., XU, J. & CAI, W. M. (2006) Preparation, characterization, and photocatalytic activity of visible light driven chlorine-doped TiO2. *Chinese Journal of Catalysis,* 27**,** 890-894.

CHEN, S. F., CHEN, L., GAO, S. & CAO, G. Y. (2005) The preparation of nitrogen-doped photocatalyst TiO2-xNx by ball milling. *Chemical Physics Letters,* 413**,** 404-409.

CHOI, H., STATHATOS, E. & DIONYSIOU, D. D. (2006) Sol-gel preparation of mesoporous photocatalytic TiO2 films and TiO2/Al2O3 composite membranes for environmental applications. *Applied Catalysis B-Environmental,* 63**,** 60-67.

CIRCA (2005) *Quality Standards (EQS) substance data sheet: Tributyltin compounds (TBT-ion)*, CIRCA publisher.

CLARK, E. A., STERRITT, R. M. & LESTER, J. N. (1988) The fate of tributyltin in the aquatic environment - a look at the data. *Environmental Science & Technology,* 22**,** 600-604.

CLARKSON, T. W. (1991) *Inorganic and organometal pesticides,* New York, Eds. Academic Press.

COLOMBINI, V., BANCON-MONTIGNY, C., YANG, L., MAXWELL, P., STURGEON, R. E. & MESTER, Z. (2004) Headspace single-drop microextration for the detection of organotin compounds. *Talanta,* 63**,** 555-560.

CROFTON, K. M., DEAN, K. F., BONCEK, V. M., ROSEN, M. B., SHEETS, L. P., CHERNOFF, N. & REITER, L. W. (1989) Prenatal or postnatal exposure to bis(tri-normal-butyltin) oxide in the rat - postnatal evaluation of teratology and behavior. *Toxicology and Applied Pharmacology,* 97**,** 113-123.

DIMITRIOU-CHRISTIDIS, P., HARRIS, B. C., MCDONALD, T. J., REESE, E. & AUTENRIETH, R. L. (2003) Estimation of selected physicochemical properties for methylated naphthalene compounds. *Chemosphere,* 52**,** 869-881.

DO, D. D. (1998) *Adsorption Analysis: Equilibria and Kinetics,* London, UK, Imperial College Press.

EBDON, L. & ALONSO, J. I. G. (1987) Determination of tributyltin ions in estuarine waters by high-performance liquid-chromatography with fluorometric detection using morin in a micellar solution. *Analyst,* 112**,** 1551-1554.

EPA (1996) Endocrine Disruptor Screening Program (EDSP): http://www.epa.gov/endo/pubs/edspoverview/whatare.htm

Washington, DC, USA, United States Environmental Protection Agency.

EPA (1999) *Understanding variation in partition coefficient, Kd, values (EPA 402-R-99-004A),* Washington, DC, USA, United States Environmental Protection Agency.

EPA (2008) *Revised production chemistry chapter for the tributyltin (DC 20460),* Washington, DC, USA, United States Environmental Protection Agency.

EPA (2009) Internation Estimation Program Interface (EPI) Suite Version 4.0: http://www.epa.gov/oppt/exposure/pubs/episuite.htm. Washington, DC, USA, United States Environmental Protection Agency.

EUROPA (2003) Regulation (EC) No 782/2003 of the european parliament and of the council on the prohibition of organotin compounds on ships. *journal of the European Union***,** L115/1-11.

EUROPA (2008) Directive 2008/105/EC of the european paliment and the council on environmental quality standards in the field of water policy. *journal of the European Union***,** L 348/84-96.

EXTOXNET (1996) Extension toxicology network, pesticide information profiles: http://extoxnet.orst.edu/pips/tributyl.htm. Oregon State University.

FENT, K. (1996) Ecotoxicology of organotin compounds. *Critical Reviews in Toxicology,* 26**,** 1-117.

FENT, K. & HUNN, J. (1991) Phenyltins in water, sediment, and biota of fresh-water marinas. *Environmental Science & Technology,* 25**,** 956-963.

FENT, K. & LOOSER, P. W. (1995) Bioaccumulation and bioavailability of tributyltin chloride - influence of pH and humic acids. *Water Research,* 29**,** 1631-1637.

FENT, K. & MULLER, M. D. (1991) Occurrence of organotins in municipal waste-water and sewage-sludge and behavior in a treatment-plant. *Environmental Science & Technology,* 25**,** 489-493.

FORSYTH, D. S., SUN, W. F. & DALGLISH, K. (1994) Survey of organotin compounds in blended wines. *Food Additives and Contaminants,* 11**,** 343-350.

GADD, G. M. (2000) Microbial interactions with tributyltin compounds: detoxification, accumulation, and environmental fate. *Science of the Total Environment,* 258**,** 119-127.

GOH, C. L. (1985) Irritant dermatitis from tri-n-butyl tin oxide in paint. *Contact Dermatitis,* 12**,** 161-163.

GOMES, R. L., SCRIMSHAW, M. D. & LESTER, J. N. (2003) Determination of endocrine disrupters in sewage treatment and receiving waters. *Trac-Trends in Analytical Chemistry,* 22**,** 697-707.

GOMEZARIZA, J. L., MORALES, E. & RUIZBENITEZ, M. (1992) Simultaneous speciation of butyltin and phenyltin compounds in the waters of south-west spain. *Analyst,* 117**,** 641-644.

GOOGLEMAP (2009) Google maps of UK: http://maps.google.co.uk/. London, UK.

GOSS, K. U., ARP, H. P. H., BRONNER, G. & NIEDERER, C. (2008) Partition behavior of hexachlorocyclohexane isomers. *Journal of Chemical and Engineering Data,* 53**,** 750-754.

GOUIN, T., COUSINS, I. & MACKAY, D. (2004) Comparison of two methods for obtaining degradation half-lives. *Chemosphere,* 56**,** 531-535.

GREENPEACE (1999) TBT: A global problem for the marine environment: http://archive.greenpeace.org/toxics/reports/tbtfactsheet.html

GURUGE, K. S., TANABE, S., IWATA, H., TAKSUKAWA, R. & YAMAGISHI, S. (1996) Distribution, biomagnification, and elimination of butyltin compound residues in common cormorants (Phalacrocorax carbo) from Lake Biwa, Japan. *Archives of Environmental Contamination and Toxicology,* 31**,** 210-217.

HALL, L. W., BUSHONG, S. J., HALL, W. S. & JOHNSON, W. E. (1988) Acute and chronic effects of tributyltin on a chesapeake bay copepod. *Environmental Toxicology and Chemistry,* 7**,** 41-46.

HALL, L. W., SCOTT, M. C., KILLEN, W. D. & UNGER, M. A. (2000) A probabilistic ecological risk assessment of tributyltin in surface waters of the Chesapeake Bay watershed. *Human and Ecological Risk Assessment,* 6**,** 141-179.

HARINO, H., FUKUSHIMA, M., KUROKAWA, Y. & KAWAI, S. (1997a) Degradation of the tributyltin compounds by the microorganisms in water and sediment collected from the harbour area of Osaka City, Japan. *Environmental Pollution,* 98**,** 163-167.

HARINO, H., FUKUSHIMA, M., KUROKAWA, Y. & KAWAI, S. (1997b) Susceptibility of bacterial populations to organotin compounds and microbial degradation of organotin compounds in environmental water. *Environmental Pollution,* 98**,** 157-162.

HARINO, H., FUKUSHIMA, M. & TANAKA, M. (1992) Simultaneous determination of butyltin and phenyltin compounds in the aquatic environment by gas-chromatography. *Analytica Chimica Acta,* 264**,** 91-96.

HARINO, H., OHJI, M., WATTAYAKORN, G., ARAI, T., RUNGSUPA, S. & MIYAZAKI, N. (2006) Occurrence of antifouling biocides in sediment and green mussels from Thailand. *Archives of Environmental Contamination and Toxicology,* 51**,** 400-407.

HARRIS, J. R. W., CLEARY, J.J. (1987) Particle water partitioning and organotin dispersal in an estury. *Proceeding of the fourth international organotin symposium.*

HOANG, T. V., MICHEL, A. & GUYOT, A. (1982) Polyvinylchloride stabilisation with organotin compounds—Part III: Effect of lewis acidity and co-ordination of organotin chlorides upon their catalytic activity towards dehydrochlorination. *Polymer Degradation and Stability,* 4**,** 213-222.

HOCH, M. (2001) Review: Organotin compounds in the environment - an overview. *Applied geochemistry,* 16**,** 719-743.

HOCH, M. (2004) Assessment of salinity variations in TBT adsorption onto kaolinite and montmorillonite at different pH levels. *Water Air and Soil Pollution,* 152**,** 349-362.

HOCH, M., ALONSO-AZCARATE, J. & LISCHICK, M. (2002) Adsorption behavior of toxic tributyltin to clay-rich sediments under various environmental conditions. *Environmental Toxicology and Chemistry,* 21**,** 1390-1397.

HOCH, M., ALONSO-AZCARATE, J. & LISCHICK, M. (2003) Assessment of adsorption behavior of dibutyltin (DBT) to clay-rich sediments in comparison to the highly toxic tributyltin (TBT). *Environmental Pollution,* 123**,** 217-227.

HORIKOSHI, S., KAJITANI, M. & SERPONE, N. (2007) The microwave-/photo-assisted degradation of bisphenol-A in aqueous TiO2 dispersions revisited - Re-assessment of the microwave non-thermal effect. *Journal of Photochemistry and Photobiology a-Chemistry,* 188**,** 1-4.

HUANG, J. H., SCHWESIG, D. & MATZNER, E. (2004) Organotin compounds in precipitation, fog and soils of a forested ecosystem in Germany. *Environmental Pollution,* 130**,** 177-186.

IMO (2002) International maritime organization TBT antifouling ban: Account of discussion at IMO-MEPC47: http://www.imo.org/. London, UK.

IP, S. W. & TOGURI, J. M. (1994) The equivqlency of surface tension, surface energy and surface free energy. *Journal of Materials Science,* 29**,** 688-692.

IPCS (1990) Environmental health criteria 116: Tributyltin compounds: http://www.inchem.org/documents/ehc/ehc/ehc116.htm#SubSectionNumber:4.2.1. *International Programme on Chemical Safety.*

JACOBSON, A. H. & WILLINGHAM, G. L. (2000) Sea-nine antifoulant: an environmentally acceptable alternative to organotin antifoulants. *Science of the Total Environment,* 258**,** 103-110.

JIANG, G. B., LIU, J. Y. & YANG, K. W. (2000) Speciation analysis of butyltin compounds in Chinese seawater by capillary gas chromatography with flame photometric detection using in-situ hydride derivatization followed by headspace solid-phase microextraction. *Analytica Chimica Acta,* 421**,** 67-74.

JIE, H., PARK, H., CHAE, K. H., ANPO, M. & PARK, J. K. (2009) Suppressed recombination of electrons and holes and its role on the improvement of photoreactivity of flame-synthesized TiO2 nanopowders. *Chemical Physics Letters,* 470**,** 269-274.

KALOYANOVA, F. P., EL BATAWI, M.A. (1991) *In: Human toxicology of pesticides,* Florida, CRC Press.

KAMRUDDIN, S. K., CHATTOPADHYAYA, T. K., ROY, A. & TIEKINK, E. R. T. (1996) Biocidal organotin compounds .2. Synthesis, characterization and biocidal properties of triorganotin(IV) hydantoic acid derivatives and the crystal structures of triphenyltin and tricyclohexyltin hydantoates. *Applied Organometallic Chemistry,* 10, 513-521.

KEENAN, H. E., SAKULTANTIMETHA, A., BANGKEDPHOL, S. (2008) Environmental fate and partition co-efficient of oestrogenic compounds in sewage treatment process. *Environmental Research,* 106**,** 313-318.

KERK, G. J. M. V. D. (1975) Present status of the use of organotin compounds. *Chemiker-Zeitung* 99**,** 26-32.

KIRK-OTHMER (1981) *Encyclopedia of chemical technology,* New York, USA, Wiley & Sons

KONSTANTINOU, I. K. & ALBANIS, T. A. (2004) Worldwide occurrence and effects of antifouling paint booster biocides in the aquatic environment: a review. *Environment International,* 30**,** 235-248.

KRAJNC, E. I., WESTER, P. W., LOEBER, J. G., VANLEEUWEN, F. X. R., VOS, J. G., VAESSEN, H. & VANDERHEIJDEN, C. A. (1984) Toxicity of bis(tri-normal-butyltin) oxide in the rat. short-term effects on general parameters and on the endocrine and lymphoid systems. *Toxicology and Applied Pharmacology,* 75**,** 363-386.

KSIBI, M., ROSSIGNOL, S., TATIBOUET, J. M. & TRAPALIS, C. (2008) Synthesis and solid characterization of nitrogen and sulfur-doped TiO2 photocatalysts active under near visible light. *Materials Letters,* 62**,** 4204-4206.

LANDMEYER, J. E., TANNER, T. L. & WATT, B. E. (2004) Biotransformation of tributyltin to tin in freshwater river-bed sediments contaminated by an organotin release. *Environmental Science & Technology,* 38**,** 4106-4112.

LANGSETH, W. (1984) Determination of diphenyltin and dialkyltin homologs by HPLC with morin in the eluent. *Talanta,* 31**,** 975-978.

LANGSTON, W. J. & POPE, N. D. (1995) Determinants of TBT adsorption and desorption in estuarine sediments. *Marine Pollution Bulletin,* 31**,** 32-43.

LASCOURREGES, J. F., CAUMETTE, P. & DONARD, O. F. X. (2000) Toxicity of butyltin, phenyltin and inorganic tin compounds to sulfate-reducing bacteria isolated from anoxic marine sediments. *Applied Organometallic Chemistry,* 14**,** 98-107.

LAUGHLIN, R. B., FRENCH, W. & GUARD, H. E. (1986) Accumulation of bis(tributyltin) oxide by the marine mussel mytilus-edulis. *Environmental Science & Technology,* 20**,** 884-890.

LAWLER, I. F. & ALDRICH, J. C. (1987) Sublethal effects of bis(tri-normal-butyltin) oxide on crassostrea-gigas spat. *Marine Pollution Bulletin,* 18**,** 274-278.

LE GAC, M., LESPES, G. & POTIN-GAUTIER, M. (2003) Rapid determination of organotin compounds by headspace solid-phase microextraction. *Journal of Chromatography A,* 999**,** 123-134.

LINSEBIGLER, A. L., LU, G. Q. & YATES, J. T. (1995) Photocatalysis on Tio_2 surfaces - principles, mechanisms, and selected results. *Chemical Reviews,* 95**,** 735-758.

LOCH, J. P. G., GREVE, P. A. & VANDERBERG, S. (1990) Accumulation and leaching of the fungicide fentin acetate and intermediates in sandy soils. *Water Air and Soil Pollution,* 53**,** 119-129.

MACHIDA, M., AIKAWA, M. & TATSUMOTO, H. (2005) Prediction of simultaneous adsorption of Cu(II) and Pb(II) onto activated carbon by conventional Langmuir type equations. *Journal of Hazardous Materials,* 120**,** 271-275.

MACKAY, D. (2001) *Multimedia environmental models: The fugacity approach* London, Lewis Publishers.

MACKAY, D. & PATERSON, S. (1981) Calculating Fugacity. *Environmental Science & Technology,* 15**,** 1006-1014.

MAGUIRE, R. J. & TKACZ, A. J. (1985) Degradation of the tri-n-butyltin species in water and sediment from Toronto Harbour. *Journal of agricultural and food chemistry,* 33**,** 947-953.

MANESS, P. C., SMOLINSKI, S., BLAKE, D. M., HUANG, Z., WOLFRUM, E. J. & JACOBY, W. A. (1999) Bactericidal activity of photocatalytic TiO2 reaction: Toward an understanding of its killing mechanism. *Applied and Environmental Microbiology,* 65**,** 4094-4098.

MARSHALL, P., CHRISTIE, C., DOBB, K., GREEN, A., HAYNES, D., BRODIE, J., MICHALEK-WAGNER, K., SMITH, A., STORRIE, J. & TURAK, E. (2002) Grounded ship leaves TBT-based antifoulant on the Great Barrier Reef: An overview of the environmental response. *Spill Science & Technology Bulletin,* 7**,** 215-221.

MARTINEZ, K., FERRER, I. & BARCELO, D. (2000) Part-per-trillion level determination of antifouling pesticides and their by products in seawater samples by off-line solid-phase extraction followed by high-performance liquid chromatography-atmospheric pressure chemical ionization mass spectrometry. *Journal of Chromatography A,* 879**,** 27-37.

MATHIAS, P. M., KUMAR, R., MOYER, J. D., SCHORK, J. M., SRINIVASAN, S. R., AUVIL, S. R. & TALU, O. (1996) Correlation of multicomponent gas adsorption by the dual-site Langmuir model. Application to nitrogen/oxygen adsorption on 5A-zeolite. *Industrial & Engineering Chemistry Research,* 35**,** 2477-2483.

MATSUI, H., WADA, O., MANABE, S., ONO, T., IWAI, H. & FUJIKURA, T. (1982) [Properties and mechanism of hyperlipidemia induced in rabbits by tributyltin fluoride]. *Sangyo Igaku,* 24**,** 163-71.

MATTHIESSEN, P. & GIBBS, P. E. (1998) Critical appraisal of the evidence for tributyltin-mediated endocrine disruption in mollusks. *Environmental Toxicology and Chemistry,* 17**,** 37-43.

MCKAY, D. (2001) *Multimedia environmental models: The fugacity approach* London, Lewis Publishers.

MILLER, J. N. & MILLER, J. C. (2000) *Statistics and chemometrics for analytical chemistry,* Harlow, USA, Pearson Education Limited.

MOENS, L., DESMAELE, T., DAMS, R., VANDENBROECK, P. & SANDRA, P. (1997) Sensitive, simultaneous determination of organomercury, -lead, and -tin compounds with headspace solid phase microextraction capillary gas chromatography combined with inductively coupled plasma mass spectrometry. *Analytical Chemistry,* 69**,** 1604-1611.

MORIKAWA, T., ASAHI, R., OHWAKI, T., AOKI, K. & TAGA, Y. (2001) Band-gap narrowing of titanium dioxide by nitrogen doping. *Japanese Journal of Applied Physics Part 2-Letters,* 40**,** L561-L563.

MUGGLI, D. S. & DING, L. F. (2001) Photocatalytic performance of sulfated TiO2 and Degussa P-25TiO(2) during oxidation of organics. *Applied Catalysis B-Environmental,* 32**,** 181-194.

MULLER, M. D. (1987) Comprehensive trace level determination of organotin compounds in environmental-samples using high-resolution gas-chromatography with flame photometric detection. *Analytical Chemistry,* 59**,** 617-623.

NAGAVENI, K., SIVALINGAM, G., HEDGE, M. S. & MADRAS, G. (2004) Solar photocatalytic degradation of dyes: high activity of combustion synthesized nano TiO2. *Applied Catalysis B-Environmental,* 48**,** 83-93.

NAKAMURA, R., TANAKA, T. & NAKATO, Y. (2004) Mechanism for visible light responses in anodic photocurrents at N-doped TiO2 film electrodes. *Journal of Physical Chemistry B,* 108**,** 10617-10620.

NAKANO, Y., MORIKAWA, T., OHWAKI, T. & TAGA, Y. (2007) Origin of visible-light sensitivity in N-doped TiO2 films. *Chemical Physics,* 339**,** 20-26.

NAVIO, J. A., CERRILLOS, C. & MACIAS, M. (2009) Degradation of n-butyl tin chlorides in waters. A comparative assessment of the process by photo-assisted and chemical- treatment methods. *Journal of Advanced Oxidation Technologies,* 12**,** 158-163.

NAVIO, J. A., CERRILLOS, C., MARCHENA, F. J., PABLOS, F. & PRADERA, M. A. (1996) Photoassisted degradation of n-butyltin chlorides in air-equilibrated aqueous TiO2 suspension. *Langmuir,* 12**,** 2007-2014.

NAVIO, J. A., MARCHENA, F. J., CERRILLOS, C. & PABLOS, F. (1993) UV photolytic degradation of butyltin chlorides in water. *Journal of Photochemistry and Photobiology a-Chemistry,* 71**,** 97-102.

NIEDERER, C. & GOSS, K. U. (2008) Effect of ortho-chlorine substitution on the partition behavior of chlorophenols. *Chemosphere,* 71**,** 697-702.

NIEHS (2006): National Institute of Environmental Health Sciences; Endocrine disruptors: http://www.niehs.nih.gov. North Carolina, USA.

O'NEILL, P. (1998) *Environmental chemistry,* London, UK, Blackie Academic & Profersional, an imprint of Thomson Science.

OCALLAGHAN, J. P. & MILLER, D. B. (1988) Acute exposure of the neonatal rat to triethyltin results in persistent changes in neurotypic and gliotypic proteins. *Journal of Pharmacology and Experimental Therapeutics,* 244**,** 368-378.

OECD (1995)*: Organization for Economic Cooperation and Development (OECD) guideline for the testing of chemical: water solubility (105),* Paris, OECD publidher.

OHNO, T., SARUKAWA, K., TOKIEDA, K. & MATSUMURA, M. (2001) Morphology of a TiO2 photocatalyst (Degussa, P-25) consisting of anatase and rutile crystalline phases. *Journal of Catalysis,* 203**,** 82-86.

OMAE, I. (2003) Organotin antifouling paints and their alternatives. *Applied Organometallic Chemistry,* 17**,** 81-105.

PATTERSON, A. L. (1939) The Scherrer formula for X-Ray particle size determination. *Physical Review,* 56**,** 978.

PELIKAN, Z. & CERNY, E. (1968) The toxic effects of tri-n butyl tin compounds on white mice. *Archives of Toxicology,* 23**,** 283-292.

PRAET, A., DEWAELE, C., VERDONCK, L. & VANDERKELEN, G. P. (1990) Liquid-chromatography of organotin compounds on cyanopropyl silica-gel. *Journal of Chromatography,* 507**,** 427-437.

PRI (2008): The permaculture research institue; http://permaculture.org.au/. Australia.

QOURZAL, S., ASSABBANE, A. & AIT-ICHOU, Y. (2004) Synthesis of TiO2 via hydrolysis of titanium tetraisopropoxide and its photocatalytic activity on a suspended mixture with activated carbon in the degradation of 2-naphthol. *Journal of Photochemistry and Photobiology a-Chemistry,* 163**,** 317-321.

QUEVAUVILLER, P., DONARD, O. F. X. & ETCHEBER, H. (1994) Butyltin distribution in a sediment core from Arcachon harbor (France). *Environmental Pollution,* 84**,** 89-92.

RAJESH, K. N. (1999) *Endocrine Disruptors: Effects on Male and Female Reproductive Systems,* USA, CRC Press, LLC.

REUTHER, R., JAEGER, L. & ALLARD, B. (1999) Determination of organometallic forms of mercury, tin and lead by in situ derivatization, trapping and gas chromatography - atomic emission detection. *Analytica Chimica Acta,* 394**,** 259-269.

RINKER, E. B., OELSCHLAGER, D. W., COLUSSI, A. T., HENRY, K. R., SANDALL, O. C. (1994) Viscosity, density, and surface tension of binary mixtures of water and N-methyldiethanolamine and water and diethanolamine and tertiary mixtures of these amines with water over the temperature range 20-100 degree C. *Journal of Chemical and Engineering Data,* 39**,** 392-395.

RYDBERG, J., COX, M., MUSIKAS, C., CHOPPIN, G.R. (2004) *Solvent extraction principles and practice*, Marcel Dekker, Inc., New York, USA.

SAEKI, K., NABESHIMA, A., KUNITO, T. & OSHIMA, Y. (2007) The stability of butyltin compounds in a dredged heavily-contaminated sediment. *Chemosphere,* 68**,** 1114-1119.

SAINT-LOUIS, R. & PELLETIER, E. (2004) Sea-to-air flux of contaminants via bubbles bursting. An experimental approach for tributyltin. *Marine Chemistry,* 84**,** 211-224.

SAMIULLAH, Y. (1990) *Prediction of the environmental fate of chemicals.,* New York, USA, Elsevier applied science.

SANDERSON, H., FAUSER, P., THOMSEN, M. & SORENSEN, P. B. (2007) PBT screening profile of chemical warfare agents (CWAs). *Journal of Hazardous Materials,* 148**,** 210-215.

SANTISTEBAN, J. I., MEDIAVILLA, R., LOPEZ-PAMO, E., DABRIO, C. J., ZAPATA, M. B. R., GARCIA, M. J. G., CASTANO, S. & MARTINEZ-ALFARO, P. E. (2004) Loss on ignition: a qualitative or quantitative method for organic matter and carbonate mineral content in sediments? *Journal of Paleolimnology,* 32**,** 287-299.

SEINEN, W., HELDER, T., VERNIJ, H., PENNINKS, A. & LEEUWANGH, P. (1981) Short-term toxicity of tri-n-butyltinchloride in rainbow-trout (salmo-gairdneri richardson) yolk-sac fry. *Science of the Total Environment,* 19**,** 155-166.

SEPA (2003) Assessment of TBT impacts and concentrations in Scotland http://www.sepa.org.uk/science_and_research/data_and_reports/water.aspx. Glasgow, UK, Scottish Environment Protection Agency publisher.

SERRA, H. & NOGUEIRA, J. M. F. (2005) Organotin speciation in environmental matrices by automated on-line hydride generation-programmed temperature vaporization-capillary gas chromatography-mass spectrometry detection. *Journal of Chromatography A,* 1094**,** 130-137.

SHIOJI, H., TSUNOI, S., HARINO, H. & TANAKA, M. (2004) Liquid-phase microextraction of tributyltin and triphenyltin coupled with gas chromatography-tandem mass spectrometry - Comparison between 4-fluorophenyl and ethyl derivatizations. *Journal of Chromatography A,* 1048**,** 81-88.

SHORT, J. W., THROWER, F.P. (1986) *Accumulation of butyltins in muscle tissue of chinook salmon reared in sea pens treated with tri n butyltin,* Auke bay, U.S. National Oceanic and Atmospheric Administration.

SIRISAKSOONTORN, W., THACHEPAN, S. & SONGSASEN, A. (2009) Photodegradation of phenanthrene by N-doped TiO2 photocatalyst. *Journal of Environmental Science and Health Part a-Toxic/Hazardous Substances & Environmental Engineering,* 44**,** 841-846.

SIVALINGAM, G., NAGAVENI, K., HEGDE, M. S. & MADRAS, G. (2003) Photocatalytic degradation of various dyes by combustion synthesized nano anatase TiO2. *Applied Catalysis B-Environmental,* 45**,** 23-38.

SMITH, B. S. (1981) Male characteristics on female mud snails nassarius-obsoletus caused by anti fouling bottom paints. *Journal of Applied Toxicology,* 1**,** 22-25.

SPARKS, D. L. (1995) *Environmental soil chemistry,* San Diego, California, Academic Press, INC.

SPURR, R. A. & MYERS, H. (1957) Quantitative analysis of anatase-rutile mixtures with an X-ray diffractometer. *Analytical Chemistry,* 29**,** 760-762.

STEFAN, W. (2009) Permaculture Research Institue. The pollution issues; http://www.pollutionissues.com/A-Bo/Bioaccumulation.html. Australia.

SUEHIRO, F., KOBAYASHI, T., NONAKA, L., TUYEN, B. C. & SUZUKI, S. (2006) Degradation of tributyltin in microcosm using Mekong River sediment. *Microbial Ecology,* 52**,** 19-25.

SUN, B., VORONTSOV, A. V. & SMIRNIOTIS, P. G. (2003) Role of platinum deposited on TiO2 in phenol photocatalytic oxidation. *Langmuir,* 19**,** 3151-3156.

SZPUNARLOBINSKA, J., CEULEMANS, M., LOBINSKI, R. & ADAMS, F. C. (1993) Flow-injectionsample preparation for organotin speciation analysis of water by capillary gas-chromatography microwave-induced plasma-atomic emission-spectrometry. *Analytica Chimica Acta,* 278**,** 99-113.

TAKAHASHI, S., MUKAI, H., TANABE, S., SAKAYAMA, K., MIYAZAKI, T. & MASUNO, H. (1999) Butyltin residues in livers of humans and wild terrestrial mammals and in plastic products. *Environmental Pollution,* 106**,** 213-218.

TAN, K. H. (1998) *Principles of Soil Chemistry,* New York, USA, Marcel Dekker Inc.

THOMAS, K. V., FILEMAN, T. W., READMAN, J. W. & WALDOCK, M. J. (2001) Antifouling paint booster biocides in the UK coastal environment and potential risks of biological effects. *Marine Pollution Bulletin,* 42**,** 677-688.

TSOUKLERIS, D. S., MAGGOS, T., VASSILAKOS, C. & FALARAS, P. (2007) Photocatalytic degradation of volatile organics on TiO2 embedded glass spherules. *Catalysis Today,* 129**,** 96-101.

UNEP (2005) *Report of the interim chemical review committee: tributyltin compounds* Nairobi, UNEP publisher.

UNGER, M. A. (1988) Sorption behaviour of butyltin on estuarine and freshwater sediments. *Environmental Toxicology and Chemistry,* 7**,** 907-915.

USEPA (1985) *Technical Support Document: Tributyltin,* Washington DC, USEPA office of pesticide programs publisher.

VERCAUTEREN, J., DE MEESTER, A., DE SMAELE, T., VANHAECKE, F., MOENS, L., DAMS, R. & SANDRA, P. (2000) Headspace solid-phase microextraction-capillary gas chromatography-ICP mass spectrometry for the determination of the organotin pesticide fentin in environmental samples. *Journal of Analytical Atomic Spectrometry,* 15**,** 651-656.

VERCAUTEREN, J., PERES, C., DEVOS, C., SANDRA, P., VANHAECKE, F. & MOENS, L. (2001) Stir bar sorptive extraction for the determination of ppq-level traces of organotin compounds in environmental samples with thermal desorption-capillary gas Chromatography - ICP mass spectrometry. *Analytical Chemistry,* 73**,** 1509-1514.

VOMVAS, A., POMONI, K., TRAPALIS, C. & TODOROVA, N. (2007) Photoconductivity in sol-gel TiO2 thin films with and without ammonia treatment. *Materials Science-Poland,* 25**,** 809-816.

WANG, X. P., DING, L., ZHANG, H. R., CHENG, J. H., YU, A. M., ZHANG, H. Q., LIU, L., LIU, Z. H. & LI, Y. (2006) Development of an analytical method for organotin compounds in fortified flour samples using microwave-assisted extraction and normal-phase HPLC with UV detection. *Journal of Chromatography B-Analytical Technologies in the Biomedical and Life Sciences,* 843**,** 268-274.

WANG, Z. P., CAI, W. M., HONG, X. T., ZHAO, X. L., XU, F. & CAI, C. G. (2005) Photocatalytic degradation of phenol in aqueous nitrogen-doped TiO2 suspensions with various light sources. *Applied Catalysis B-Environmental,* 57**,** 223-231.

WEBER, J. H. (1970) *Mechanism of adsorption of s-triazines by clay colloids and factors affecting plant availability,* New York, USA, Springer-Verlag.

WESTER, P. W., KRAJNC, E. I., VANLEEUWEN, F. X. R., LOEBER, J. G., VANDERHEIJDEN, C. A., VAESSEN, H. & HELLEMAN, P. W. (1990) Chronic toxicity and carcinogenicity of bis(tri-normal-butyltin) oxide (Tbto) in the rat. *Food and Chemical Toxicology,* 28**.**

WFD (2005)*: Water Framework Directive, "Environmental Quality Standards (EQS) Substance Data Sheet: Tributyltin compounds (TBT-ion)," Common Implementation Strategy for the Water Framework Directive, 15 January 2005,* Brussel, Water Framework Directive.

WHO (2002): World Health Organisation; The International Programme on Chemicals Safety (IPCS): Global assessment of the state-of-the-science of the endocrine disruptors: http://www.who.int/ipcs/publications/new_issues/endocrine_disruptors/en/. USA.

WUERTZ, S., MILLER, C. E., PFISTER, R. M. & COONEY, J. J. (1991) Tributyltin-resistant bacteria from estuarine and fresh-water sediments. *Applied and Environmental Microbiology,* 57**,** 2783-2789.

YEBRA, D. M., KIIL, S. & DAM-JOHANSEN, K. (2004) Antifouling technology - past, present and future steps towards efficient and environmentally friendly antifouling coatings. *Progress in Organic Coatings,* 50**,** 75-104.

ZACHAREWSKI, T. (1998) Identification and assessment of endocrine disruptors: Limitations of in vivo and in vitro assays. *Environmental Health Perspectives,* 106**,** 577-582.

ZHANG, L. H., LI, P. J., GONG, Z. Q. & LI, X. M. (2008) Photocatalytic degradation of polycyclic aromatic hydrocarbons on soil surfaces using TiO2 under UV light. *Journal of Hazardous Materials,* 158**,** 478-484.

Appendices

Appendix A

- The polarity of the mobile phase on the HPLC separation

- Calculation of t-test and limit of detection (LOD)

Appendix Table A1 The polarity of the mobile phase on the HPLC separation

Mobile phases	Retention time (min)		
	TBT	DBT	MBT
Hexane	5.4	11.8	-
Hexane containing ethanol, 1% v/v	5.6	17.4	-
Hexane containing methanol, 1% v/v	5.5	18.6	-
Hexane containing water, 4% v/v	5.6	24.7	-

The optimised HPLC procedure was compared with the standard GC-MS method using the paired t-test at 95% confidence interval (Miller and Miller, 2000).

Appendix Table A2 The calculation of t-test between developed HPLC and standard GC-MS on various concentration of TBT in the samples

Batch	Concentration (mg L^{-1})	Concentration by HPLC (mg L^{-1})	Concentration by GC-MS (mg L^{-1})	Difference value : d	$t = \frac{\bar{d}\sqrt{n}}{S_d}$
1	5	4.85	5.15	-0.3	
2	10	10.03	9.72	0.31	
3	15	15.38	14.84	0.54	
4	20	20.06	20.20	-0.14	
5	25	24.69	24.92	-0.23	
6	30	29.92	30.16	-0.24	0.778
7	35	35.55	35.02	0.53	(t value)
8	40	39.82	39.6	0.22	
9	45	45.41	45.13	0.28	
10	50	50.08	50.24	-0.16	
n = 10			$\sum d$	0.81	
			Average d: $\bar{d}$	0.081	$t_{9\ (0.05)}$ = 2.26
			S_d	0.329	(t critical)

$H_o : \mu_d = 0$

$H_1 : \mu_d \neq 0$

From t-test, t calculated value < t critical
Therefore, null hypothesis is accepted. There are no different between two methods

Appendix Table A3 The calculation of t-test between developed HPLC and standard GC-MS on various concentration of DBT in the samples

Batch	Concentration ($mg\ L^{-1}$)	Concentration by HPLC ($mg\ L^{-1}$)	Concentration by GC-MS ($mg\ L^{-1}$)	Difference value : d	$t = \frac{\overline{d}\sqrt{n}}{S_d}$
1	5	4.89	5.25	-0.36	
2	10	10.42	10.18	0.24	
3	15	15.55	15.06	0.49	
4	20	20.93	20.97	-0.04	
5	25	25.42	24.54	0.88	
6	30	29.55	29.76	-0.21	1.077
7	35	34.98	35.23	-0.25	(t value)
8	40	40.14	39.23	0.91	
9	45	44.69	45.25	-0.56	
10	50	50.64	49.88	0.76	
n = 10			$\sum d$	1.86	$t_{9\ (0.05)}$ = 2.26
			Average d: $\overline{d}$	0.186	(t critical)
			S_d	0.546	

$H_o : \mu_d = 0$

$H_1 : \mu_d \neq 0$

From t-test, t calculated value < t critical
Therefore, null hypothesis is accepted. There are no different between two methods

Calculation of limit of detection (LOD) for TBT determined by NPHPLC (Miller and Miller, 2000)

Appendix Table A4 Calculation data of TBT

Concentration (mg L^{-1})	Average peak area, y_i	Signal from regression line, [$\hat{y}$] $\hat{y}$ = 815.44X+ 35.999 R^2 = 0.9998	y-residuals $[y_i - \hat{y}]^2$
3	2419	2482	3967
5	4070	4113	1837
10	7970	8190	48575
15	12512	12267	59894
20	16516	16344	29424
50	40718	40808	8039

Calculation

To obtain the calculation, substitute a and $S_{y/x}$ in LOD signal = a + $3S_{y/x}$

When: a is intercept of regression line

$S_{y/x}$ is $\sqrt{\frac{\Sigma[y_i - \hat{y}]^2}{n-2}}$, n = 6

Therefore: LOD signal = (35.999) + 3(194.768)

= 620.305

From the formula of regression line is Y = 815.44X+ 35.999

When: Y = LOD signal , and X = LOD

Therefore: LOD = 0.71 mg L^{-1}

Calculation of limit of detection (LOD) for DBT determined by NPHPLC (Miller and Miller, 2000)

Appendix Table A5 Calculation data of DBT

Concentration (mg L^{-1})	Average peak area, y_i	Signal from regression line, [$\hat{y}$] $\hat{y}$ = 1531.6X+808.44 R^2 = 0.997	y-residuals $[y_i - \hat{y}]^2$
1	1610	2340	532958
3	4723	5403	462273
5	7121	8466	1809312
10	18163	16124	4157086
15	23338	23782	197527
20	33516	31440	4307949
50	76474	77388	836201

Calculation

To obtain the calculation, substitute a and $S_{y/x}$ in LOD signal = a + $3S_{y/x}$

When: a is intercept of regression line

$S_{y/x}$ is $\sqrt{\frac{\Sigma[y_i-\hat{y}]^2}{n-2}}$, n = 7

Therefore: LOD signal = (808.44) + 3(1568.65) = 5514.388

From the formula of regression line is Y = 1531.6X+808.44

When: Y = LOD signal , and X = LOD

Therefore: LOD = 0.50 mg L^{-1}

Calculation of limit of detection (LOD) for TBT determined by GC-MS (Miller and Miller, 2000)

Appendix Table A6 Calculation data of TBT

Concentration (mg L^{-1})	Average peak area, y_i	Signal from regression line, [$\hat{y}$] $\hat{y}$ = 182908X + 148765 R^2 = 0.9977	y-residuals $[y_i - \hat{y}]^2$
0.5	187000	240219	2832261961
1	324069	331673	57825885
5	1127344	1063305	4100993521
10	2025398	1977845	2261319511
15	2841621	2892385	2577017539

Calculation

To obtain the calculation, substitute a and $S_{y/x}$ in LOD signal = a + $3S_{y/x}$

When: a is intercept of regression line

$S_{y/x}$ is $\sqrt{\frac{\Sigma[y_i-\hat{y}]^2}{n-2}}$, n = 5

Therefore: LOD signal = (148765) + 3(62794.42)

= 337148.27

From the formula of regression line is Y = 182908X + 148765

When: Y = LOD signal , and X = LOD

Therefore: LOD = 1.03 mg L^{-1}

Calculation of limit of detection (LOD) for DBT determined by GC-MS (Miller and Miller, 2000)

Appendix Table A7 Calculation data of DBT

Concentration (mg L^{-1})	Average peak area, y_i	Signal from regression line, [$\hat{y}$] $\hat{y}$ = 186909X + 116133 R^2 = 0.9967	y-residuals $[y_i - \hat{y}]^2$
0.5	135560	209588	5480120108
1	301324	303042	2950379
5	1143120	1050678	8545584992
10	2019833	1985223	1197829027
15	2868468	2919768	2631724200

Calculation

To obtain the calculation, substitute a and $S_{y/x}$ in LOD signal = a + $3S_{y/x}$

When: a is intercept of regression line

$S_{y/x}$ is $\sqrt{\frac{\Sigma[y_i - \hat{y}]^2}{n-2}}$, n = 5

Therefore: LOD signal = (116133) + 3(77153.98)

= 347594.93

From the formula of regression line is Y = 186909X + 116133

When: Y = LOD signal , and X = LOD

Therefore: LOD = 1.24 mg L^{-1}

Calculation of limit of detection (LOD) for MBT determined by GC-MS (Miller and Miller, 2000)

Appendix Table A8 Calculation data of MBT

Concentration (mg L^{-1})	Average peak area, y_i	Signal from regression line, [$\hat{y}$] $\hat{y}$ = 183376X - 41614 R^2 = 0.9932	y-residuals $[y_i - \hat{y}]^2$
0.5	7739	50074	1792280448
1	68287	141762	5398624608
5	1008836	875266	17840855853
10	1853518	1792146	3766563299
15	2629905	2709026	6260079894

Calculation

To obtain the calculation, substitute a and $S_{y/x}$ in LOD signal = a + $3S_{y/x}$

When: a is intercept of regression line

$S_{y/x}$ is $\sqrt{\frac{\Sigma[y_i-\hat{y}]^2}{n-2}}$, n = 5

Therefore: LOD signal = (41614) + 3(108102.4)

= 347594.93

From the formula of regression line is Y = 183376X - 41614

When: Y = LOD signal , and X = LOD

Therefore: LOD = 2.22 mg L^{-1}

Appendix B

- The XRD diffraction patterns of illite and montmorillonite

- The X-ray diffraction 2θ d-spacing and specific density conversion tables

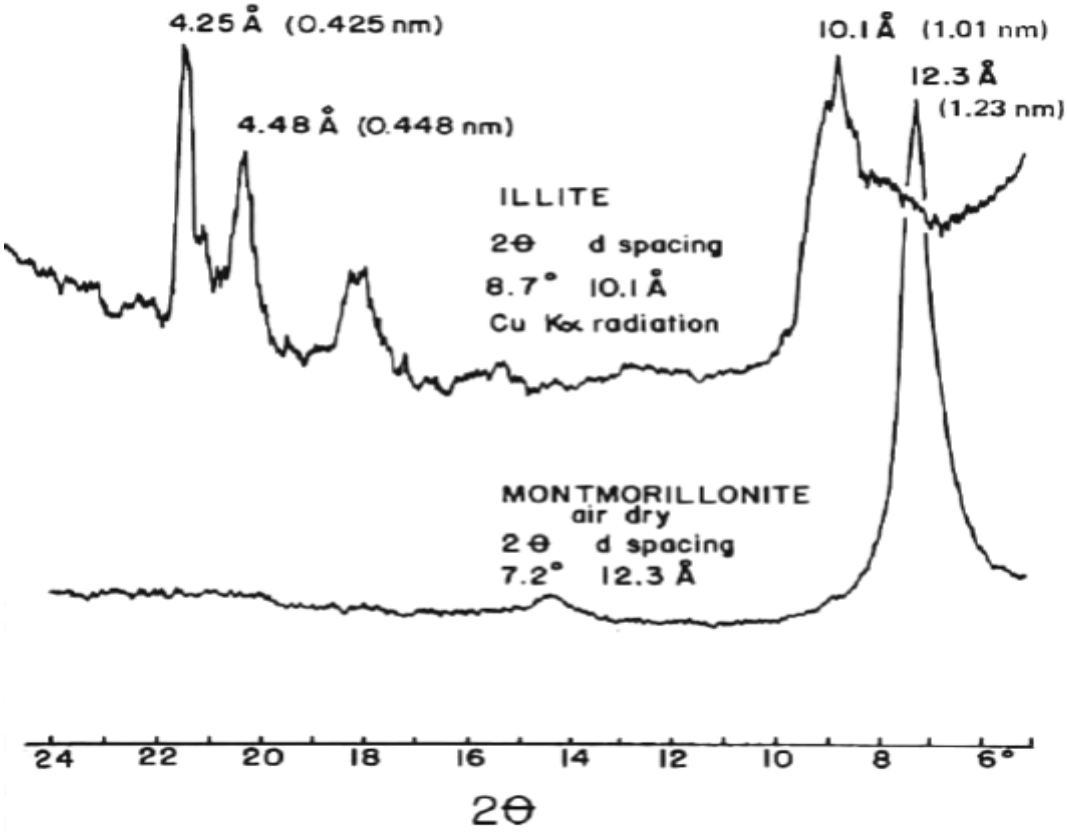

Appendix Figure B1 The interpretation and identification of illite and montmorillonite using XRD pattern. A first order diffraction peaks at $2\theta = 8.7^{o}$ and 7.2^{o} are diagnostic for the presence of illite and montmorillonite, respectively (Tan, 1998).

Appendix Table B1 The X-ray diffraction 2θ d-spacing conversion table

2θ d Spacing Values for Cu Kα Radiation with λ = 1.5405 Å (0.1540 nm)

2θ	0.0	0.1	0.2	0.3	0.4	0.5	0.6	0.7	0.8	0.9
0	∞	882.63	441.32	294.21	220.66	176.53	147.11	126.09	110.33	98.076
1	88.263	80.245	73.555	67.897	63.047	58.845	55.167	51.922	49.038	46.457
2	44.135	42.033	40.122	38.378	36.779	35.308	33.950	32.693	31.526	30.440
3	29.425	28.476	27.587	26.751	25.964	25.223	24.522	23.859	23.232	22.636
4	22.071	21.532	21.020	20.531	20.065	19.619	19.193	18.785	18.394	18.018
5	17.659	17.312	16.979	16.660	16.352	16.054	15.768	15.491	15.225	14.967
6	14.717	14.476	14.243	14.017	13.798	13.586	13.381	13.181	12.988	12.800
7	12.617	12.440	12.267	12.099	11.936	11.777	11.622	11.471	11.325	11.182
8	11.042	10.906	10.773	10.644	10.517	10.394	10.273	10.155	10.040	9.9270
9	9.8168	9.7098	9.6042	9.5010	9.4001	9.3015	9.2053	9.1105	9.0173	8.9264
10	8.8378	8.7500	8.6645	8.5506	8.4989	8.4181	8.3387	8.2609	8.1847	8.1100
11	8.0360	7.9644	7.8935	7.8234	7.7549	7.6880	7.6220	7.5571	7.4932	7.4305
12	7.3688	7.3081	7.2484	7.1897	7.1320	7.0751	7.0192	6.9642	6.9100	6.8567
13	6.8042	6.7524	6.7015	6.6513	6.6019	6.5532	6.5053	6.4550	6.4114	6.3655
14	6.3203	6.2757	6.2317	6.1883	6.1456	6.1035	6.0619	6.0209	5.9804	5.9405
15	5.9011	5.8623	5.8239	5.7860	5.7488	5.7119	5.6755	5.6395	5.6041	5.5691
16	5.5345	5.5004	5.4666	5.4333	5.4004	5.3679	5.3358	5.3040	5.2727	5.2417
17	5.2111	5.1809	5.1510	5.1214	5.0922	5.0633	5.0348	5.0065	4.9787	4.9511
18	4.9238	4.8968	4.8701	4.8437	4.8176	4.7918	4.7663	4.7410	4.7160	4.6913
19	4.6669	4.6426	4.6187	4.5950	4.5715	4.5482	4.5253	4.5026	4.4801	4.4577
20	4.4357	4.4138	4.3922	4.3708	4.3496	4.3287	4.3079	4.2872	4.2669	4.2467
21	4.2267	4.2069	4.1872	4.1678	4.1486	4.1295	4.1106	4.0919	4.0733	4.0550
22	4.0367	4.0187	4.0008	3.9831	3.9656	3.9481	3.9309	3.9139	3.8969	3.8801
23	3.8635	3.8469	3.8306	3.8144	3.7983	3.7824	3.7666	3.7509	3.7354	3.7200
24	3.7047	3.6896	3.6746	3.6596	3.6449	3.6302	3.6157	3.6013	3.5870	3.5728
25	3.5587	3.5448	3.5309	3.5172	3.5036	3.4901	3.4767	3.4634	3.4502	3.4371
26	3.4241	3.4112	3.3984	3.3857	3.3731	3.3606	3.3482	3.3359	3.3236	3.3115
27	3.2995	3.2875	3.2758	3.2639	3.2522	3.2406	3.2291	3.2176	3.2063	3.1951
28	3.1839	3.1727	3.1617	3.1508	3.1399	3.1291	3.1184	3.1078	3.0973	3.0868
29	3.0763	3.0660	3.0557	3.0455	3.0354	3.0253	3.0153	3.0054	2.9955	2.9857
30	2.9760	2.9664	2.9568	2.9472	2.9377	2.9283	2.9190	2.9098	2.9005	2.8914
31	2.8823	2.8732	2.8643	2.8553	2.8465	2.8376	2.8289	2.8202	2.8116	2.8029
32	2.7945	2.7859	2.7775	2.7691	2.7608	2.7526	2.7443	2.7362	2.7281	2.7200
33	2.7120	2.7040	2.6961	2.6882	2.6804	2.6727	2.6649	2.6573	2.6496	2.6420
34	2.6345	2.6270	2.6195	2.6121	2.6048	2.5974	2.5902	2.5830	2.5757	2.5686
35	2.5615	2.5541	2.5474	2.5404	2.5334	2.5295	2.5196	2.5129	2.5060	2.4993
36	2.4926	2.4859	2.4793	2.4727	2.4661	2.4596	2.4531	2.4466	2.4402	2.4338
37	2.4274	2.4211	2.4149	2.4086	2.4024	2.3962	2.3901	2.3840	2.3779	2.3719
38	2.3659	2.3599	2.3540	2.3480	2.3421	2.3362	2.3305	2.3247	2.3189	2.3131
39	2.3074	2.3018	2.2962	2.2905	2.2849	2.2794	2.2739	2.2684	2.2629	2.2574

Appendix Table B2 The specific gravity conversion table

Specific Gravity	Grams Soil/L	Specific Gravity	Grams Soil/L	Specific Gravity	Grams Soil/L
1.0024	0.0	1.0136	18.0	1.0247	36.0
1.0027	0.5	1.0139	18.5	1.0250	36.5
1.0030	1.0	1.0142	19.0	1.0253	37.0
1.0033	1.5	1.0145	19.5	1.0257	37.5
1.0036	2.0	1.0148	20.0	1.0260	38.0
1.0040	2.5	1.0151	20.5	1.0263	38.5
1.0043	3.0	1.0154	21.0	1.0266	39.0
1.0046	3.5	1.0157	21.5	1.0269	39.5
1.0049	4.0	1.0160	22.0	1.0272	40.0
1.0052	4.5	1.0164	22.5	1.0275	40.5
1.0055	5.0	1.0167	23.0	1.0278	41.0
1.0058	5.5	1.0170	23.5	1.0281	41.5
1.0061	6.0	1.0173	24.0	1.0284	42.0
1.0064	6.5	1.0176	24.5	1.0288	42.5
1.0067	7.0	1.0179	25.0	1.0291	43.0
1.0071	7.5	1.0182	25.5	1.0294	43.5
1.0074	8.0	1.0185	26.0	1.0297	44.0
1.0077	8.5	1.0188	26.5	1.0300	44.5
1.0080	9.0	1.0191	27.0	1.0303	45.0
1.0083	9.5	1.0195	27.5	1.0306	45.5
1.0086	10.0	1.0198	28.0	1.0309	46.0
1.0089	10.5	1.0201	28.5	1.0312	46.5
1.0092	11.0	1.0204	29.0	1.0315	47.0
1.0095	11.5	1.0207	29.5	1.0319	47.5
1.0098	12.0	1.0210	30.0	1.0322	48.0
1.0102	12.5	1.0213	30.5	1.0325	48.5
1.0105	13.0	1.0216	31.0	1.0328	49.0
1.0108	13.5	1.0219	31.5	1.0331	49.5
1.0111	14.0	1.0222	32.0	1.0334	50.0
1.0114	14.5	1.0226	32.5	1.0337	50.5
1.0117	15.0	1.0229	33.0	1.0340	51.0
1.0120	15.5	1.0232	33.5	1.0343	51.5
1.0123	16.0	1.0235	34.0	1.0346	52.0
1.0126	16.5	1.0238	34.5	1.0350	52.5
1.0129	17.0	1.0241	35.0	1.0353	53.0
1.0133	17.5	1.0244	35.5	1.0356	53.5
				1.0359	54.0
				1.0362	54.5
				1.0365	55.0

Appendix C

- Calculation of crystallite sizes, phase composition and unit cell volume

The crystallite size was also calculated applying the Sherrer's equation as shown in Equation 1

$$d = \frac{k\lambda}{\beta \cos\theta_B} \qquad \text{.....(Equation 1)}$$

where d is the crystallite size (nm)

k is the constant whose value is approximately 0.9

λ is the wavelength of the X-ray radiation source (0.154 nm for Cu Kα)

β is the full width at half maximum intensity (FWHM) (radians)

θ_B is the Bragg angle at the position of the peak maximum

This is an example of finding all constants involved in the Sherrer's equation.

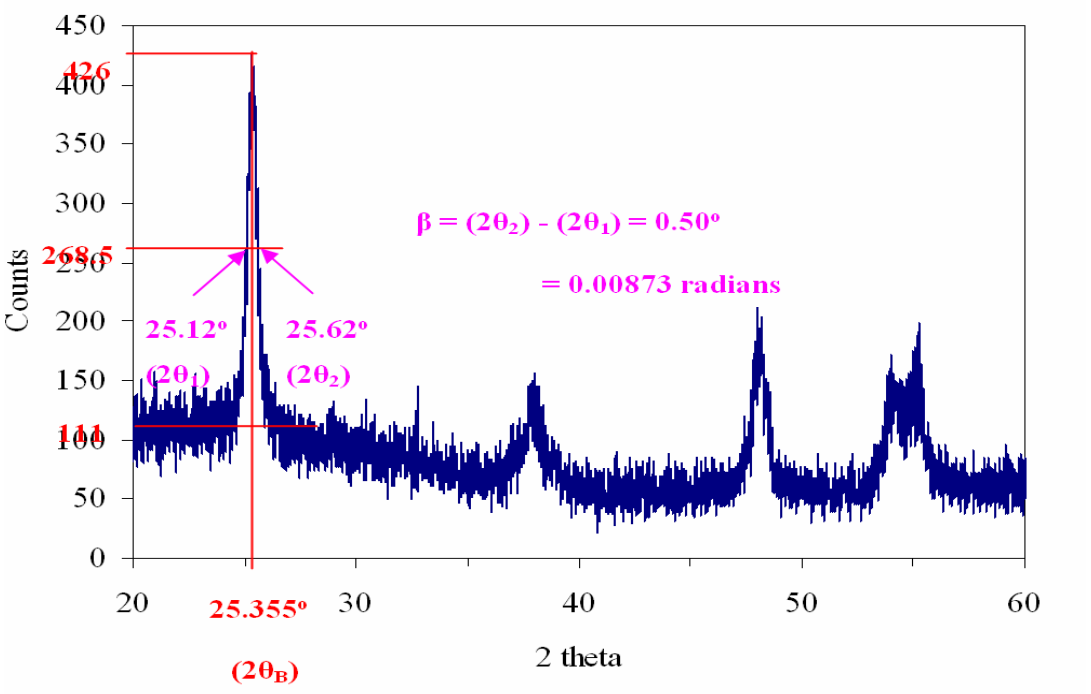

Appendix Figure C1 The XRD pattern of N-doped TiO_2 using titanium(IV) tetraisopropoxide mixed with NH_3 and calcined at 400 ºC.

Note: All color-labelled numbers were average values from the XRD raw data

The content of anatase was also calculated applying Spurr-Myers equation as shown in Equation 2.

$$w_A = \frac{1}{(1+1.26\frac{I_R}{I_A})} \qquad \text{.....(Equation 2)}$$

where w_A is the weight fraction of anatase in the mixture

I_R is the intensity of the diffraction peak of rutile

I_A is the intensity of the diffraction peak of anatase

This is an example of finding all constants involved in the Spurr-Myers equation.

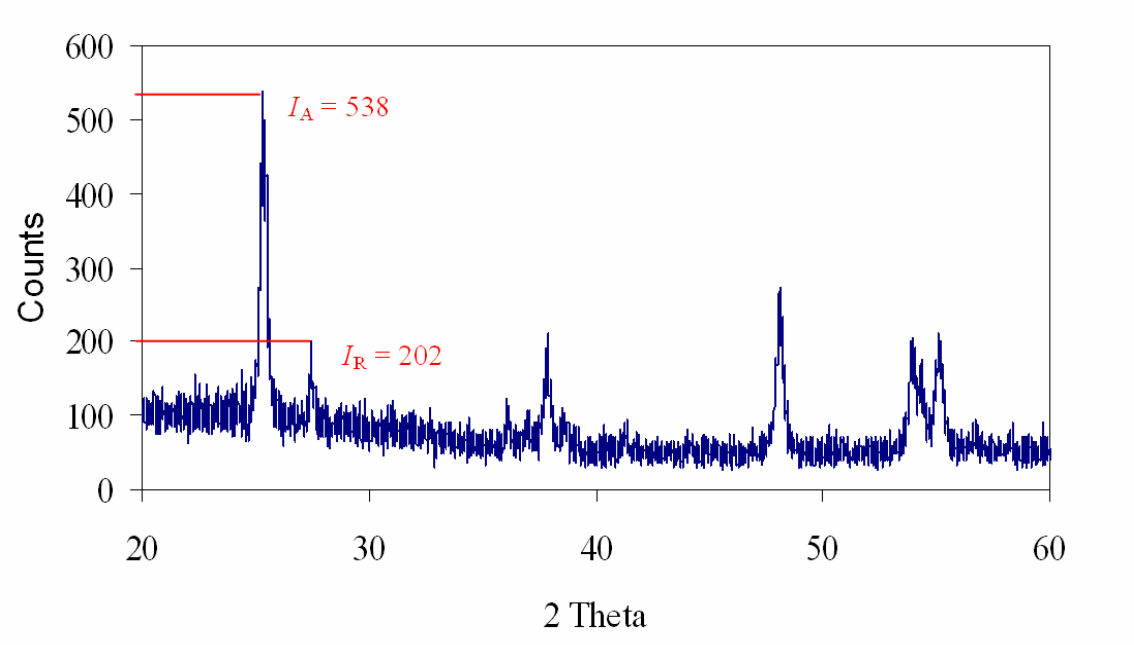

Appendix Figure C2 The XRD pattern of N-doped TiO_2 using titanium(IV) tetraisopropoxide mixed with NH_3 and calcined at 600 ºC.

Note: All color-labelled numbers were average values from the XRD raw data

The unit cell volume was calculated from the product of three lattice parameters (a, b and c), which can be equated for the tetragonal system (a≠b=c) as follows;

$$\frac{1}{d^2} = \frac{h^2 + k^2}{a^2} + \frac{l^2}{c^2} \qquad \text{.....(Equation 3)}$$

where d is a lattice spacing between the planes in the atomic lattice

h, k and l are the Miller indices

a, b and c are the lattice parameters

This is an example of finding all constants involved in the Equation 3. Firstly, the *d*-spacing value was calculated from Bragg's equation as shown below.

$$2d\sin\theta_B = n\lambda \qquad \text{.....(Equation 4)}$$

where θ_B is a Bragg's angle

n is an integer determined by the order given (n = 1)

λ is the wavelength of x-rays ($\lambda_{Cu\ K\alpha}$ = 0.154 nm)

From the XRD pattern (for anatase) as depicted in Appendix Figure C3, at $2\theta_B$ of 25.355^o and 38.875^o the *d*-spacing values were 0.3509 and 0.2373 nm, respectively. Secondly, the *d*-spacing values and the Miller indices were replaced into the Equation 3.

For the (101) plane;

$$\frac{1}{0.3509^2} = \frac{1^2+0^2}{a^2} + \frac{1^2}{c^2} \qquad \text{.....(Equation 5)}$$

For the (004) plane;

$$\frac{1}{0.2373^2} = \frac{0^2+0^2}{a^2} + \frac{4^2}{c^2} \qquad \text{.....(Equation 6)}$$

Last, from the Equations 5 and 6, a and c lattice constants will be obtained; a = 0.9492 nm and c = 0.3777 nm. Hence, the unit cell volume is finally equal to 0.1354 nm^3. For rutile cell volume, the specified $2\theta_B$ of 27.495 ^{o} and 54.385 ^{o} were shown in Appendix Figure C4. Therefore, the unit cell volume of rutile is equal to 0.0619 nm^3.

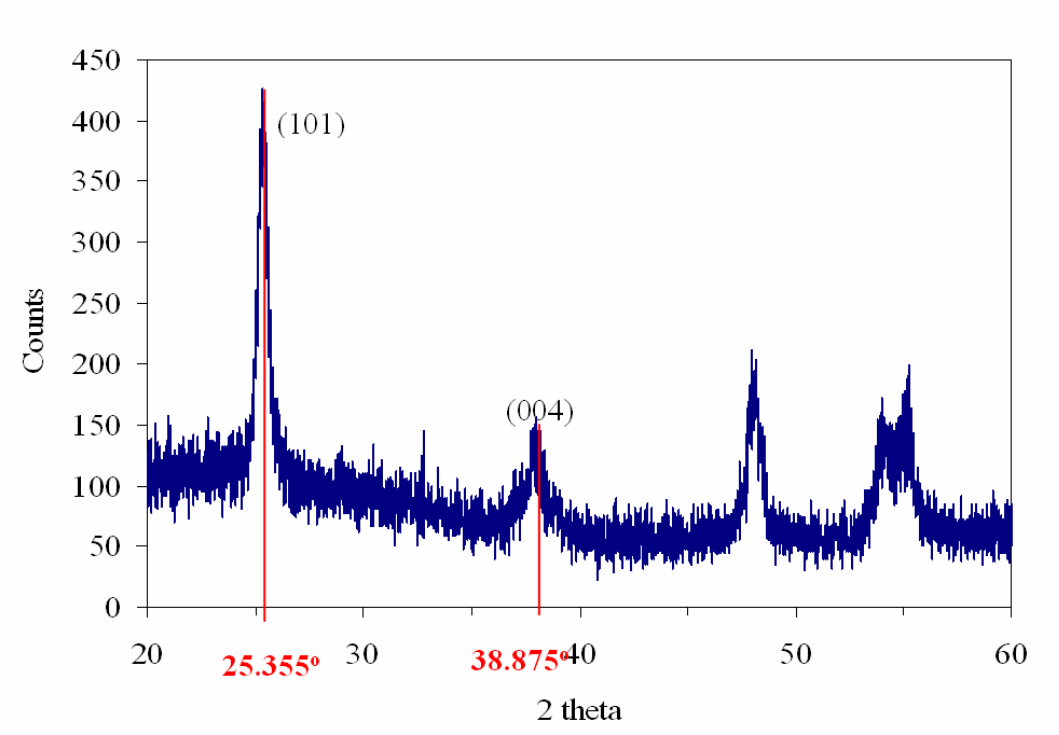

Appendix Figure C3 The XRD pattern of N-doped TiO_2 using titanium(IV) tetraisopropoxide mixed with NH_3 and calcined at 400 ºC

Note: All red-labelled numbers shown diffraction peaks of anatase

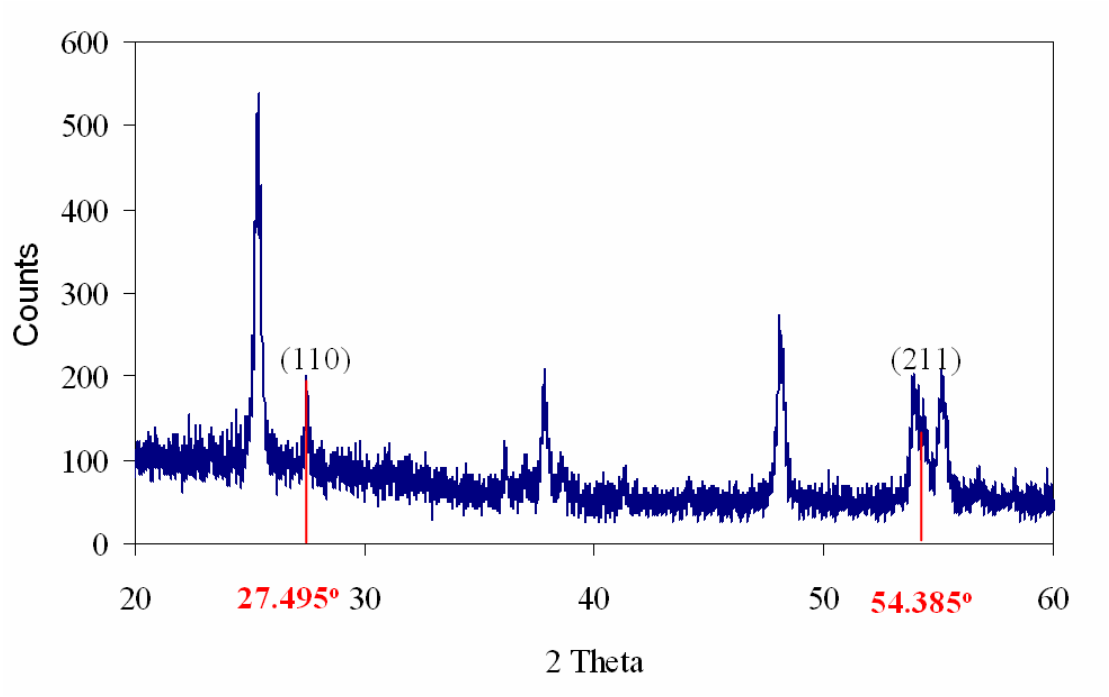

Appendix Figure C4 The XRD pattern of N-doped TiO_2 using titanium(IV) tetraisopropoxide mixed with NH_3 and calcined at 600 ºC.

Note: All red-labelled numbers shown diffraction peaks of rutile

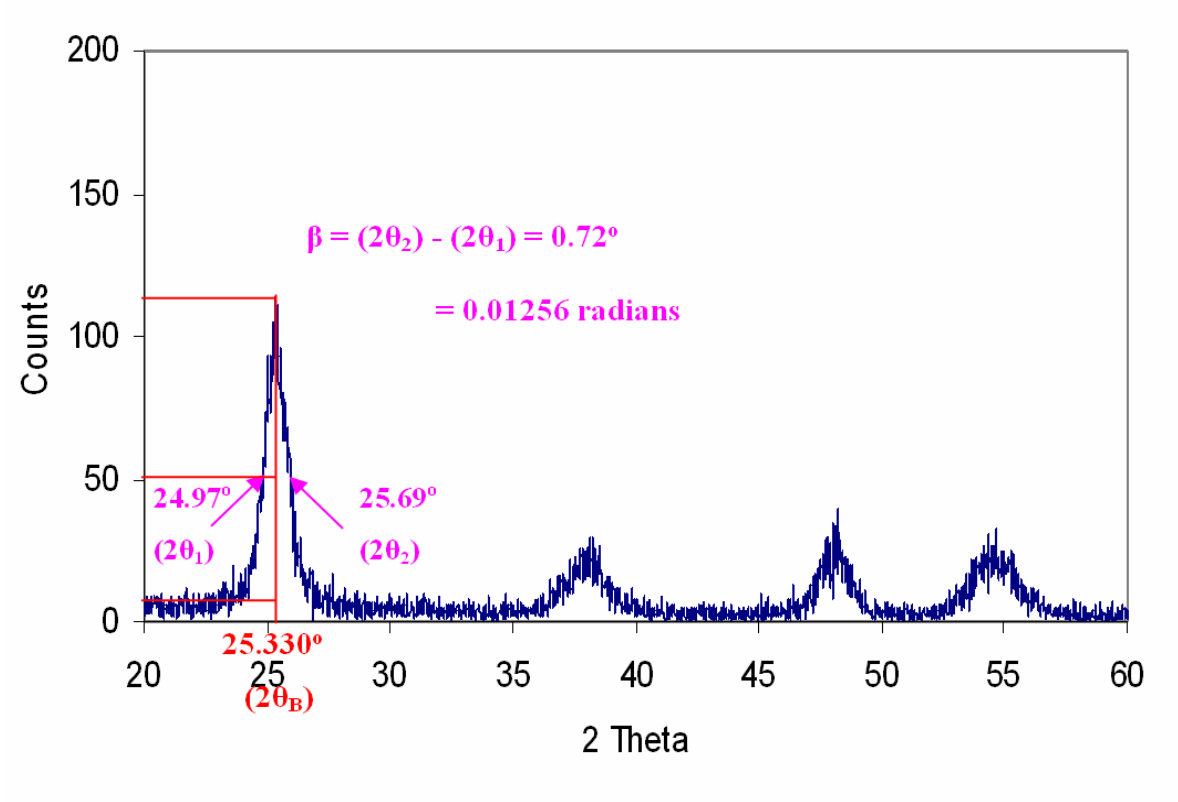

Appendix Figure C5 The of XRD pattern undoped TiO_2

Appendix Table C1 Calcination temperatures on the crystallite sizes and phase content of undoped TiO_2 which calcined at 400 °C

Catalyst	Calcination temperature (°C)	Phase[a]	2θ (degree)	Cosθ	β (degree)	β (radian)	Crystallite size (nm)[b]	Intensity (A)	Intensity (R)	% A[c]	% R[d]
Undoped TiO_2	400	A	25.330	0.976	0.72	0.01256	11.3	114	-	100	0

[a]A and R are stand for anatase and rutile, respectively

[b]The crystallite size was calculated by using Scherrer's equation.

[c]The relative anatase content was calculated by applying Spurr-Myers equation.

[d]The relative rutile content was calculated by 100% - Anatase%.

Appendix Table C2 Calcination temperatures on the unit cell volume of undoped TiO_2

Titania precursor	Calcination temperature (°C)	Phase	Lattice parameters (nm)			Unit cell volume (nm^3)
			a	b	c	
Undoped TiO_2	400	A	0.9269	0.3790	0.3790	0.1332

Appendix D

-The photocatalyst mechanism and raw data of all photo-degradation reactions

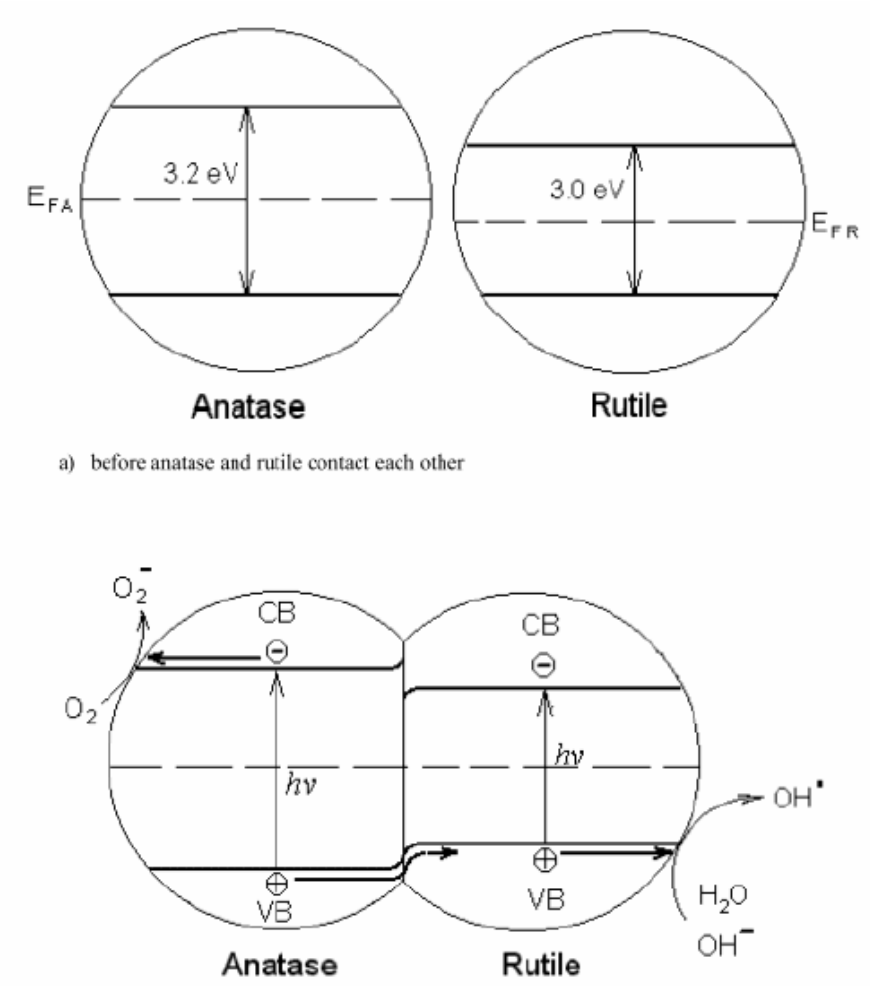

Appendix Figure D1 The mechanism of electron-hole separation in P25-TiO_2 during photo catalysis (Sun et al., 2003)

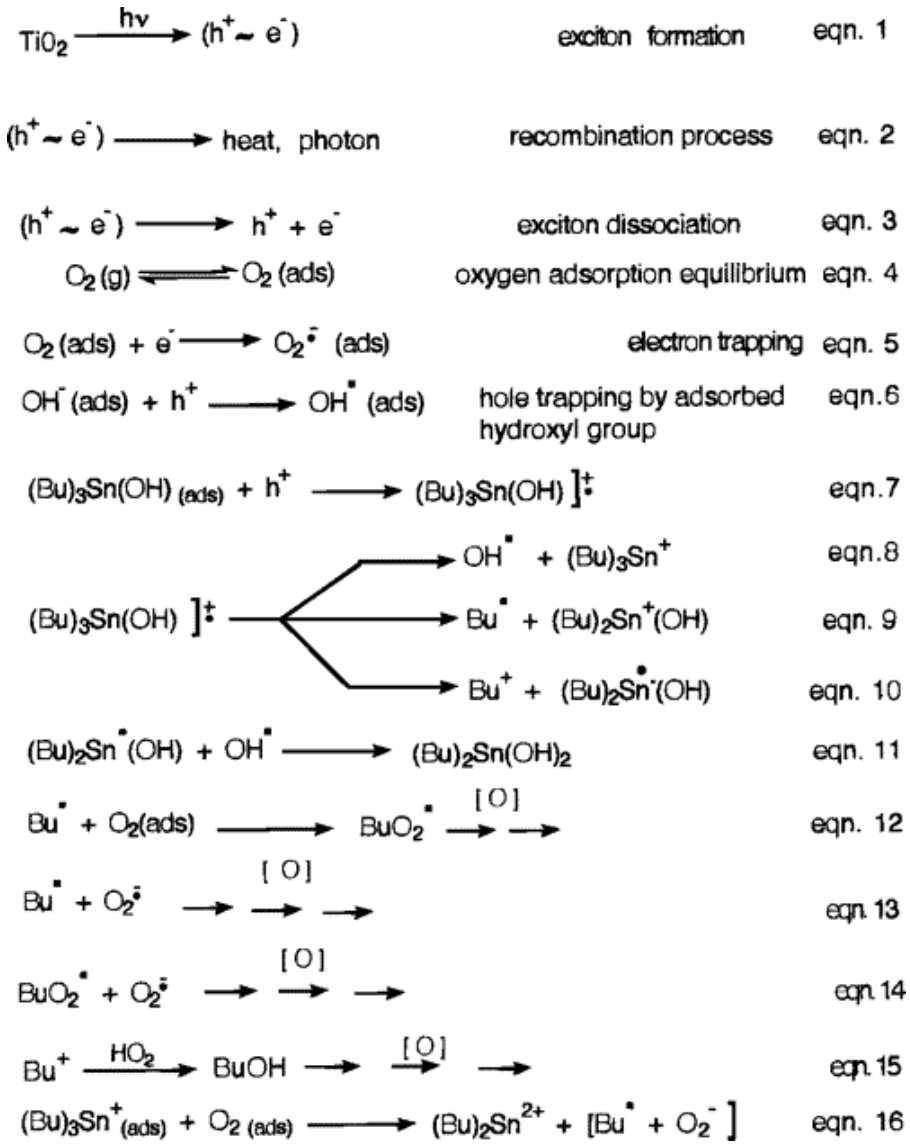

Appendix Figure D2 The proposed mechanism for the TiO_2-photocatalytic degradation of TBT (Navio et al., 1996).

Appendix Table D1 Raw data of the photo-degradation reaction of TBT under ***visible light***

Degrading time (h)	Concentration (μg mL^{-1})			Relative concentration (C/C_o)				
	C_1	C_2	C_3	C_1/C_o	C_2/C_o	C_3/C_o	$(C/C_o)_{ave}$	Std $_{(C/Co)}$
0	10.243	10.265	10.288	0.998	1.000	1.002	1	0.002
0.5	10.365	10.260	10.326	1.010	1.000	1.003	1.005	0.005
1	10.256	9.998	10.557	0.999	0.974	1.028	1.001	0.027
1.5	9.986	10.523	10.452	0.973	1.025	1.018	1.005	0.028
2	10.568	10.360	10.364	1.029	1.009	1.010	1.016	0.012
3	9.999	10.433	9.996	0.974	1.016	0.974	0.988	0.024

Appendix Table D2 Raw data of the photo-degradation reaction of TBT by Undoped TiO_2 under ***visible light***

Degrading time (h)	Concentration (μg mL^{-1})			Relative concentration (C/C_o)				
	C_1	C_2	C_3	C_1/C_o	C_2/C_o	C_3/C_o	$(C/C_o)_{ave}$	Std $_{(C/Co)}$
0	9.862	9.852	9.869	1.000	0.999	1.001	1	0.001
0.5	9.743	9.756	9.755	0.988	0.989	0.989	0.989	0.001
1	9.636	9.696	9.601	0.977	0.983	0.974	0.978	0.005
1.5	9.523	9.501	9.427	0.966	0.963	0.956	0.962	0.005
2	9.402	9.366	9.263	0.953	0.950	0.939	0.948	0.007
3	9.084	9.189	9.174	0.921	0.932	0.930	0.928	0.006

Appendix Table D3 Raw data of the photo-degradation reaction of TBT by P25-TiO_2 under ***visible light***

Degrading time (h)	Concentration (μg mL^{-1})			Relative concentration (C/C_o)				
	C_1	C_2	C_3	C_1/C_o	C_2/C_o	C_3/C_o	$(C/C_o)_{ave}$	Std $_{(C/Co)}$
0	8.632	8.625	8.665	0.999	0.998	1.003	1.000	0.002
0.5	8.449	8.569	8.356	0.978	0.992	0.967	0.979	0.012
1	8.184	7.856	8.295	0.947	0.909	0.960	0.939	0.026
1.5	7.771	7.756	7.776	0.899	0.898	0.900	0.899	0.001
2	7.740	7.735	7.730	0.896	0.895	0.895	0.895	0.001
3	7.423	7.416	7.460	0.859	0.858	0.863	0.860	0.003

Appendix Table D4 Raw data of the photo-degradation reaction of TBT by N-doped TiO_2 under ***visible light***

Degrading time (h)	Concentration (μg mL^{-1})			Relative concentration (C/C_o)				
	C_1	C_2	C_3	C_1/C_o	C_2/C_o	C_3/C_o	$(C/C_o)_{ave}$	Std $_{(C/Co)}$
0	9.706	9.896	9.710	0.993	1.013	0.994	1.000	0.011
0.5	9.354	9.371	9.596	0.957	0.959	0.982	0.966	0.014
1	9.003	8.611	8.657	0.921	0.881	0.886	0.896	0.022
1.5	8.550	8.601	8.676	0.875	0.880	0.888	0.881	0.006
2	8.286	8.269	8.127	0.848	0.846	0.832	0.842	0.009
3	7.611	7.603	7.672	0.779	0.778	0.785	0.781	0.004

Appendix Table D5 Raw data of the photo-degradation reaction of TBT under ***natural light***

Degrading time (h)	Concentration (μg mL^{-1})			Relative concentration (C/C_o)				
	C_1	C_2	C_3	C_1/C_o	C_2/C_o	C_3/C_o	$(C/C_o)_{ave}$	Std $_{(C/Co)}$
0	10.837	10.475	10.656	1.017	0.983	1.000	1.000	0.017
0.5	10.8.8	10.521	10.665	1.014	0.987	1.001	1.001	0.013
1	10.821	10.771	10.592	1.015	1.011	0.994	1.006	0.011
1.5	10.618	10.462	10.540	0.996	0.982	0.989	0.989	0.007
2	10.568	10.360	10.764	0.992	0.972	1.010	0.991	0.019
3	10.799	10.433	10.366	1.013	0.979	0.973	0.988	0.022
4	10.792	10.799	10.596	1.013	1.012	0.994	1.007	0.011
5	10.744	10.602	10.373	1.008	0.995	0.973	0.992	0.018
2 days	10.428	10.330	10.924	0.979	0.969	1.025	0.991	0.030
3 days	10.719	10.173	10.446	1.006	0.955	0.980	0.980	0.026
4 days	10.312	10.789	10.146	0.968	1.012	0.952	0.977	0.031
5 days	10.574	10.412	10.133	0.992	0.977	0.951	0.973	0.021

Appendix Table D6 Raw data of the photo-degradation reaction of TBT by Undoped TiO_2 under ***natural light***

Degrading time (h)	Concentration (μg mL^{-1})			Relative concentration (C/C_o)				
	C_1	C_2	C_3	C_1/C_o	C_2/C_o	C_3/C_o	$(C/C_o)_{ave}$	Std $_{(C/Co)}$
0	10.422	10.330	10.376	1.004	0.996	1.000	1.000	0.004
0.5	10.339	10.217	10.278	0.996	0.985	0.991	0.991	0.006
1	9.803	9.634	9.718	0.945	0.928	0.937	0.937	0.008
1.5	9.320	9.432	9.376	0.898	0.909	0.904	0.904	0.005
2	9.104	9.324	9.214	0.877	0.899	0.888	0.888	0.011
3	8.796	8.881	8.838	0.848	0.856	0.852	0.853	0.004
4	8.682	8.539	8.611	0.837	0.823	0.830	0.831	0.007
5	8.483	8.480	8.482	0.818	0.816	0.817	0.817	0.001
2 days	6.924	6.324	6.814	0.667	0.609	0.657	0.644	0.031
3 days	4.796	4.881	4.838	0.462	0.470	0.466	0.467	0.004
4 days	2.682	2.569	2.681	0.258	0.248	0.258	0.255	0.006
5 days	0.682	0.589	0.661	0.066	0.057	0.064	0.062	0.005

Appendix Table D7 Raw data of the photo-degradation reaction of TBT by P25-TiO_2 under ***natural light***

Degrading time (h)	Concentration (μg mL^{-1})			Relative concentration (C/C_o)				
	C_1	C_2	C_3	C_1/C_o	C_2/C_o	C_3/C_o	$(C/C_o)_{ave}$	Std $_{(C/Co)}$
0	10.631	9.750	10.190	1.043	0.957	1.000	1.000	0.043
0.5	9.656	9.606	9.632	0.948	0.943	0.946	0.945	0.002
1	9.610	9.644	9.627	0.943	0.946	0.945	0.945	0.002
1.5	8.882	8.886	8.884	0.872	0.873	0.872	0.872	0.001
2	8.569	8.730	8.649	0.841	0.857	0.849	0.850	0.008
3	8.329	8.377	8.353	0.817	0.822	0.820	0.821	0.002
4	8.097	8.187	8.142	0.795	0.803	0.799	0.799	0.004
5	7.855	7.759	7.807	0.771	0.761	0.766	0.766	0.005
2 days	6.359	5.930	6.149	0.624	0.582	0.603	0.604	0.021
3 days	3.933	3.877	3.853	0.386	0.380	0.378	0.382	0.004
4 days	1.097	0.997	0.842	0.108	0.098	0.083	0.096	0.013
5 days	ND[a]	ND	ND	-	-	-	-	-

ND[a] non detectable

Appendix Table D8 Raw data of the photo-degradation reaction of TBT by N-doped TiO_2 under ***natural light***

Degrading time (h)	Concentration (μg mL^{-1})			Relative concentration (C/C_o)				
	C_1	C_2	C_3	C_1/C_o	C_2/C_o	C_3/C_o	$(C/C_o)_{ave}$	Std $_{(C/Co)}$
0	9.917	10.008	9.962	0.995	1.005	1.000	1.000	0.005
0.5	9.654	9.537	9.596	0.969	0.957	0.963	0.963	0.006
1	9.003	9.311	9.157	0.904	0.935	0.919	0.920	0.015
1.5	8.550	8.401	8.476	0.858	0.843	0.851	0.852	0.007
2	7.886	7.869	8.127	0.771	0.791	0.816	0.792	0.022
3	7.411	6.903	7.157	0.744	0.693	0.719	0.718	0.025
4	6.583	6.568	6.575	0.661	0.659	0.660	0.660	0.001
5	6.039	6.273	6.156	0.606	0.630	0.618	0.619	0.012
2 days	4.686	4.269	4.127	0.470	0.429	0.414	0.438	0.029
3 days	1.411	1.873	1.137	0.142	0.188	0.114	0.148	0.037
4 days	ND[a]	ND	ND	-	-	-	-	-
5 days	ND	ND	ND	-	-	-	-	-

ND[a] non detectable